The evolution of Troodos ophiolite dikes and their relationship with the spreading ridge-transform fault system on Cyprus

Anke van Grieken (6014135)

Faculty of Geosciences, Utrecht University, December 2023

Supervisors: dr. R.J.F. Wessels, dr. A. Beniest, prof. dr. M.R. Drury

Utrecht University

Acknowledgements

Abstract

As windows into fossil oceanic crust, ophiolites provide unique information on processes such as crust formation, seafloor spreading and hydrothermal alteration. The Troodos ophiolite is located on Cyprus, an island on the southern Anatolian plate in the eastern Mediterranean. The ophiolite formed during the Late Cretaceous (90-92 Ma) and contains the full ophiolitic sequence: ultramafic cumulates, gabbros, mafic and felsic sheeted dikes, pillow lavas and a sedimentary cover. The southeast of the ophiolite is cut by the Arakapas fossil spreading ridge-transform fault system. It connects two parts of a spreading ridge, which in turn is the origin of the Troodos dikes. The influence of the Arakapas Transform Fault activity on the intrusive sequence is not yet known. In addition, more information on both evolution within the dike complex and between dike types is needed.

This thesis aims to fill these knowledge gaps by conducting fieldwork and microscopic research. Dikes are classified into groups, sampled, and studied with optical microscopy, Scanning Electron Microscopy (SEM) and Energy-dispersive X-ray Spectroscopy (EDS). Two important alteration trends are identified from the geochemistry: alteration from pyroxene to amphibole and from Ca-rich plagioclase to Na-rich plagioclase is observed, indicating a decrease in calcium and an increase in sodium. Additionally, bulk rock data show an increase in SiO_2 content. An increase in scale allows for determining the degree of alteration per dike type at set distances from the Arakapas Fault. No correlation is found; no influence of the Arakapas Fault activity on the dikes can be identified from this study. Next, the degree of alteration per dike type, irrespective of the distance to the transform fault, was established. The degree of alteration varied between groups, possibly caused by compositional diversity. The presence or absence of certain minerals may lead to differences in susceptibility to alteration or differences in permeability. Finally, the possibility of black smoker hydrothermal system activity in these rocks is explored, which explains K and Ca depletion and can induce an increase in permeability.

Contents

1. Introduction

1.1 General introduction

Windows into a fossil oceanic crust: ophiolites are invaluable in the understanding of Earth's history. Ophiolites are segments of oceanic lithosphere that are subaerially exposed. These segments can be emplaced onto continental or oceanic crust through obduction (e.g. Searle & Cox, 1999) or are uplifted due to isostatic processes (e.g. Evans et al., 2021).

Ophiolites can provide information on processes such as oceanic crust formation, seafloor spreading and hydrothermal alteration by studying their overall structure, mineral content, microstructures and elemental composition (Dilek, 2003).

During the 1972 GSA Penrose Conference, the ideal, complete sequence for ophiolites was described from bottom to top as follows: an ultramafic complex, a gabbroic complex, a mafic sheeted dike complex, a mafic volcanic pillowed complex, and an overlying sedimentary layer (Figure 1) (e.g. Dilek, 2003; McClain, 2003).

Ophiolites can be classified based on the presence or absence of certain units described in the Penrose sequence; not all types contain all units. Ophiolites of the Tethyan (or Mediterranean (Dilek, 2003)) type do usually contain all units. They are covered by pelagic sedimentary rocks and are separated from the underlying crust by a metamorphic sole (Dilek, 2003; Moores, 1982). The sheeted dike complex in this type is not always well-developed (Dilek, 2003; Robinson et al., 2008).

Figure 1 | Stratigraphy of an ideal ophiolite (after McClain, 2003)

Sheeted dike complexes form in extensional environments: narrow, elongate magma bodies are injected in host rock perpendicular to the lowest stress direction and parallel to the spreading axis (Robinson et al., 2008). A balance between spreading rate and magma supply results in a well-developed sheeted dike complex, as is often the case at mid-ocean ridges (MORs) (Niu & Batiza, 1993; Purdy et al., 1992; Small, 1994). Thus, initially, sheeted dike complexes in ophiolites were interpreted as evidence for an MOR origin in extensional setting (e.g. Gass, 1968; Hynes, 1975; Moores & Vine, 1971).

However, some ophiolites with a well-developed sheeted dike complex did not show the expected MOR geochemical signature. This sparked a heated debate on the origin of ophiolites. Some important arguments were that the presence of both tholeiitic and calc-alkalic compositions in the lower pillow lavas and sheeted dikes indicated an island arc setting (e.g. Miyashiro, 1973, 1975, 1975) and that the larger thickness of modern ocean floor did not correspond to smaller ophiolite thickness (Moores, 1982).
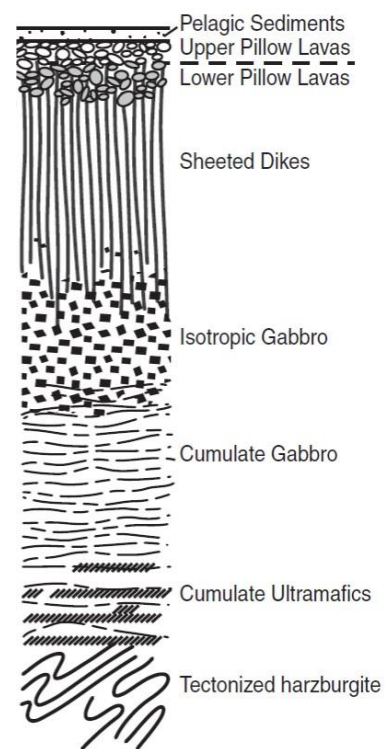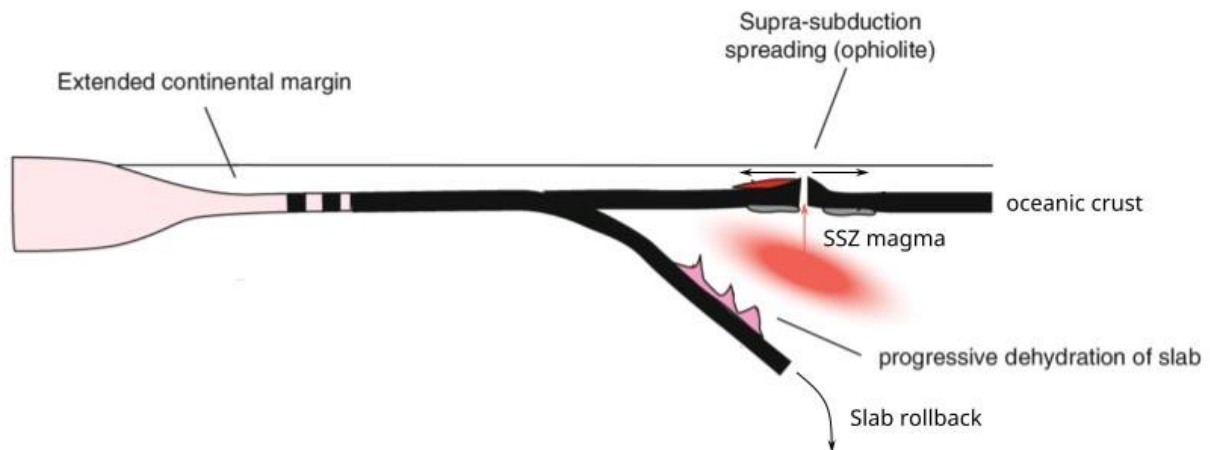
Figure 2 | Schematic cross-section of the formation of supra-subduction ophiolitic crust. The downgoing slab rolls back, creating tension in the overriding plate, while its melting generates magma with an SSZ geochemistry (modified after Herrington & Brown, 2011)).

From these arguments evolved the concept of ophiolites that formed in a supra-subduction zone setting (SSZ) (Moores et al., 1984). This concept merges observations of both the MOR and island arc theories. It is theorized that the crust was formed above a subduction zone. In such a system, slab rollback of the downgoing plate causes tension in the overriding plate, which creates space for sheeted dike intrusions (Figure 2). Dehydration of the downgoing plate generates partial melting of the mantle above, creating magma with a subduction-influenced geochemical signature (Osozawa et al., 2012; Pearce et al., 1984). The geochemical issue of calc-alkalic rocks being present is also explained: they are not only characteristic for island arc settings, but also for convergent plate margins (Miyashiro, 1973).

One example of an SSZ ophiolite is the Troodos ophiolite, located on the island of Cyprus (Eastern Mediterranean). Its sheeted dike complex is extensive and well-developed and consists of multiple phases of distinct dike intrusions (Cooke et al., 2014). Studying and unraveling the intrusive sequence of the Troodos ophiolite will provide insights into the evolution of oceanic crust in a supra-subduction environment.

1.2 Geological setting

The African plate currently subducts northward beneath the Eurasian plate at the Cyprus Arc system (Anastasakis & Kelling, 1991; McPhee & van Hinsbergen, 2019) (Figure 3). Cyprus is situated on the southern end of the Anatolian plate and the crust of the Troodos ophiolite formed between 90 and 92 Ma during the late Cretaceous (Mukasa & Ludden, 1987).

Cyprus can be divided into four units: Kyrenia, Troodos, circum-Troodos and Mamonia (Figure 3). The Kyrenia unit is situated at the north of the island and consists of metamorphosed Jurassic carbonates and Upper Cretaceous to Pleistocene marine sediments and volcanics. Its southern edge is separated from the Mesaoria basin by a thrust fault (McPhee & van Hinsbergen, 2019; Robertson & Woodcock, 1986). The circum-Troodos area, including the Mesaoria basin, consists of Upper Cretaceous radiolarite and sediments ranging in age from Upper Cretaceous to recent. It covers the north and south of the Troodos ophiolite. The Troodos consists of mafic oceanic crust, forming a complete Penrose sequence ophiolite. It is bordered on the southwest by the Mamonia unit, which contains sediments and volcanics ranging in age from Triassic to Lower Cretaceous (McPhee & van Hinsbergen, 2019; Ring & Pantazides, 2019). It also contains minor metamorphic rocks (Malpas et al., 1992).
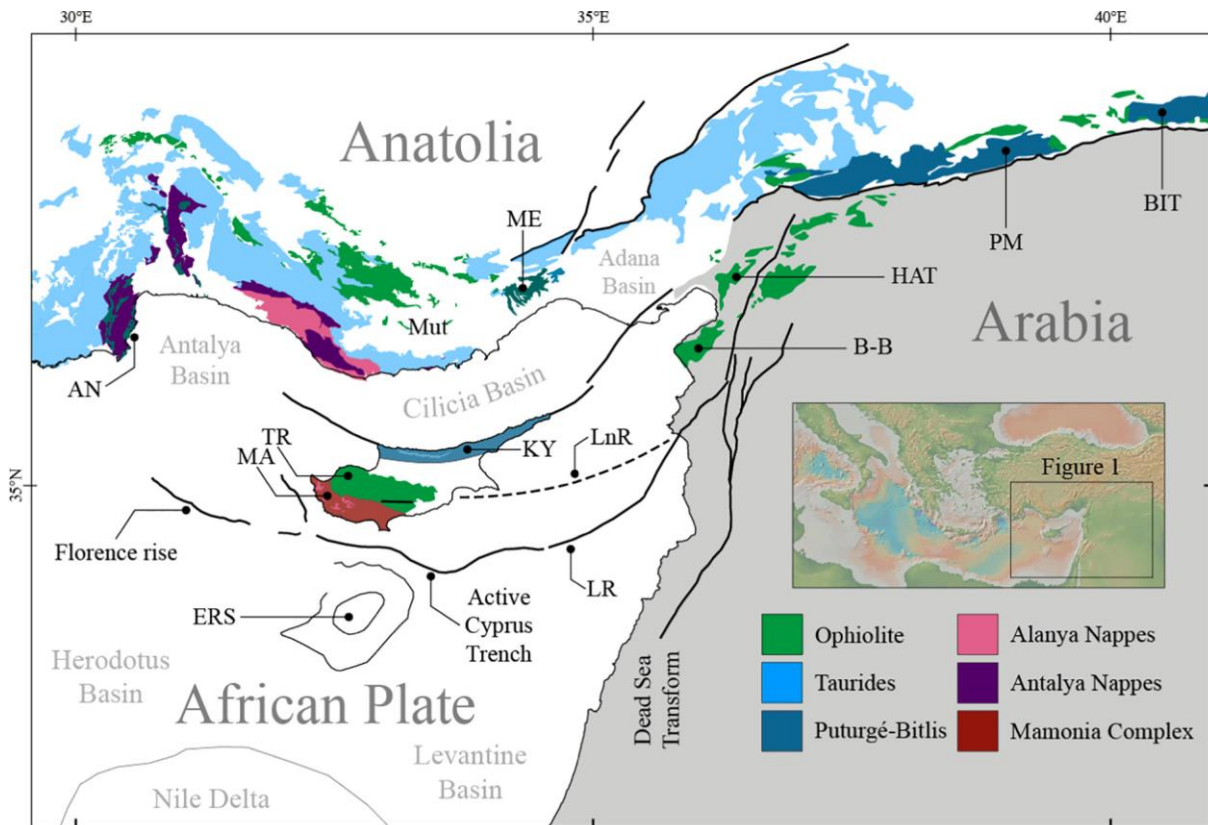
Figure 3 | Regional geological setting of Cyprus (McPhee & van Hinsbergen, 2019).

1.2.1 Troodos

The Troodos ophiolite was uplifted and emplaced during the Neogene (Freund et al., 2014; Marien et al., 2019), although the mechanism of obduction still remains unknown. It stretches out from east to west across the center of the island and measures approximately 90 km in length (NW-SE) and 30 km width (NE-SW). The ophiolite contains the complete Penrose sequence from the center of the ophiolite

to its rims (Figure 4). The ultramafic core, Mount Olympus, forms the highest point of the island at 1952 m above sea level and contains harzburgite, serpentinite, dunite, pyroxenite and wehrlite (Freund et al., 2014; Marien et al., 2019; Morag et al., 2016). This complex is surrounded by sheeted dikes, containing dikes of both mafic and felsic compositions such as gabbro, diorite and plagiogranite (Freund et al., 2014). The sheeted dikes are overlain by the lower and upper pillow lavas, which are made up of tholeiitic basalt and depleted tholeiitic to depleted boninitic basalt, respectively (Marien et al., 2019; Miyashiro, 1973). Finally, these rocks are covered by Cretaceous pelagic sediments (Marien et al., 2019). Deformation of the ophiolite into an anticlinal structure after its obduction and subsequent erosion have created the concentric structure around Mount Olympus (McPhee & van Hinsbergen, 2019; Varga, 2003). The units with the stratigraphically deepest origin are now located at the highest elevation (Marien et al., 2019; Morag et al., 2016).

In the southeast of the ophiolite, a fossil spreading ridge-transform fault system is preserved (McPhee & van Hinsbergen, 2019; Morris & Maffione, 2016). The fossil transform fault, known as the Arakapas Fault, connects two parts of a fossil spreading ridge (Figure 4). There are multiple axial valleys located within the ophiolite, which are former spreading centers; one of these, the Solea graben, is interpreted as the most recent (Morris & Maffione, 2016; Varga & Moores, 1985) and is indicated in Figure 4. The dikes of the Troodos ophiolite originated at these spreading centers. The Arakapas Fault was active during the Late Cretaceous, simultaneous with the spreading ridge activity (Morris & Maffione, 2016). It separates the Troodos from the Limassol Forest area (Morag et al., 2016). The Arakapas Fault has an E-W trend, which is perpendicular to the general strike of the sheeted dikes (Morris et al., 1990). The
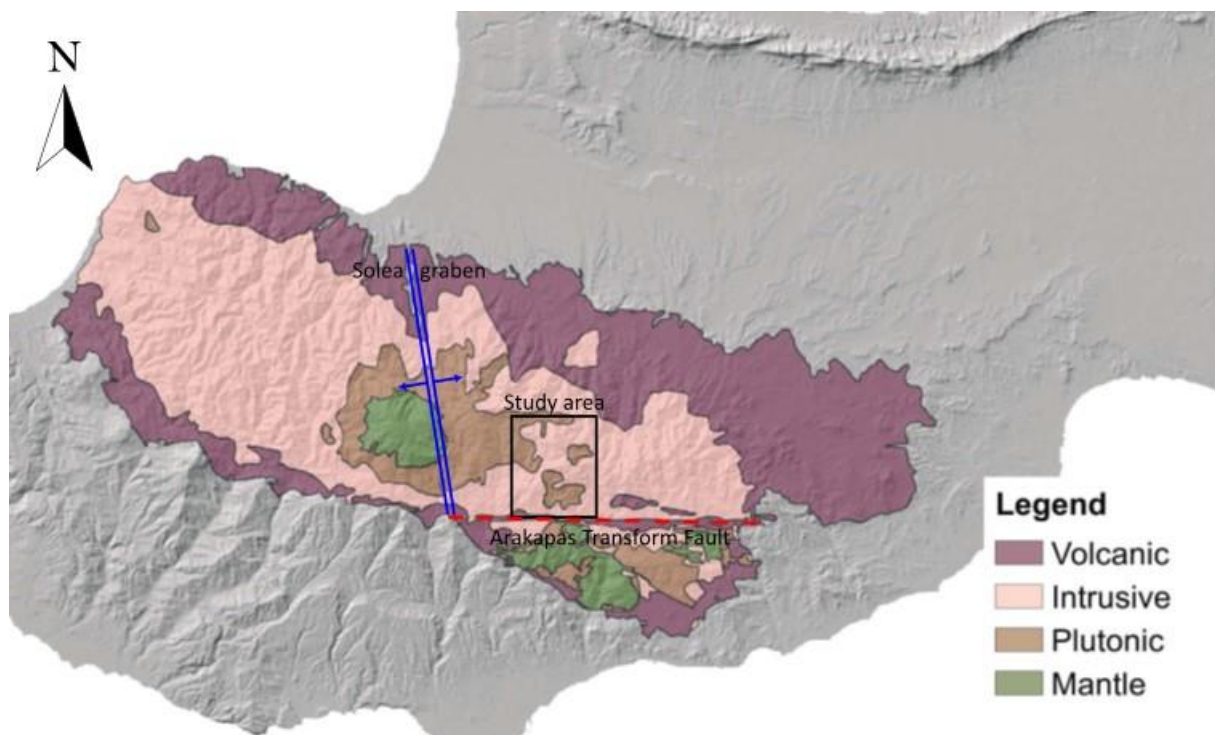

Figure 4 | Simplified geological map of Cyprus, showing the Troodos ophiolite (colored) in the center of the island surrounded by sedimentary rocks (gray). Note the concentric structure of the ophiolite around Mount Olympus (green) due to its anticlinal deformation. The Solea graben is indicated with spreading to the east and west to illustrate the fossil spreading ridge (blue). It is connected in the south to the Arakapas Fault (red). The Troodos ophiolite measures 90 km E-W and 30 km N-S (modified after Morag et al., 2016).

sense of movement along the fault is debated (McPhee & van Hinsbergen, 2019): paleomagnetic evidence suggests dextral shear (Morris et al., 1990), while dike patterns suggest sinistral movement (Varga & Moores, 1985).

1.2.2 Evolution

As noted previously, structure and geochemistry are essential to determine the geological history of an ophiolite. However, these are not the only important defining features of an ophiolite. The metamorphic sole, the slither of mafic, high-grade metamorphic rock beneath an ophiolite, also provides relevant information about its history. It is seen as the remnant of the young subducting plate beneath the ophiolite. For the Troodos ophiolite, the metamorphic sole can be found in the Mamonia complex as some separate outcrops, not as one continuous piece (Malpas et al., 1992; Osozawa et al., 2012). It contains amphibolite-grade metamorphic rocks for which hornblendes $^{40}Ar/^{39}Ar$ dating indicates a 14 million year duration of subduction activity, which is relatively long (Osozawa et al., 2012). To explain both this long duration of subduction and the creation of anomalously high temperature rocks, Osozawa et al. (2012) hypothesize the subduction of a spreading ridge situated on the downgoing plate to result in higher temperatures in the mantle. Simultaneous with the formation of the metamorphic sole, rollback of the downgoing plate caused tension in the overriding plate, creating space for SSZ magmatism.

This magmatism led to the formation of both mafic and felsic intrusions in the Troodos ophiolite. Oceanic crust generally has a mainly mafic composition, but can also contain significant amounts of felsic material (Freund et al., 2014). This can be produced by either partial melting of oceanic crust or fractional crystallization of mafic melts; the latter is the primary mechanism that formed the Troodos felsic intrusions (Freund et al., 2014; Marien et al., 2019).

Before obduction and emplacement of the ocean crust, the ophiolite rotated by 90 degrees in counterclockwise direction (Moores et al., 1984; Varga, 2003). Its mechanism of emplacement is still under debate; however, the current consensus is that emplacement of the Troodos ophiolite happened simultaneous with other ophiolites during the closing of the Tethys ocean along the southern Tethyan suture (Mukasa & Ludden, 1987; Varga, 2003).

1.3 Aim and approach

While the Troodos ophiolite has been studied extensively, it is not yet known whether the Arakapas Transform Fault activity affected the intrusive sequence. As the fault zone was active at the time of formation of the ophiolite, this would not be unlikely. Additionally, information on the evolution within the dike complex and between the different groups of intrusive dikes is lacking.

The aim of this thesis is **to investigate the evolution of the Troodos ophiolite dikes and explore the possible influence of the activity of the Arakapas Fault Zone on the intrusive sequence**. To do so, systematic observations and samples are taken along-strike of the Arakapas Transform Fault, at distances of <0.5, 1.5-2.5, and 6-9.5 km to the north of the fault trace. From this, the field characteristics of the intrusive sets and their relative timing are established. Selected outcrops are sampled and thin sections are studied with optical and scanning electron microscopy to determine mineralogy and any hydrothermal alteration, metamorphism or weathering overprint. Energy-dispersive X-ray Spectroscopy (EDS) is applied to selected samples to further investigate the geochemistry of the intrusives.

The applied methodology makes it possible to identify the evolution within the intrusive sequence and to determine if there was any effect from the Arakapas Transform Fault on the evolution of the intrusives. It also provides valuable insights on the formation and subsequent development of the ophiolite, which may be used in further research of supra-subduction zone ophiolites and their geological history.

2. Methods

2.1 Fieldwork

The fieldwork area contains well-exposed road sections in an area north of the Arakapas Fault Zone (AFZ). This region was chosen because it is structurally less complex and stratigraphically more coherent than the area south of the AFZ. The fieldwork area extended 9 km along-strike and 10 km north of the AFZ. This ensured that any influence of the Arakapas Fault Zone on the intrusive sequence would be captured, and to determine a baseline to compare observations closest to the fault with.

The field area was divided into three segments at equidistance from the Arakapas Fault Zone, at 0-0.5, 1.5-2.5 and 6-9.5 km from the fault (Figure 5). At these distances outcrops were selected along roads based on their quality and accessibility. In each outcrop, the rock types were classified in 5 groups: gabbro, early-stage grey dike, plagiogranite, late-stage grey dike and brown dike. This classification was based on field relations, color, mineralogy, shape, degree of alteration and/or grain size. The cross-cutting relationships were described and types and degree of alteration were determined. Finally, minimally weathered, representative samples were collected and labelled for further analysis.
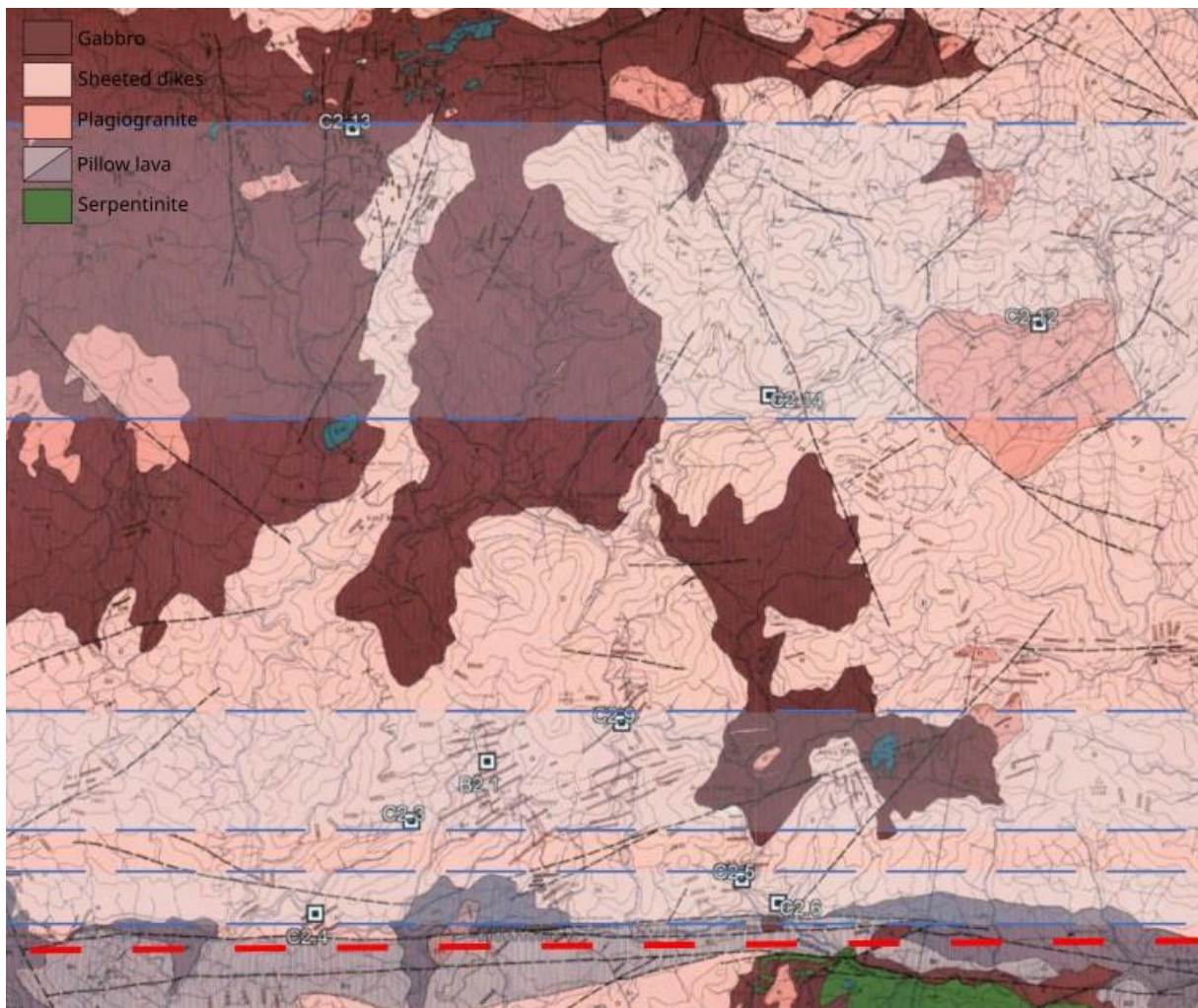

Figure 5 | Map of research area showing the segments and outcrop locations at 0-0.5 km, 1.5-2.5 km and 6-9.5 km from the Arakapas Fault Zone (red) (modified after Bear & Morel, 1960).

2.2 Sample analysis

2.2.1 Optical microscopy

The samples were prepared for sample analysis in the optical microscope. This was done by making thin sections with a thickness of 30 µm. These were subsequently digitalized with the Zeiss Axio Scan.Z1 using a 10x objective lens and brightfield illumination. They were scanned in plane polarized light in one orientation and in cross polarized light in six orientations (30° angular difference). This resulted in high resolution images (0.439 µm/pixel) which were further examined using the Zeiss Zen 3.6 (Blue Edition) software to identify their petrology and microstructures. However, most rocks had a very small grain size, making it difficult to identify minerals. Mineral identification for these rocks therefore mainly relied on SEM-EDS results.

2.2.2 Scanning Electron Microscopy (SEM) and Energy Dispersive X-ray Spectroscopy (EDS)

SEM-EDS provides information on the composition of a sample. Samples were selected for EDS analysis based on their quality, rock type, and structural position in the field. All thin sections of interest were carbon coated to prevent charging of the sample during analysis in the SEM.

The thin sections were scanned using the Zeiss EVO 15 SEM under high vacuum conditions of less than 10^{-4} Pa. The electron beam had an acceleration voltage of 15 keV and a probe current of 1 nA. More background information on SEM acquisition can be found in e.g. Goldstein et al., 2018.

For regions of interest, backscatter electron (BSE) images were obtained using the Zeiss SmartSEM software. These images were used to analyze microstructures and obtain qualitative information about the density of the different mineral phases. In addition, characteristic X-ray energy peaks, unique for each element, were detected using two Bruker XFlash 6|60 EDS detectors and analyzed with the Bruker Esprit 2.1 software. This software allows quantification of the elements present in the targeted mineral phase. A complication of this method is the occurrence of peak interferences between elements with similar X-ray peaks, such as titanium with barium or silicon with tungsten (Goldstein et al., 2018). To avoid this problem, only the elements that are most likely to be present in the sample are selected to be measured, instead of every element. The selected elements for this study were: oxygen, silicon, aluminium, titanium, magnesium, sodium, potassium, phosphorous, calcium, manganese and iron.

2.2.3 Automated quantitative mineralogy

For each thin section spot measurements were used to determine the main composition of the mineral phases. For selected samples one or two mineralogical maps were made using the Zeiss Mineralogic 1.8 software. For each rock type at least one large map was made, in addition to smaller maps. In addition to a stitched false-colored phase map and BSE map, the software provided the bulk rock composition of the mapped area and the elemental composition of the individual mineral phase. The phase map was based on a basic recipe, in which common minerals were defined using their relative elemental composition.

The Zeiss Mineralogic software uses a user-defined mineral 'recipe' based on the common minerals present in the samples and their normalized elemental weight composition over a range of possible concentrations. For each measurement on a sample, the software cycled through the recipe from first to last mineral phase and assigned the first mineral for which the element concentration matches the

measurement. Hence, it was important to consider the order of minerals in the recipe: if minerals had a similar composition, more abundant minerals were placed above less abundant minerals.

Plagioclase feldspars exist in a solid solution series, ranging from albite to anorthite. In all recipes, plagioclase feldspars were divided into 3 classes based on the amount of calcium relative to calcium and sodium combined. *Na-rich plagioclase* included albite and oligoclase, with $Ca/(Ca + Na) = 0 - 30\%$; *intermediate plagioclase* included andesine and labradorite, with $Ca/(Ca + Na) = 30 - 70\%$; and *Ca-rich plagioclase* included bytownite and anorthite, in which $Ca/(Ca + Na) = 70 - 100\%$.

Following this method, recipes were customized for each rock type using spot measurements, BSE maps and optical microscopy to determine the appropriate element concentration ranges for each mineral. The mineral phases are mostly correctly resolved on the phase maps; however, when different minerals have (nearly) identical compositions (e.g. actinolite and other amphiboles), the software has difficulty classifying them correctly. Another issue arose when a mineral could not be classified: this results in a grey spot on the map. This happened for example when a boundary between two minerals is captured in one measurement.

3. Results

A summary description of the main lithologies observed in the research area is given in section 3.1. Detailed field relations and relative timing of selected outcrops are provided in section 3.2, while mineralogy and alteration of the identified lithological groups is addressed in section 3.3. Geochemical variations and trends in the lithological groups are given in section 3.4.

3.1 Rock type field description

Intrusives found in the selected road sections were sorted in 5 groups based on color, mineralogy, morphology, relative timing, degree of alteration and/or grain size (measured in thin section). The main characteristics of these groups are summarized below. The grain sizes are determined using optical microscopy.

Gabbro

Gabbro only occurs as bodies, not as dikes. It contains mainly black pyroxene and amphibole and white plagioclase feldspar minerals. The grain size varies significantly from mm to cm scale. This is the rock type of the oldest relative age within the area of interest. In Figure 8a, blue lines indicate the gabbro body.

Early-stage grey dike

This dike type consists of microgabbro and contains plagioclase feldspar, pyroxene, amphibole and epidote. The grain size is very fine, ranging from 0.1 to 1 mm. In outcrop this rock is often heavily veined. It is the oldest dike type found in the sheeted dike area. In Figure 8a, green lines indicate the early-stage grey dike.

Plagiogranite

Plagiogranite is found both as bodies (in areas without early-stage grey dikes or gabbro) and as dikes (cutting through early-stage grey dikes). It is recognized by its yellowish/light color and mineral contents: quartz, plagioclase feldspar, chlorite and epidote. The grain size is coarser than the other dike types, ranging from 1 to 2 mm. In some outcrops the plagiogranite has a mottled appearance: it contains clusters of dark minerals, likely amphiboles. In Figure 6a, yellow lines indicate the plagiogranite body, while in Figure 8a and R4a, plagiogranite is found as dikes.

Late-stage grey dike

These dikes often have an angular morphology similar to the brown dikes described below, but have not been altered to a brown color. The grain size is very fine and is hard to distinguish in hand sample (±0.1 mm). The color is blue-grey. The mineralogy consists of plagioclase feldspar, amphibole, pyroxene and epidote. Figure 6a shows late-stage grey dikes in purple lines.

Brown dike

Brown dikes often have an angular morphology, resembling the shape of pre-existing fractures (see figures in section 3.2). The rock often easily crumbles in outcrop. The brown alteration is at least present at the edges of the dikes and often throughout the entire dike. Individual grains cannot be distinguished, grains are ±0.1 mm scale. The mineralogy consists of plagioclase feldspar, chlorite, epidote, pyroxene and amphibole. Some brown dikes also contain quartz. This youngest dike type is

found cutting through all other rock types, often in a different direction compared with the main sheeted dike trend (Figure 6a, brown lines).

For all rock types, samples were taken from parts with as little weathering as possible. This resulted in a total of 18 samples: 2 gabbro samples, 4 early-stage grey dike samples, 4 plagiogranite samples, 3 late-stage grey dike samples and 5 brown dike samples.

3.2 Field results

All pictures in this section are annotated with the same color scheme: gabbros are indicated with blue, early-stage grey dikes with green, plagiogranites with yellow, late-stage grey dikes with purple and brown dikes with brown. Table 1 shows the presence of the different groups in each outcrop and the presence of any veining. When samples are taken in an outcrop, the numbers are listed.

3.2.1 0-0.5 km distance to the Arakapas Fault

Most proximal to the Arakapas Fault, it proved difficult to find high quality outcrops, due to high density of faults and fractures. Three locations were selected where outcrop quality was sufficient: C2.4, C2.5 and C2.6 (Figure 5). The outcrops in the segment closest to the fault contain early-stage grey dikes, plagiogranite, late-stage grey dikes and brown dikes, while gabbro is absent (Table 1). The late-stage grey dikes and brown dikes are present in all three selected outcrops. Early-stage grey dikes and plagiogranite are both found in only one of the outcrops.

Outcrop C2.5 is used as the type-outcrop for this segment. It shows late-stage grey dikes and brown dikes cutting through the plagiogranite body (Figure 6). In outcrop C2.5 mottled plagiogranite is observed. It contains amphibole clusters of approximately 1 cm which have no dark minerals in their direct vicinity. In these clusters and throughout the rock the dark amphibole minerals have an elongate habit (Figure 7a). On a dm-scale, dark angular patches are incorporated in the plagiogranite (Figure 7b).

Table 1 | The different intrusion groups in each visited outcrop sorted on proximity to the transform fault. For each intrusion group any observed veining is noted. Green indicates either epidote or chlorite, as distinguishing between these two in the field proved difficult. When samples are taken, the sample number is listed.

|	Outcrop (distal - proximal from transform fault)	Gabbro	Early stage grey dike	Plagiogranite	Late stage grey dike	Brown dike
	C2.14		?		?	
6-9.5 km	veins	green, white	green	green	green	green, white
	C2.12					
	veins					
	C2.13					
	veins	green				green
	C2.3		C2.3d	C2.3c	C2.3b	C2.3f, C2.3g
1.5-2.5 km	veins		green, white	green	white	
	B2.1	B2.1d, B2.1i	B2.1c, B2.1g	B2.1ai, B2.1i	B2.1b, B2.1e	B2.1h
	veins	plagiogranite				
	C2.9					
	veins					
	C2.5			C2.5		
0-0.5 km	veins			green	green	
	C2.6					
	veins					
	C2.4					C2.4b
	veins		grey, green, white, plagiogranite		green, white	white fractures
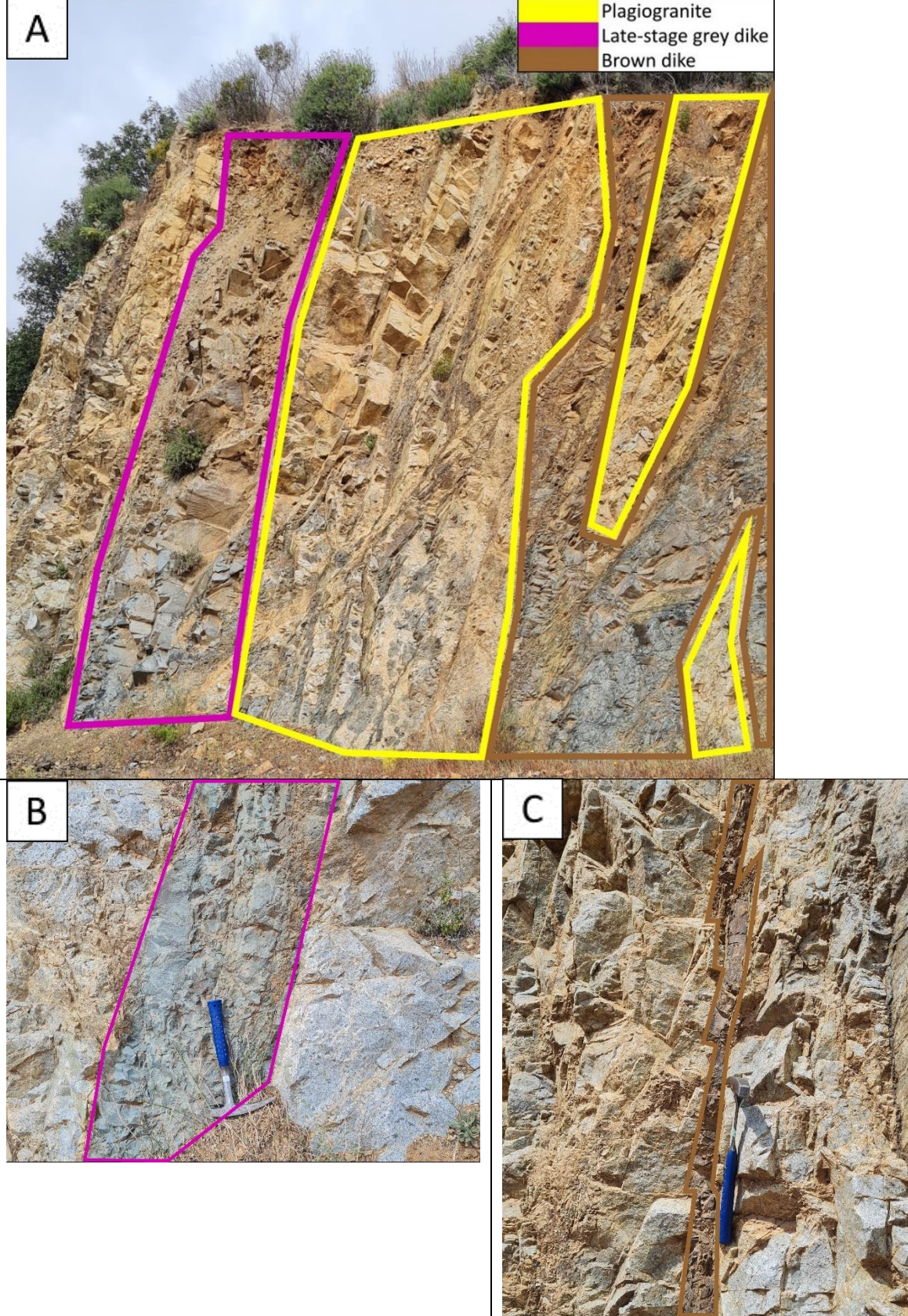
Figure 6 |a. Overview of outcrop C2.5 showing plagiogranite being cut off by brown and grey dikes. The brown dike on the right has a grey interior; it is recognized by its brown rims. Length of section: 5 m. b. Late-stage grey dike cutting through mottled plagiogranite. c. Brown dike cutting through plagiogranite, showing its angular, or serrated, morphology.
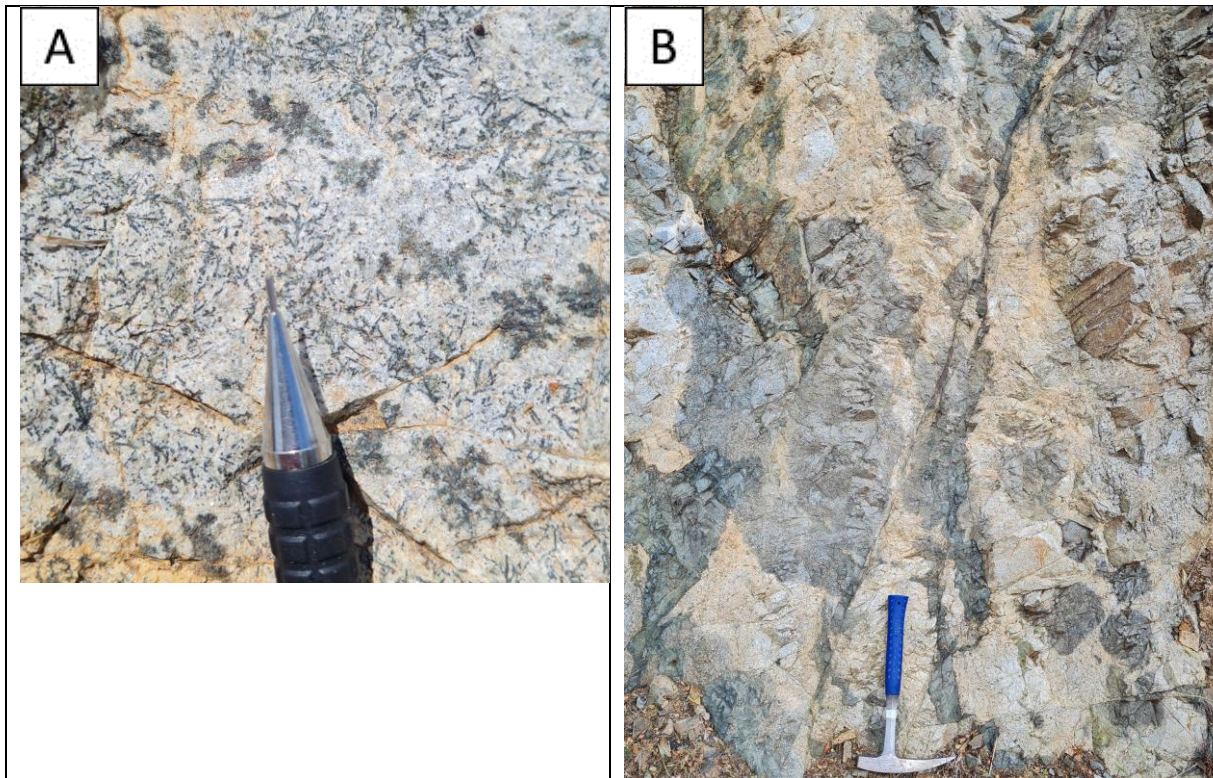
Figure 7 |a. Mottled plagiogranite with elongate dark amphiboles. b. Patches of dark material within the lighter plagiogranite.

3.2.2 1.5-2.5 km distance to the Arakapas Fault

At further distance from the fault, the outcrop quality improves and the degree of fracturing decreases. The three selected outcrops for this segment are C2.3, B2.1 and C2.9 (Figure 5). This segment contains all rock types, but gabbro and early-stage grey dikes occurred less frequently compared to the other lithological groups (Table 1).

This segment is represented best by outcrop B2.1. This outcrop is the only outcrop encountered that contains all rock types and is therefore ideal in determining their relative timing. The gabbro consists of grains with variable sizes ranging from mm to cm scale and contains some white veining. The early-stage grey dike contains extensive veining: pure white veins, white veins with black grains which are interpreted as injections of plagiogranitic material and very fine-grained grey veins which are interpreted as injections of late-stage grey dike material. The boundary of the early-stage grey dike and plagiogranite shows an interesting feature: the two rock types exhibit a swirling pattern, as if the two rock types were simultaneously in a molten state and mixed together (Figure 8b). The plagiogranite contains dark patches and is dissected by a late-stage grey dike. The late-stage grey dike has chilled margins and is fine grained throughout. The brown dike is not very cohesive and cuts through all the previous rocks. A late normal fault offsets all lithologies.

Outcrop B2.1
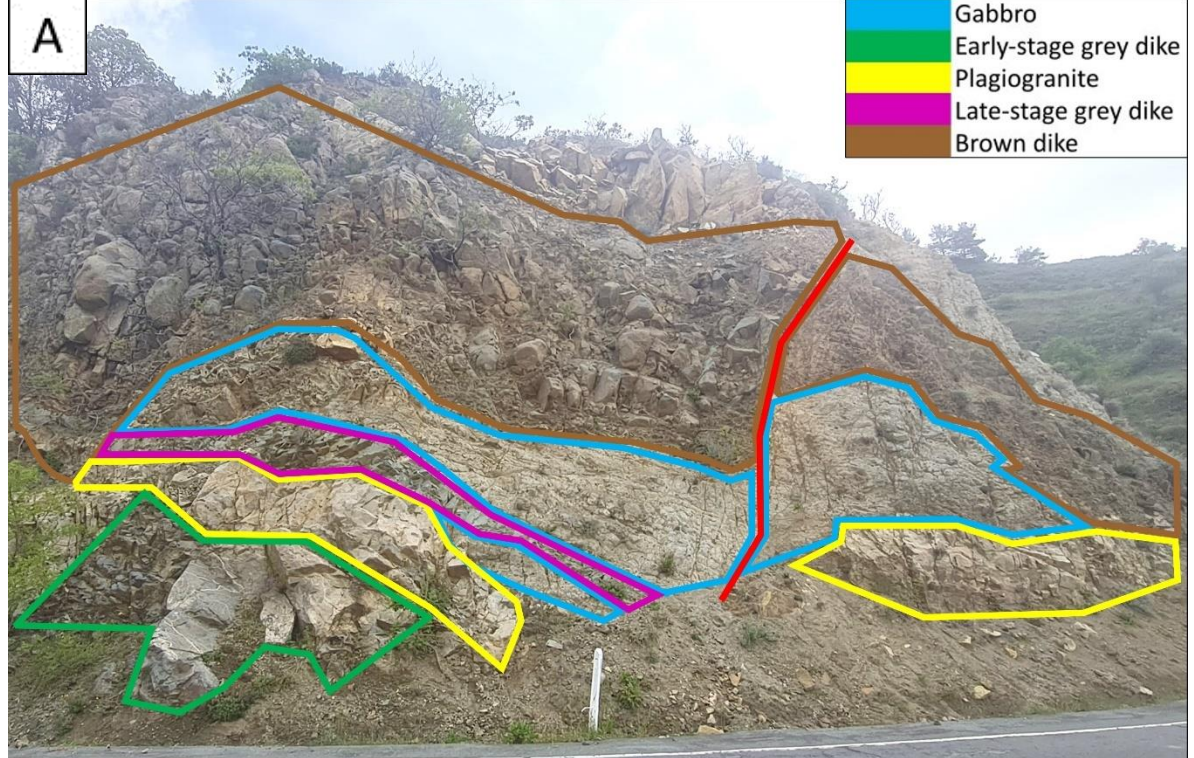
Figure 8 | a. Overview of the most complete outcrop B2.1. Outcrop length: 12 m. b. Mixing of plagiogranite (light) with early-stage grey dike (dark).

3.2.3 6-9.5 km distance to the Arakapas Fault

This segment is located at the largest distance to the transform fault and contains three selected outcrops: C2.12, C2.13 and C2.14 (Figure 5). All rock types are found in this segment (Table 1). Two of the three outcrops are located in intrusive bodies: one in a plagiogranite body and one in a gabbro body. Both are in turn intruded by other dike types. This segment is less disturbed by faults and fractures compared to the two segments closer to the transform fault.

The representative outcrop for this segment is outcrop C2.12. This is a plagiogranite body with intrusions of late-stage grey dikes and some brown dikes. The plagiogranite has both a mottled structure in some places and larger dark patches throughout. It is intruded by late-stage grey dikes with chilled margins (Figure 9b). Both contain minor white and green veins. Minor brown dikes intrude in the previous rocks.
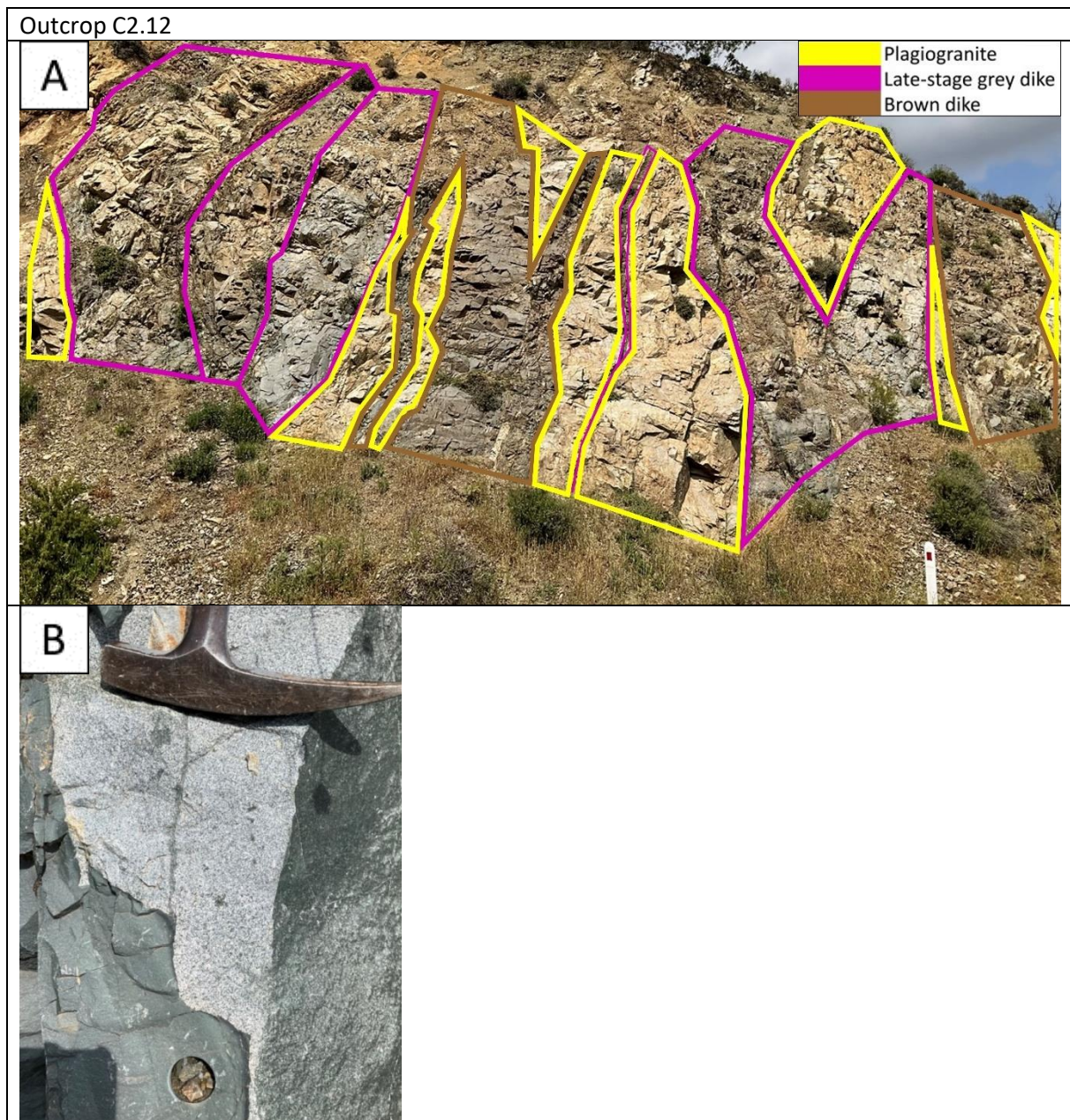
Figure 9 | a. Overview of outcrop C2.12 showing plagiogranite (yellow), late-stage grey dikes (purple) and brown dikes (brown). Length of section: 10 m. b. Plagiogranite (light) intruded by late-stage grey dikes with chilled margins, recognized by darker colors caused by a smaller grain size due to fast cooling at the edges.

3.3 SEM-EDS-AM results

The number of samples that could be processed using the Automated Mineralogy technique (AM) was limited due to issues with the SEM EVO15 at the UU Electron Microscopy center. Therefore, only 2 samples of early-stage grey dikes, 2 samples of plagiogranite, 2 samples of late-stage grey dikes and 4 samples of brown dikes could successfully be processed. For selected thin sections two maps were made. In some instances, the issues with the SEM prevented the collection of large maps, and only small maps could be obtained. This results in a total of 15 maps. No reliable AM maps could be collected for the gabbro samples, and therefore this rock type is not covered in this section.

Processing the thin sections in the SEM results in backscatter electron (BSE) maps and corresponding automated mineralogy (AM) maps. In this section these are presented side-by-side with a pie chart of the corresponding mineralogy. This will provide a clear overview of the differences and similarities within and between these dike types. The color scheme is the same for all maps and pie charts (Figure 10). Enlarged AM and BSE maps are provided in the Appendix.

■ Ca-rich plagioclase	■ Intermediate plagioclase	■ Na-rich plagioclase
■ Orthoclase	■ Chlorite	■ Amphibole
■ Pyroxene	■ Epidote	■ Calcite
■ Quartz	■ Titanite	
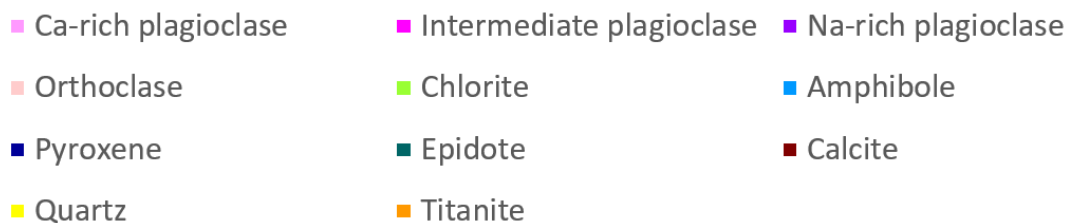
Figure 10 | Legend for maps and pie charts. All minerals that cover >1% of the map are included.

3.3.1 Early-stage grey dike

A2.3

Two small maps were made from this same thin section (Figure 11 and Figure 12). They have a similar mineralogy except for Na-rich plagioclase, which is only present in map 1, where it appears to replace Ca-rich plagioclase (Figure 11). In map 2, intermediate plagioclase can be seen along cracks in the Ca-rich plagioclase and replacing Ca-rich plagioclase in the center of grains (Figure 12). The alteration of pyroxene to amphibole is clearly visible in Figure 12, where dark blue (pyroxene) minerals are altered to light blue (amphibole) minerals. In map 1 (R7), almost all pyroxene has altered to amphibole. In map 1, a green patch is evident: this is alteration to epidote.
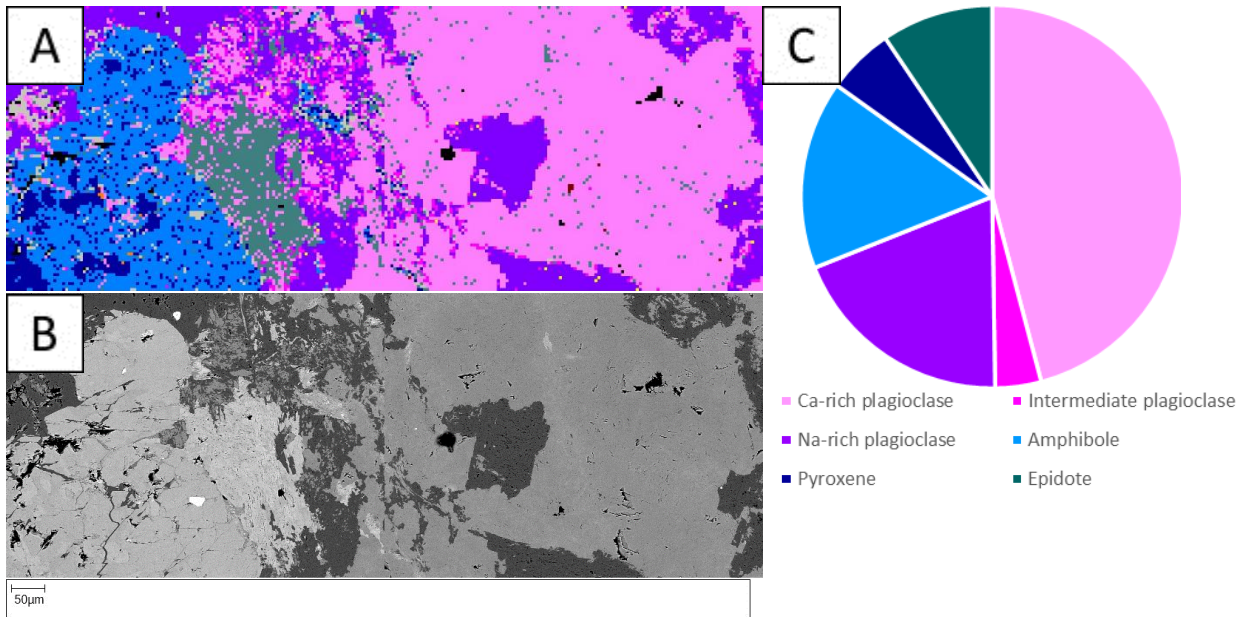
Figure 11 | AM and BSE maps and pie chart for sample A2.3 map 1.
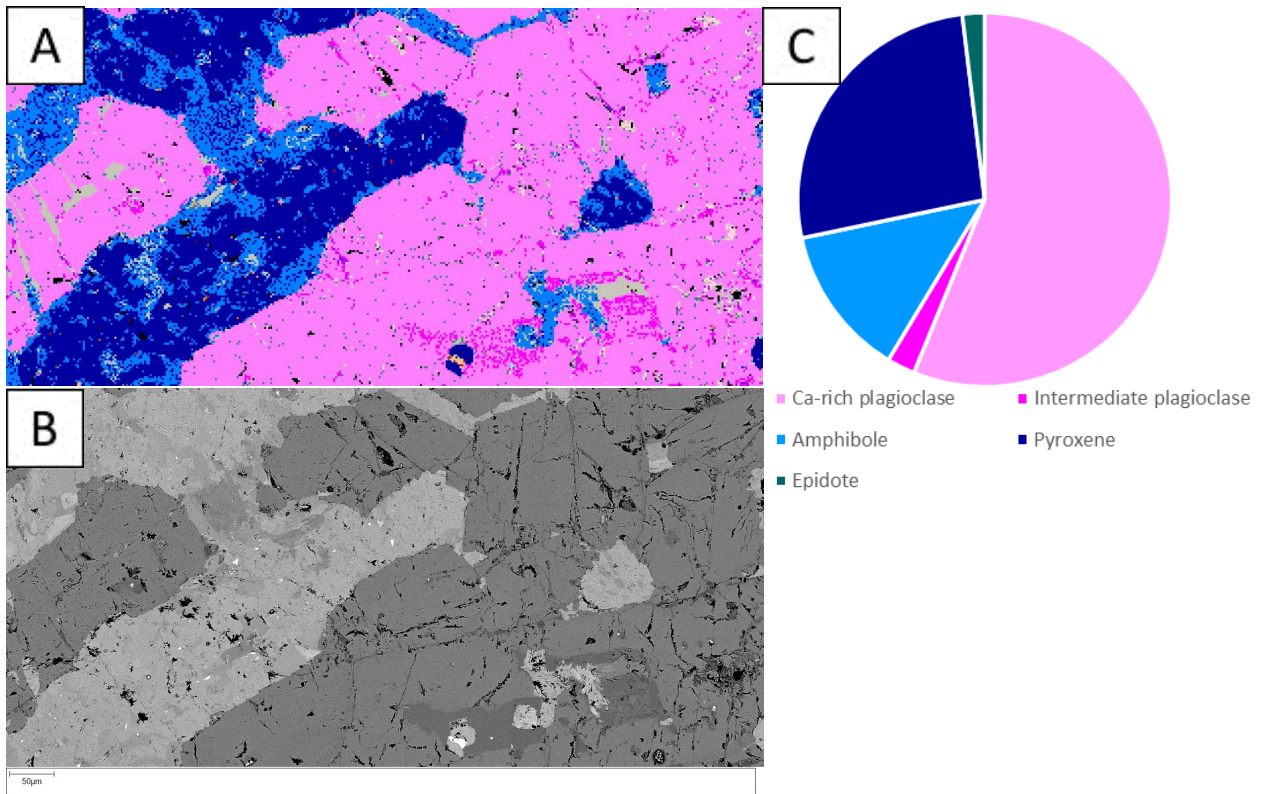
Figure 12 | AM and BSE maps and pie chart for sample A2.3 map 2.

B2.1c

This sample mostly consists of plagioclase, amphibole and pyroxene (Figure 13). The Ca-rich plagioclase is partially replaced by intermediate plagioclase, primarily along fractures and at edges of the crystals. Alteration from pyroxene to amphibole is more extensive and happens both throughout grains and along edges and fractures.
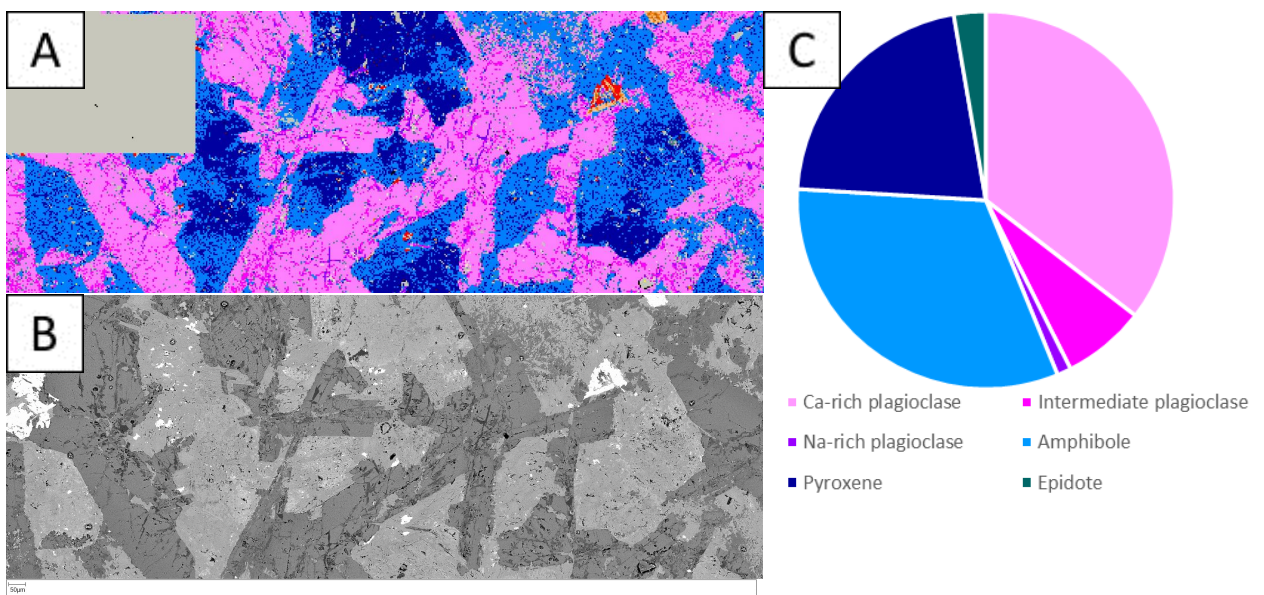
Figure 13 | AM and BSE maps and pie chart for sample B2.1c. One tile is missing in the left upper corner: the SEM failed to collect data here.

3.3.2 Plagiogranite

B2.1ai

Plagiogranite compositions are clearly different from the early-stage grey dike compositions. In this map, only four major minerals are present: Na-rich plagioclase, chlorite, epidote and quartz (Figure 14). No pyroxenes or amphiboles are present. Quartz has subhedral to anhedral crystal shapes with some porosity. In this map, no euhedral minerals are found, indicating that all minerals are secondary and none are primary. Interpretation of replacement relationships from primary to secondary phases is not possible for this sample.
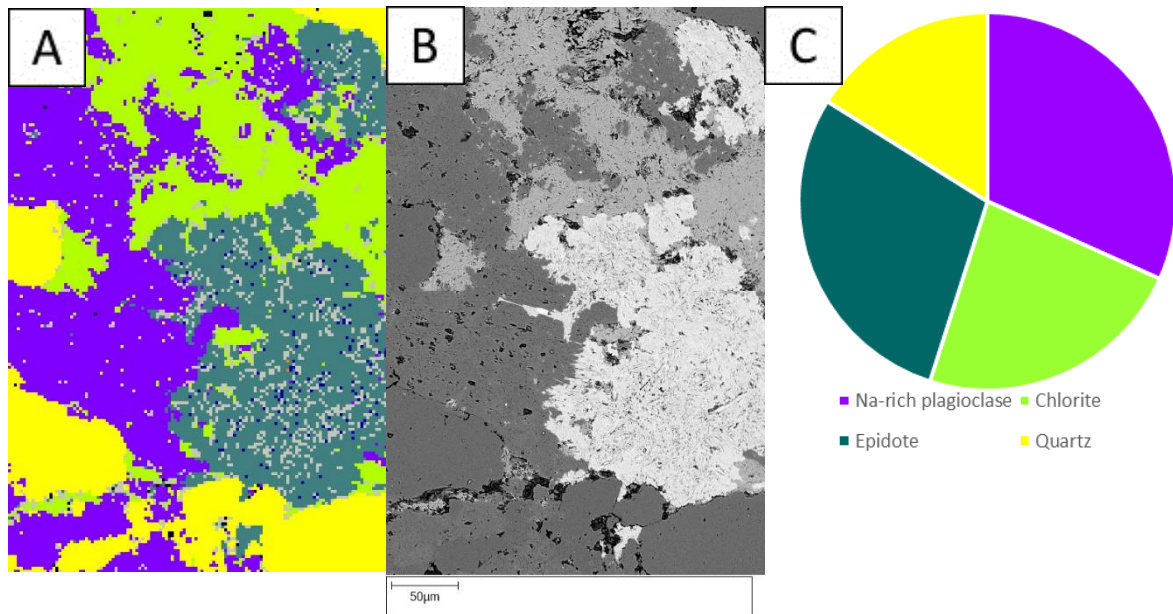
Figure 14 | AM and BSE maps and pie chart for sample B2.1ai.

C2.3c

When comparing this map with the map for B2.1ai, there is a difference in composition: intermediate plagioclase is present while chlorite is absent (Figure 15). Additionally, the texture of the plagioclase is different from sample B2.1ai: a mixture of Na-rich and intermediate plagioclase is visible. The Na-rich variety is more concentrated along the edges of the crystals and in fractures, and seemingly replaces the intermediate variety. Irregular intergrowth between quartz and plagioclase can be observed.
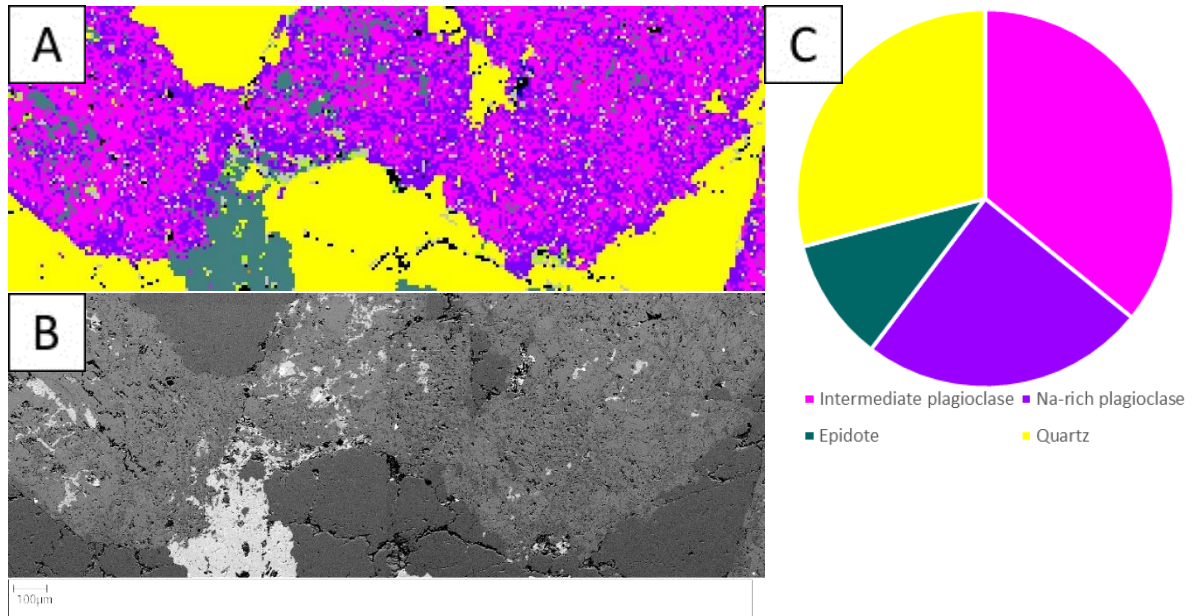
Figure 15 | AM and BSE maps and pie chart for sample C2.3c.

3.3.3 Late-stage grey dike

B2.1b

Two maps were made for this sample: one large map (Figure 16) and one small map (Figure 17). Their compositions are very similar. This sample shows thorough alteration towards a more Na-rich composition. The pyroxene is almost fully replaced by amphibole, while the shape of the original minerals can still be recognized (Figure 16 and Figure 17). Most of the intermediate plagioclase is replaced by the Na-rich variety, yet some patches of intermediate plagioclase remain, mostly along grain boundaries. In the bottom left, an epidote vein is found with minor chlorite. Titanite is relatively abundant in this sample.
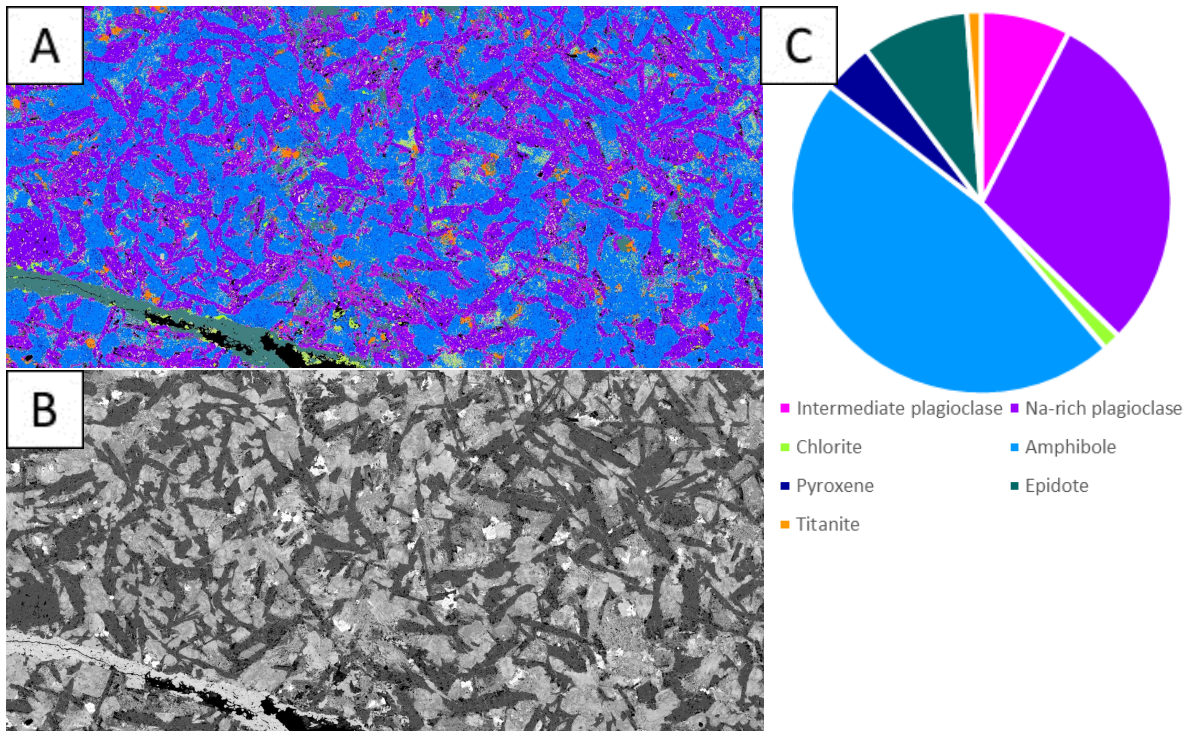
Figure 16 | AM and BSE maps and pie chart for sample B2.1b map 1.
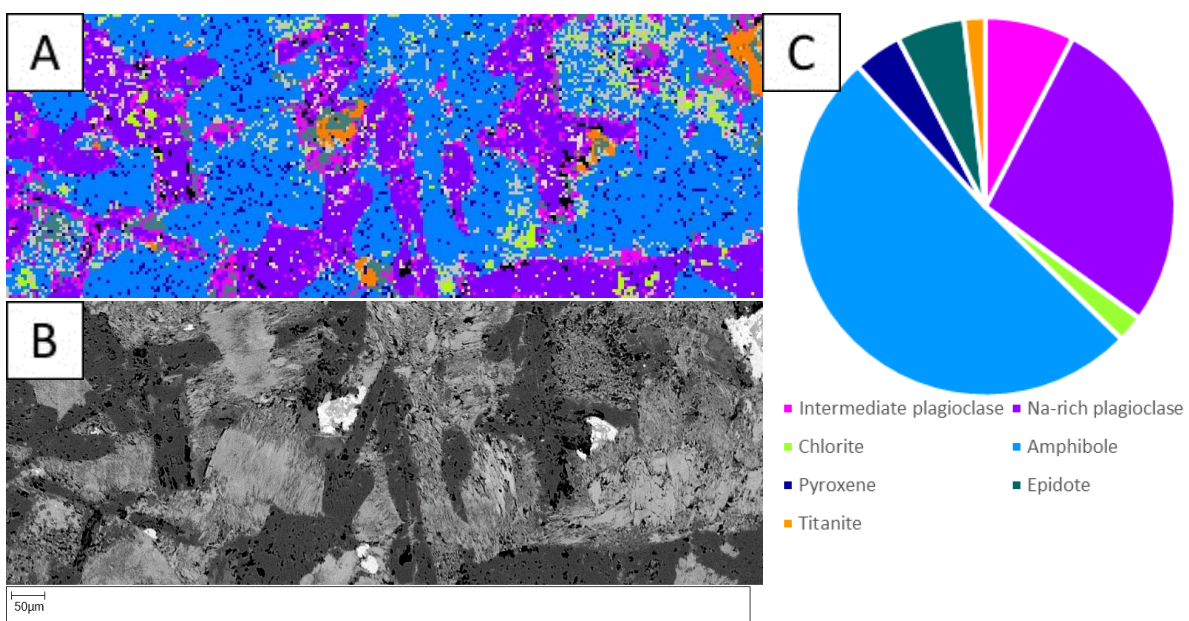
Figure 17 | AM and BSE maps and pie chart for sample B2.1b map 2.

C2.3b

Two same-size maps were made for this sample. It shows some alteration from Ca-rich to intermediate plagioclase, mostly along mineral edges and fractures. Most pyroxene has been altered to amphibole and to some epidote. Some larger titanite minerals are also found.
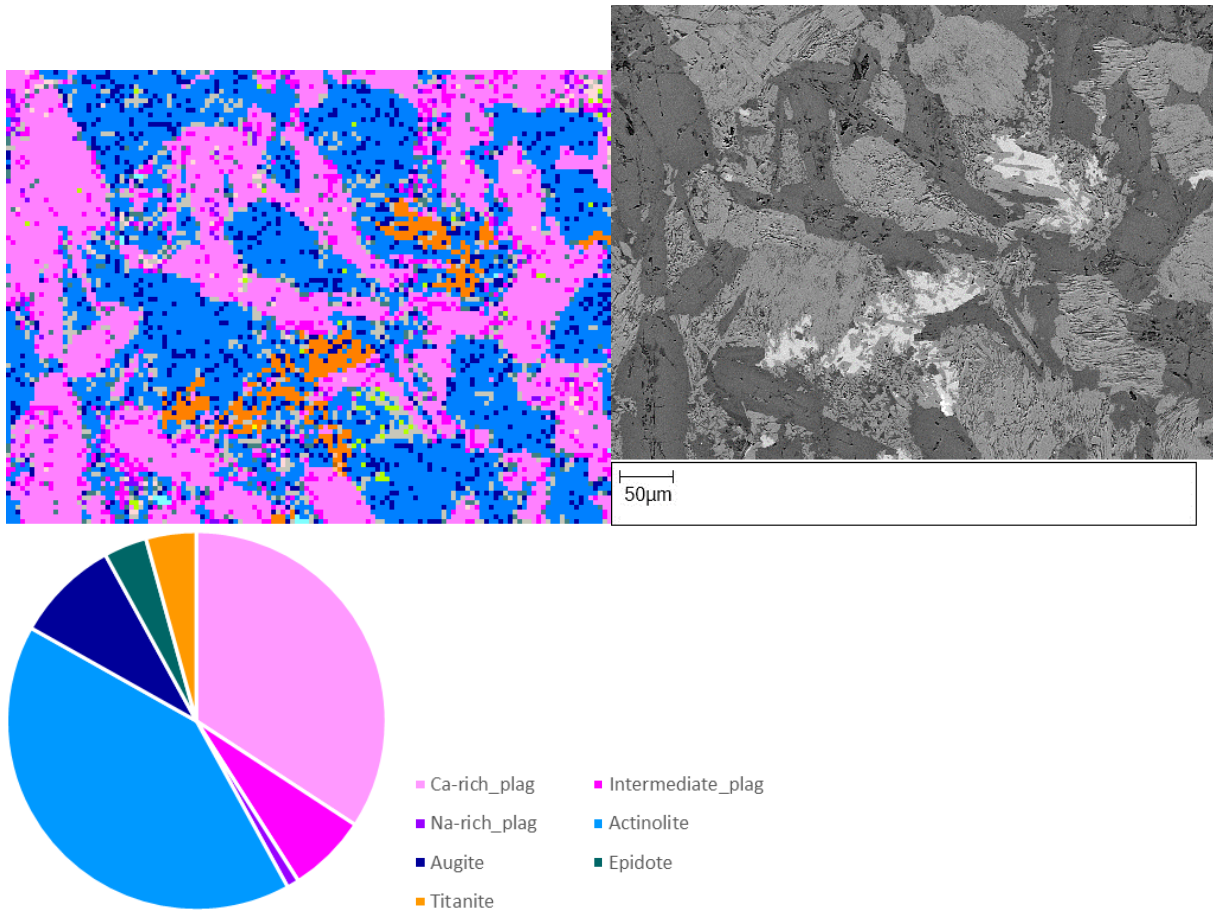
Figure 18 | AM and BSE maps and pie chart for sample C2.3b map 1.

50µm

- Ca-rich_plag
- Intermediate_plag
- Actinolite
- Augite
- Epidote
- Titanite
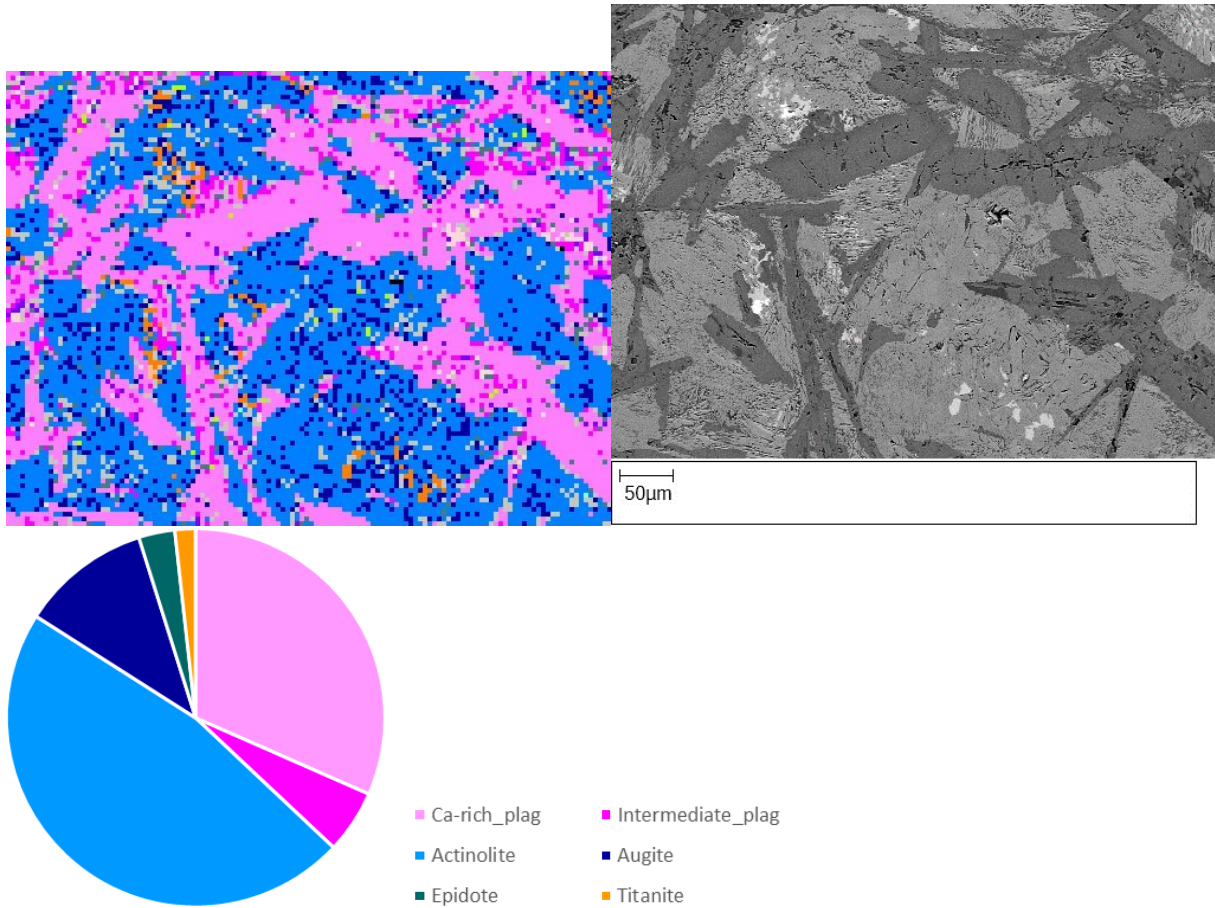
Figure 19 | AM and BSE maps and pie chart for sample C2.3b map 2.

3.3.4 Brown dike

B2.1h

Two maps were made for this sample, one large (Figure 20) and one small map (Figure 21). Alteration of intermediate to Na-rich plagioclase is almost complete, except for some areas along the edges of the minerals. Some of the pyroxene is still intact, but most is altered. Replacement by amphibole is less abundant in this sample, while there is more chlorite. In addition, significant patches of epidote are present. Small amounts of titanite and iron oxide can also be found. The iron oxides are often surrounded by a rim of epidote, while both iron oxide and titanite are spatially associated with chlorite.

The smaller map covers an area without quartz and titanite, while it contains more pyroxene. It provides a more detailed view of the pyroxene and amphibole replacement by chlorite.
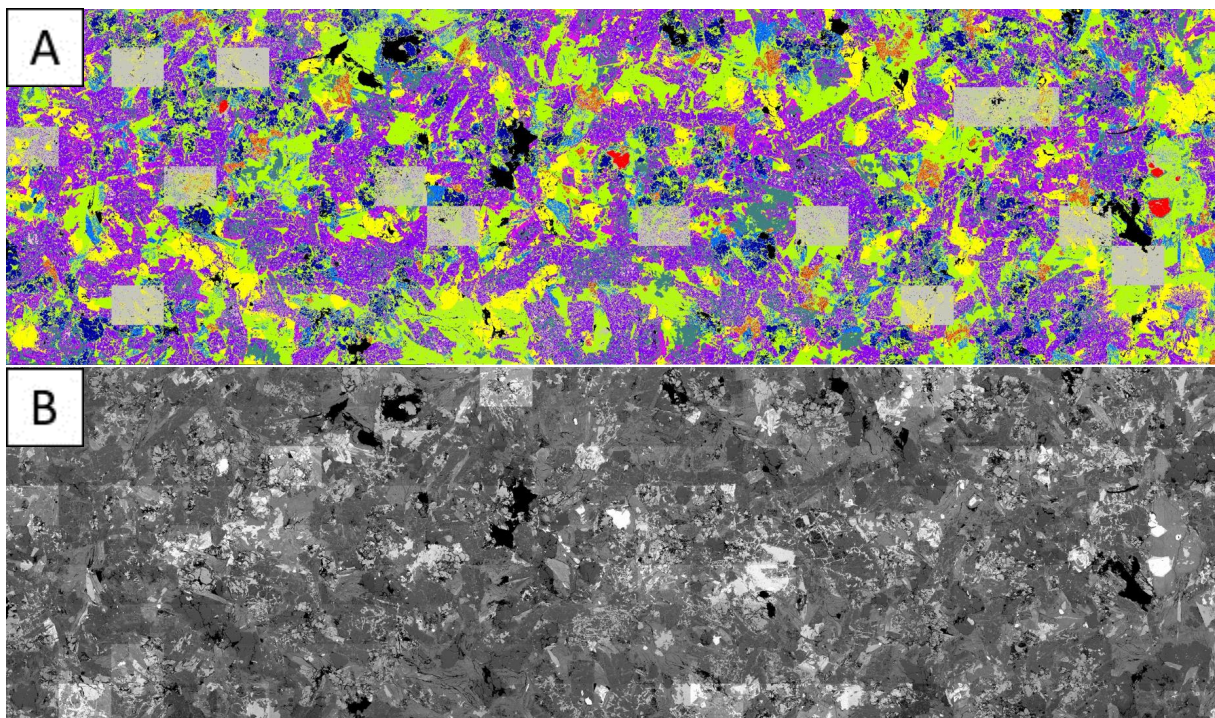
Figure 20 | AM and BSE maps and pie chart for sample B2.1h map 1. The AM map shows multiple tiles that are mostly grey and the BSE map shows difference in the grayscale between tiles, both are due to issues during acquisition.

- Intermediate plagioclase
- Na-rich plagioclase
- Chlorite
- Amphibole
- Pyroxene
- Epidote
- Quartz
- Titanite
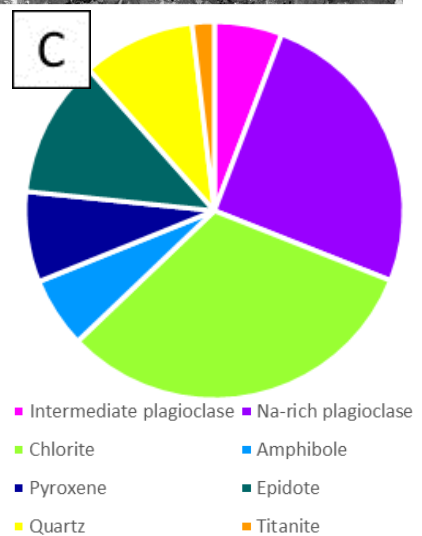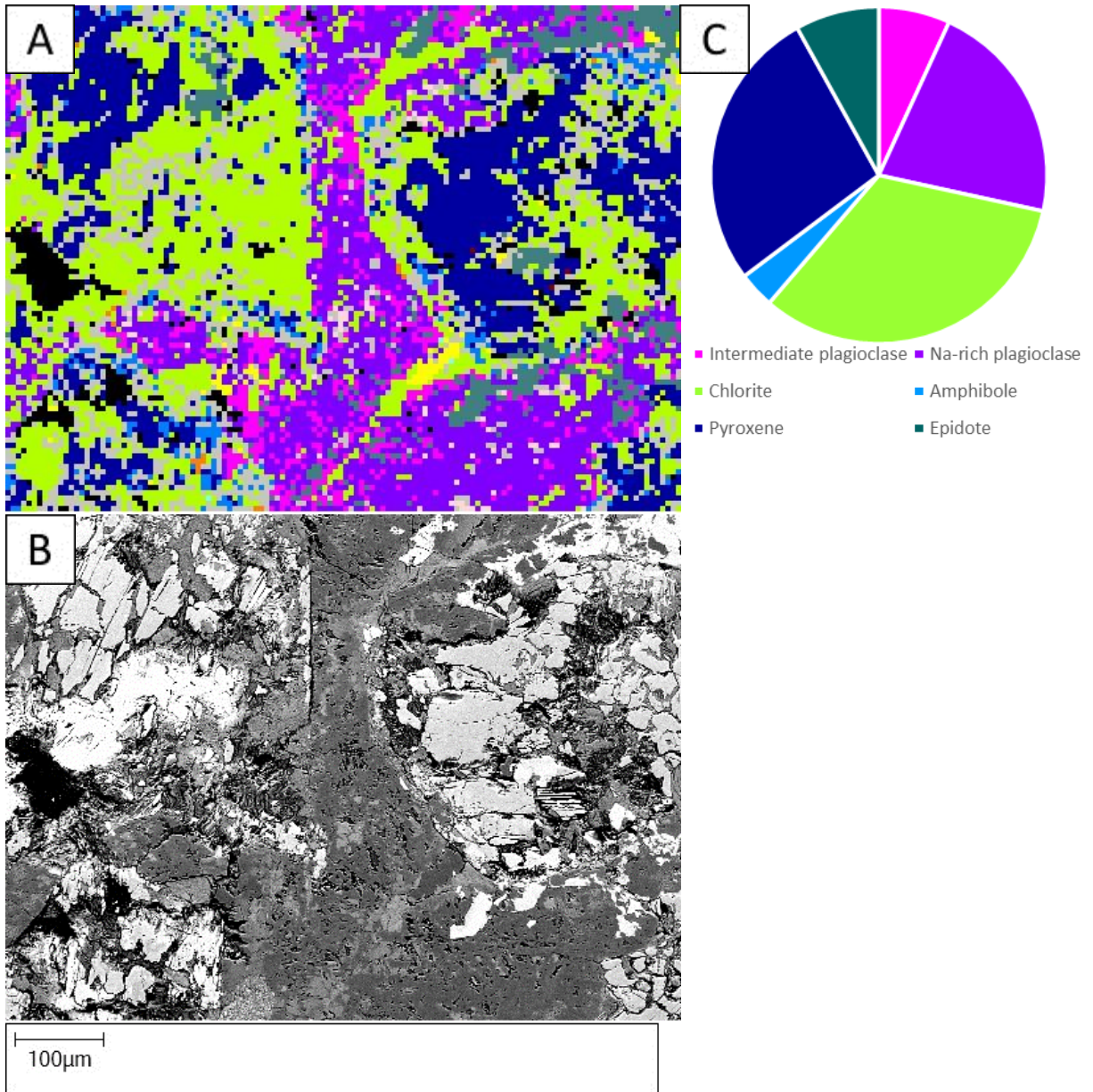
Figure 21 | AM and BSE maps and pie chart for sample B2.1h map 2.

B2.2

Two maps were made for this sample. This is the only sample where a potassium-containing mineral is found in quantities of more than 1%: 1.18% of the area of this map is orthoclase (Figure 22). Nearly all plagioclase is the Na-rich variety, only minor intermediate plagioclase can be found. This is a notable sample: neither pyroxene nor amphibole is detected; in locations where either would be expected, only chlorite is present instead (Figure 23). Relatively large patches of calcite are also present. Iron-oxides and titanite is often found in association with chlorite. Quartz is mainly anhedral with abundant porosity (vuggy appearance), and seemingly overprints or intergrows into chlorite and plagioclase.
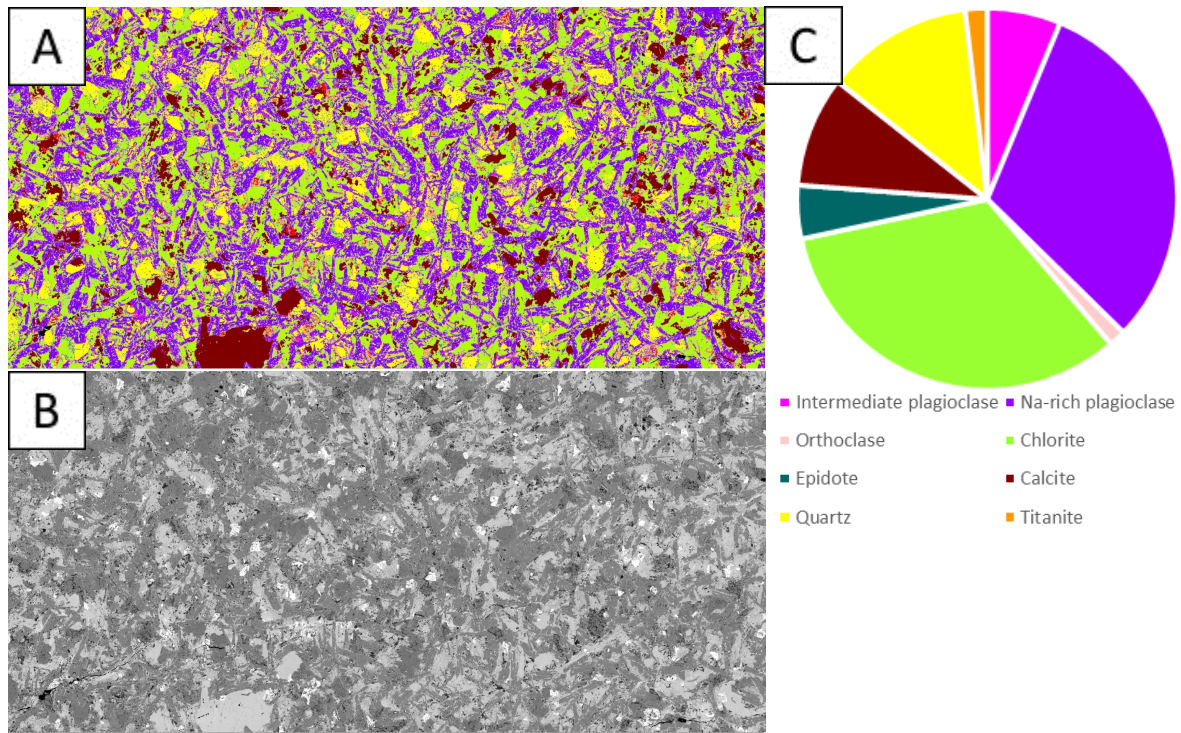
Figure 22 | AM and BSE maps and pie chart for sample B2.2 map 1.
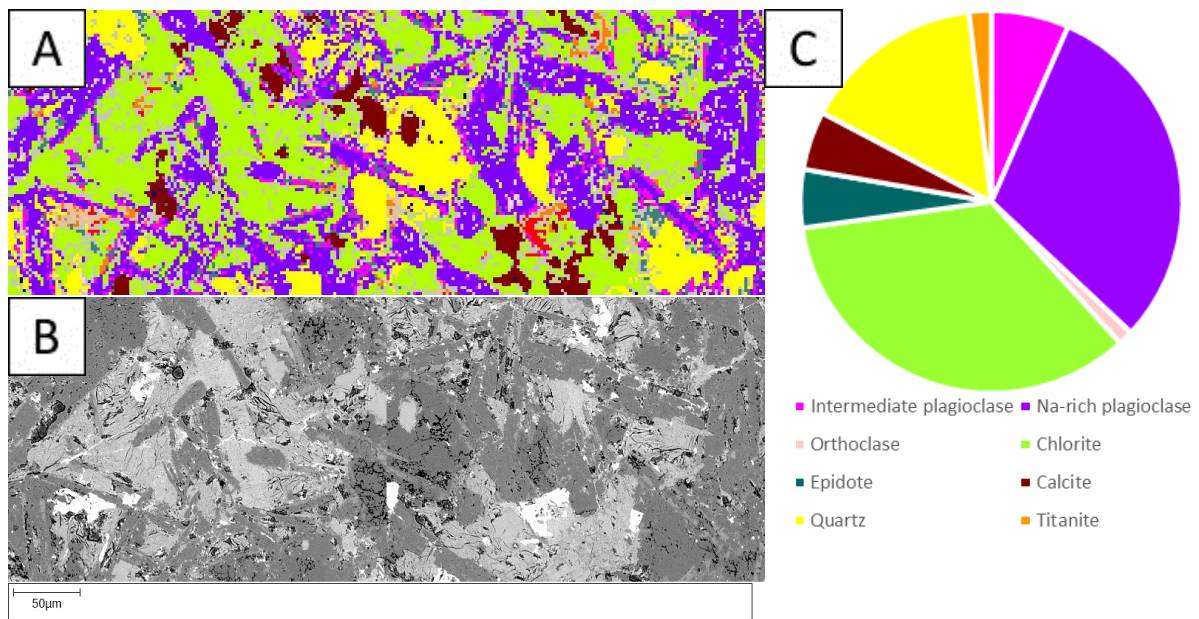
Figure 23 | AM and BSE maps and pie chart for sample B2.2 map 2.

C2.3f

One small map was made for this sample (Figure 24). Nearly all plagioclase has been altered to the Na-rich variety, while pyroxene is still observed with only minor alteration to amphibole. However, chlorite and epidote can be seen overgrowing pyroxene. Titanite and calcite are present in minor amounts, where titanite is associated with chlorite.
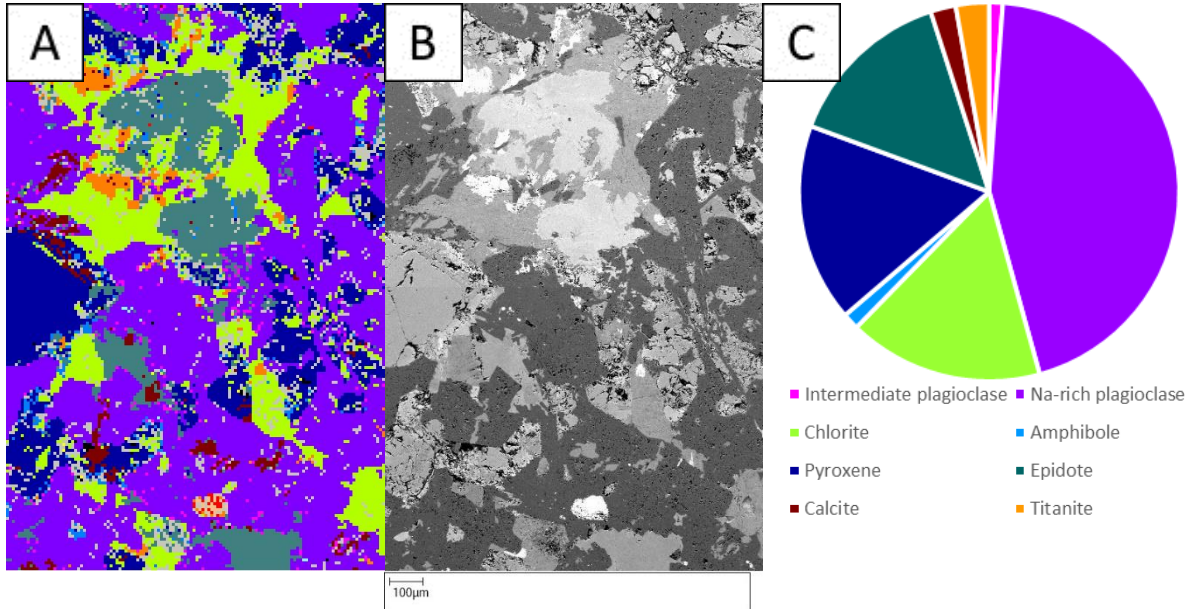

Figure 24 | AM and BSE maps and pie chart for sample C2.3f.

C2.3g

One small map was made for this sample (Figure 25). Nearly all plagioclase is replaced by Na-rich plagioclase. Pyroxene is replaced by amphibole, and subsequently by chlorite and epidote. A large quartz crystal is present, but it is unclear if this is a primary or secondary mineral.
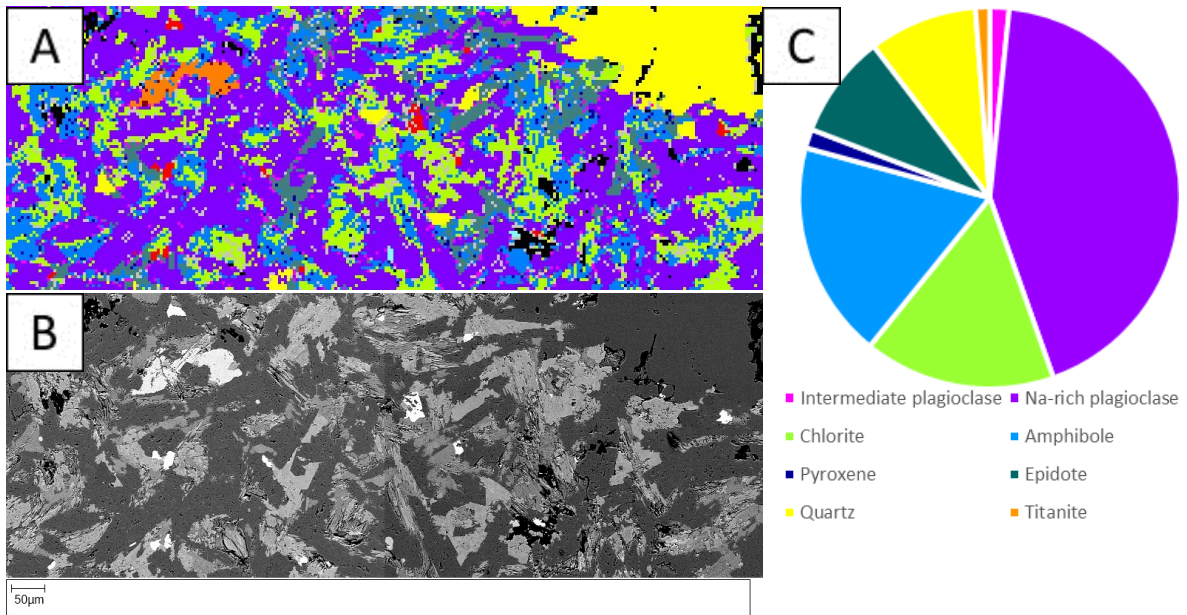
Figure 25 | AM and BSE maps and pie chart for sample C2.3g.

3.4 Processed results

3.4.1 Pyroxene plot

In five samples, SEM-EDS pyroxene spot measurements were obtained to determine the pyroxene composition. The averages per sample are visualized in Figure 26: three brown dike samples contained pyroxene, one early-stage grey dike and one plagiogranite. The number of spot measurements per sample is given in Table 2. The pyroxenes in the plagiogranite (sample C2.3c) are microscopically determined to be phenocrysts with an origin that is likely different from the rest of the rock.

The three corners of the plot represent the three end members for the possible pyroxene compositions: wollastonite, enstatite and ferrosilite. The placement of each sample on the diagram is based on its relative amounts of calcium, magnesium and iron. The samples plot slightly above the upper limit for diopside-hedenbergite (Figure 26), meaning that they are slightly more calcium rich than expected for pyroxenes.
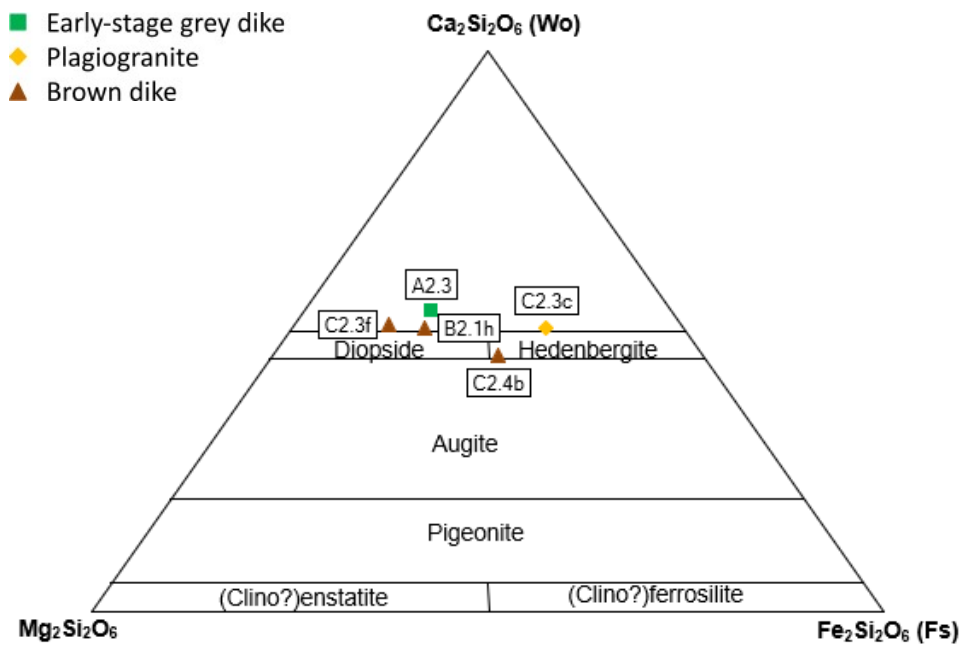

Figure 26 | Pyroxene composition plot (modified after Morimoto, 1988).

Table 2 | Number of spot measurements used to calculate average values per sample for Figure 26.

Sample name	Number of pyroxene spot measurements
A2.3	8
B2.1h	2
C2.3c	2
C2.3f	2
C2.4b	4

3.4.2 Amphibole plot

SEM-EDS spot measurements were collected for amphiboles in 10 samples (Figure 27). Placement on the diagram is based on the ratios of calcium, magnesium and iron in the sample. All amphiboles plot in the middle of the diagram in the actinolite field. The number of spot measurements per sample is given in Table 3.
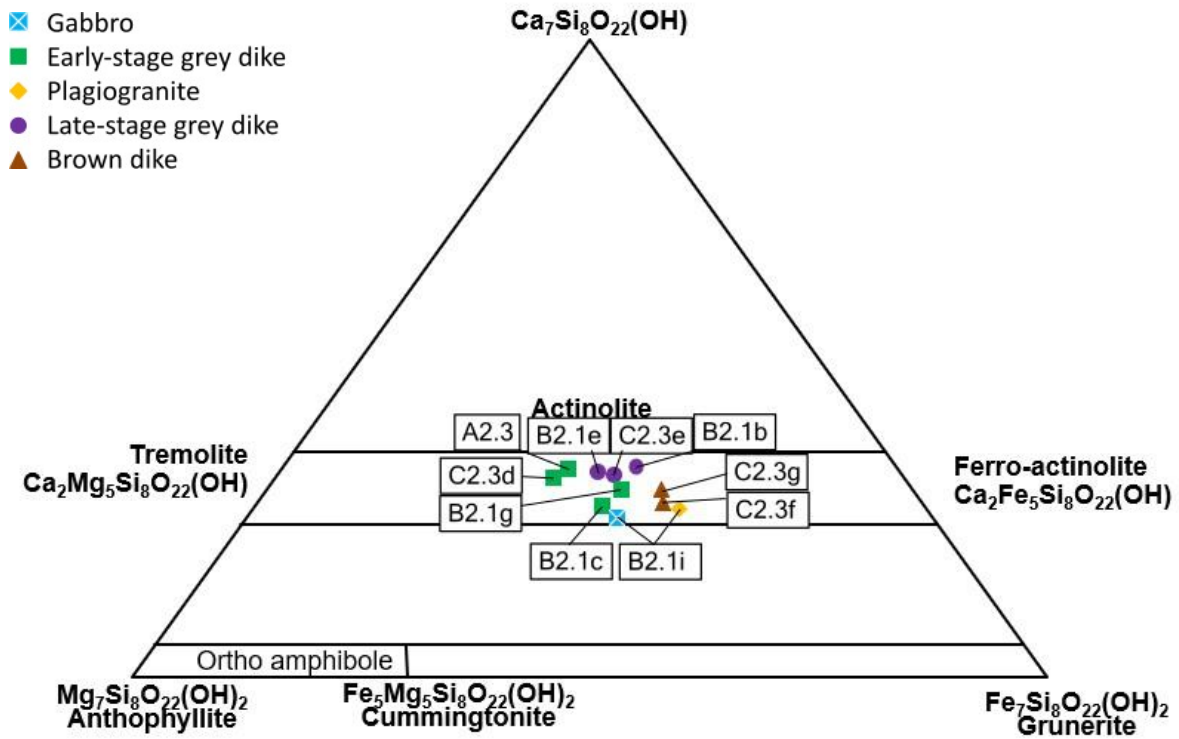

Figure 27 | Amphibole composition plot (modified after Morimoto, 1988).

Table 3 | Number of spot measurements used to calculate average values per sample for Figure 27.

Sample name	Number of amphibole spot measurements
A2.3	5
B2.1b	3
B2.1c	14
B2.1e	7
B2.1g	8
B2.1i (gabbro)	11
B2.1i (plagioclase)	4
C2.3b	3
C2.3d	8
C2.3f	1
C2.3g	2

3.4.3 Plagioclase plot

For all samples, the plagioclase feldspars were divided into three categories in the automated mineralogy analysis: Na-rich, intermediate and Ca-rich. For each sample, the average composition per category and per dike type (if present) is given below (Figure 28). Alteration towards a more Na-rich composition is visible by following the horizontal lines from right to left: if two measurements of the same dike type are on the same line, meaning they are from the same sample, this indicates the presence of multiple varieties of plagioclase in the sample. The BSE and AM maps (Section 3.3) show that the more Ca-rich plagioclases are replaced by more Na-rich varieties.
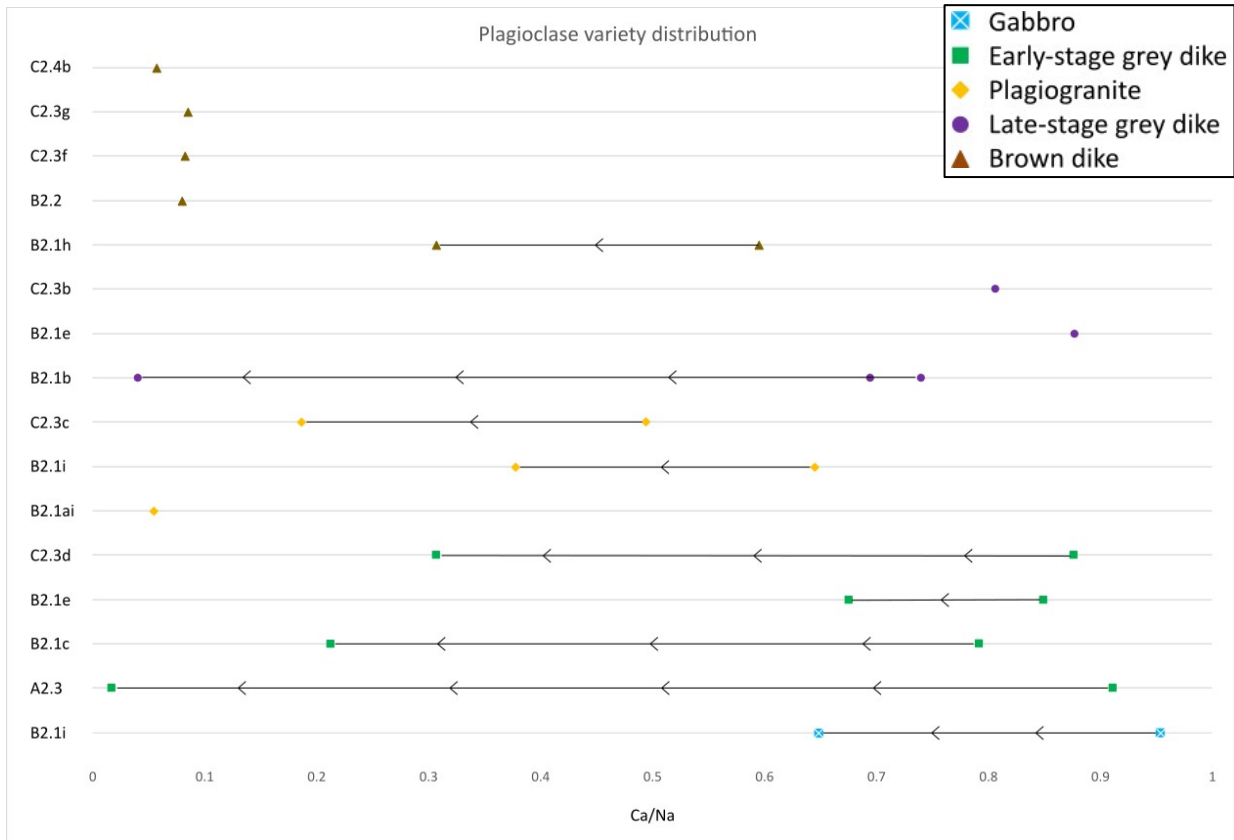
Figure 28 | Plagioclase variety distribution plot per sample. Alteration towards a more Na-rich composition is visible by following the horizontal lines.

3.4.4 SiO₂ content

The bulk rock SiO_2 content for all samples is given in these plots. If two maps were made for one sample, the bulk rock composition of the largest map was used. The SiO_2 content has been normalized to exclude calcite, which is not a phase of interest.

Two diagrams are constructed: one where all silica is included (Figure 29a), and one where quartz is excluded (Figure 29b) (see discussion). The measurements are ordered per dike type. This shows a general increase in SiO_2 content for progressively younger dike types.
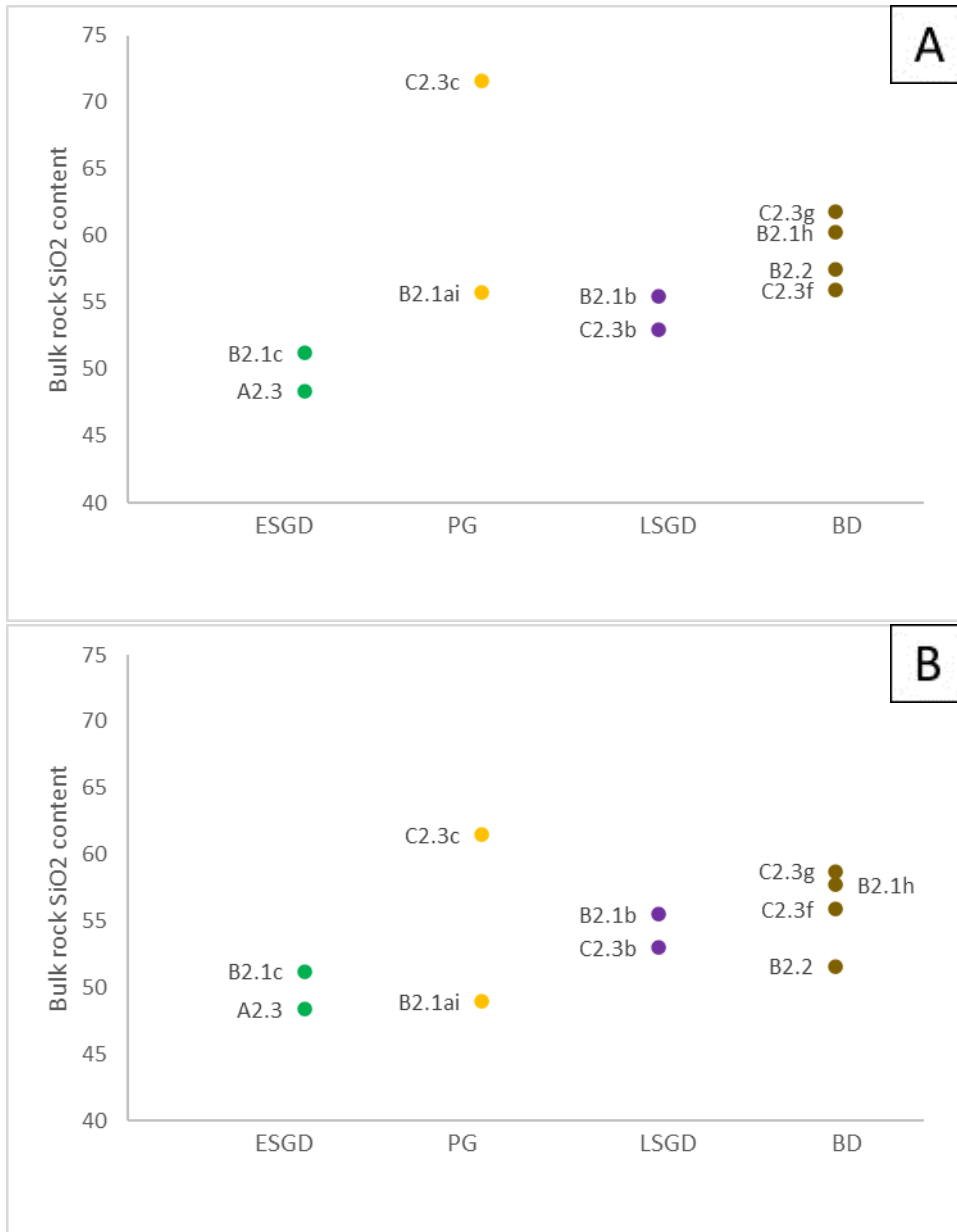
Figure 29 | Increase of bulk rock SiO_2 content through time (left is the oldest rock, right is most recent). a. Bulk rock SiO_2 content normalized to exclude calcite. b. Bulk rock SiO_2 content normalized to exclude both calcite and quartz.

4. Discussion

Types of alteration and alteration minerals are discussed in section 4.1. The pyroxene, amphibole and plagioclase diagrams presented in section 3.4 of results are discussed in section 4.2. In section 4.3, the implications of alteration are discussed in relation to the Arakapas Fault, to the variable degrees of alteration and to black smoker hydrothermal systems. Finally, an evolutionary overview of the Troodos intrusives is given in section 4.4.

For this section, it is important to note that the malfunctioning of the SEM caused multiple issues, affecting the reliability of the data. About half of the SEM maps could not be used due to too low spectrum counts, which in itself already meant that the amount of data would be meagre. Moreover, for all dike types one large map and one or more small maps were made, but for plagiogranite and early-stage grey dike the large maps were unusable. This negatively impacted the reliability of the available bulk rock data for these dike types as small maps were often focused on interesting features and were not representative of the whole sample. Lastly, none of the maps for gabbro were usable, making it impossible to include gabbro in this study. The ideas in the following section are thus based on the data that was available, and may need to be revised if more data becomes available.

4.1 Alteration minerals

The encountered mineral assemblage does not contain only primary minerals. In fact, a majority of the minerals are interpreted to be secondary: intermediate and Na-rich plagioclase, calcite, amphibole, epidote, chlorite, titanite and in some cases quartz. The remaining primary minerals are mainly Ca-rich plagioclase, pyroxene and possibly quartz.

The most commonly encountered minerals in the samples are the plagioclase varieties. They have been divided into three groups: Ca-rich plagioclase which includes bytownite and anorthite, intermediate plagioclase which includes andesine and labradorite and Na-rich plagioclase which includes albite and oligoclase. The BSE and AM maps show replacement of Ca-rich plagioclase by more Na-rich varieties. A clear example for this is sample B2.1c: the light pink colored mineral is more prominent in this sample, while the darker pink mineral is more prevalent at fractures and edges of the mineral. Fractures and edges of minerals act as fluid pathways and are often the first parts of a mineral to be altered, so this color change indicates alteration from a Ca-rich to a more Na-rich variety.

Plagioclase minerals can also alter to epidote (Figure 11). However, epidote is more often encountered as an alteration product of amphibole or pyroxene (Figure 25). It is also found in veins (Figure 16).

The chlorite group consists of multiple minerals and is used as the diagnostic mineral for the greenschist facies (Klein & Dutrow, 2007). It forms by alteration of mafic minerals, which are in this case likely to be pyroxenes and amphiboles. See for example Figure 23: the plagioclase minerals are surrounded by chlorite while in other samples the groundmass consists of plagioclase with pyroxene and/or secondary amphibole (Figure 16).

Titanite is often found within or bordering chlorite domain (Figure 24). This association with chlorite leads to the interpretation that titanite itself is also a secondary mineral.

Pyroxene is often observed to alter to amphibole in these rocks. See for example Figure 12, where the remnants of pyroxene (dark blue) are surrounded by amphibole (light blue). Alteration is mostly to actinolite and in some cases to other amphiboles.

Calcite forms by precipitation of calcium-rich water. Significant twinning would be expected when calcite undergoes metamorphism (Burkhard, 1993), which is not observed in the calcites in the thin sections under the optical microscope. It is thus interpreted that calcite is a late-stage mineral phase that post-dates most of the deformation in the area.

In the plagiogranite, quartz could either be interpreted as a primary or a secondary mineral. However, quartz is also found in brown dikes, where the vuggy anhedral nature and overprinting relations suggest a secondary origin. This leads to the interpretation that the presence of quartz is a result of later stage alteration, at least in the brown dikes. For the plagiogranite this is unclear: quartz can be partly or fully a primary mineral or fully a secondary mineral. Optical microscope and SEM data have not made this clear.

The dikes containing some combination of most of these minerals are classified as microgabbro with a greenschist facies mineral assemblage (Cann et al., 2012; Jowitt et al., 2012). Greenschist develops at temperatures between 300-450°C and pressures between 0.1 and 0.9 GPa (Bucher & Grapes, 2011a). Even though the name *greenschist* implies a certain level of schistosity, this is not the case in these rocks: many plated minerals, such as micas, contain kalium, which is (nearly) absent in these rocks. This means they cannot be classified as true greenschists, but they do have a greenschist facies mineral assemblage (Bucher & Grapes, 2011b). The exceptions that do not contain a majority of the minerals above are the plagiogranites: they contain only chlorite, epidote, quartz and plagioclase. The lack of mafic minerals clearly distinguishes the felsic plagiogranites from the other intrusive groups.

4.2 Trends in diagrams

4.2.1 Ca-Na trend

Both the amphibole and the pyroxene plot (Figure 26 and R23) are based on the relative amounts of calcium, magnesium and iron. When comparing the two, it becomes evident that the pyroxene samples are richer in calcium than the amphiboles. As amphibole is an alteration product of pyroxene, this means that alteration leads to less calcium in the system, showing a trend of decreasing calcium content for progressively younger dike types. Noticeably, there is more variation in composition for the pyroxenes than for the amphiboles, which cluster tightly in the actinolite field. This could indicate that all the amphiboles crystallized under similar conditions.

The same overall trend is observed in the plagioclase feldspars: alteration from Ca-rich varieties to Na-rich varieties can be seen in the SEM-EDS data (Section 3.3) and in Figure 28. This albitization occurs throughout most of the samples, however, there are some inconsistencies. Most alteration found in both pyroxene-amphibole and plagioclase starts from grain boundaries or fractures and progress inward. However, sample B2.2, sample B2.1h and sample B2.1b show a concentration of intermediate plagioclase along boundaries and fractures in Na-rich grains, indicating either alteration from Na-rich composition to less Na-rich composition or alteration from grain center to edges. This is the opposite from what is expected based on findings in the rest of the samples. The cause of this remains unknown and could be the subject of further research.

4.2.2 SiO2 trend

Calcite is excluded from calculations in the SiO_2 content graphs, as this is not a magmatic phase or part of the greenschist facies mineral assemblage (Figure 29). It likely originates from a more recent alteration phase and is thus irrelevant in providing information about the origin or alteration history of the rock. In Figure 29b, quartz has been removed from the calculations as well as calcite. As it is unknown whether quartz is a more recent alteration, both graphs are included in the results.

Both graphs show an overall increase in SiO_2 content through time. The plagiogranites are outliers in this trend: Figure 29a (including quartz) shows both samples as higher than expected and for Figure 29b (excluding quartz), still one of the two values (sample C2.3c) is higher. However, a shared source for the felsic and mafic dikes should not be assumed, as plagiogranite formed after fractional crystallization of mafic magma. Previous work shows SiO_2 values for plagiogranite of up to 73%, which is in agreement with the values found here (Veit, 1996).

Without the plagiogranite, the increasing SiO2 trend becomes more evident. Combined with the fractional crystallization as cause for the plagiogranite formation, this leads to an interpretation of fractional crystallization throughout the magma source, with plagiogranite at the top. This corresponds to field observations: plagiogranite bodies are found on the boundary between gabbro bodies and sheeted dikes. Crystallization of more mafic magma and precipitation at the bottom of the magma chamber leads to a more SiO_2-rich magmatic composition over time. This is in agreement with the increasing SiO_2 trend seen in the mafic dikes of the ophiolite.

4.3 Implications of alteration

4.3.1 Alteration versus distance to the Arakapas Fault

The division in primary and secondary minerals (section 4.1) is an efficient way to visualize the alteration in these rocks. The relationship between alteration and distance from the transform fault per dike type is shown in Figure 30. An increase in mineral alteration close to the transform fault should be observed if the fault influenced the alteration process of the area. This scenario would be expected based on the simultaneous activity of the transform fault and formation of the ophiolite. However, a correlation between distance and alteration cannot be determined based on this figure.

A more convincing figure would include data for plagiogranite and late-stage grey dike alteration at 0-0.5 km distance from the transform fault; unfortunately this data is unavailable due to the aforementioned issues with the SEM. Based on the available data there is no correlation between intensity of alteration and distance to fault: early-stage grey dikes show a slight decrease in primary minerals with increasing distance, which is contrary to the expected trend in case of influence of the fault. Brown dikes do show a slight increase in primary minerals with increasing distance. Furthermore, no correlation is found between amount and type of veining versus distance to fault.
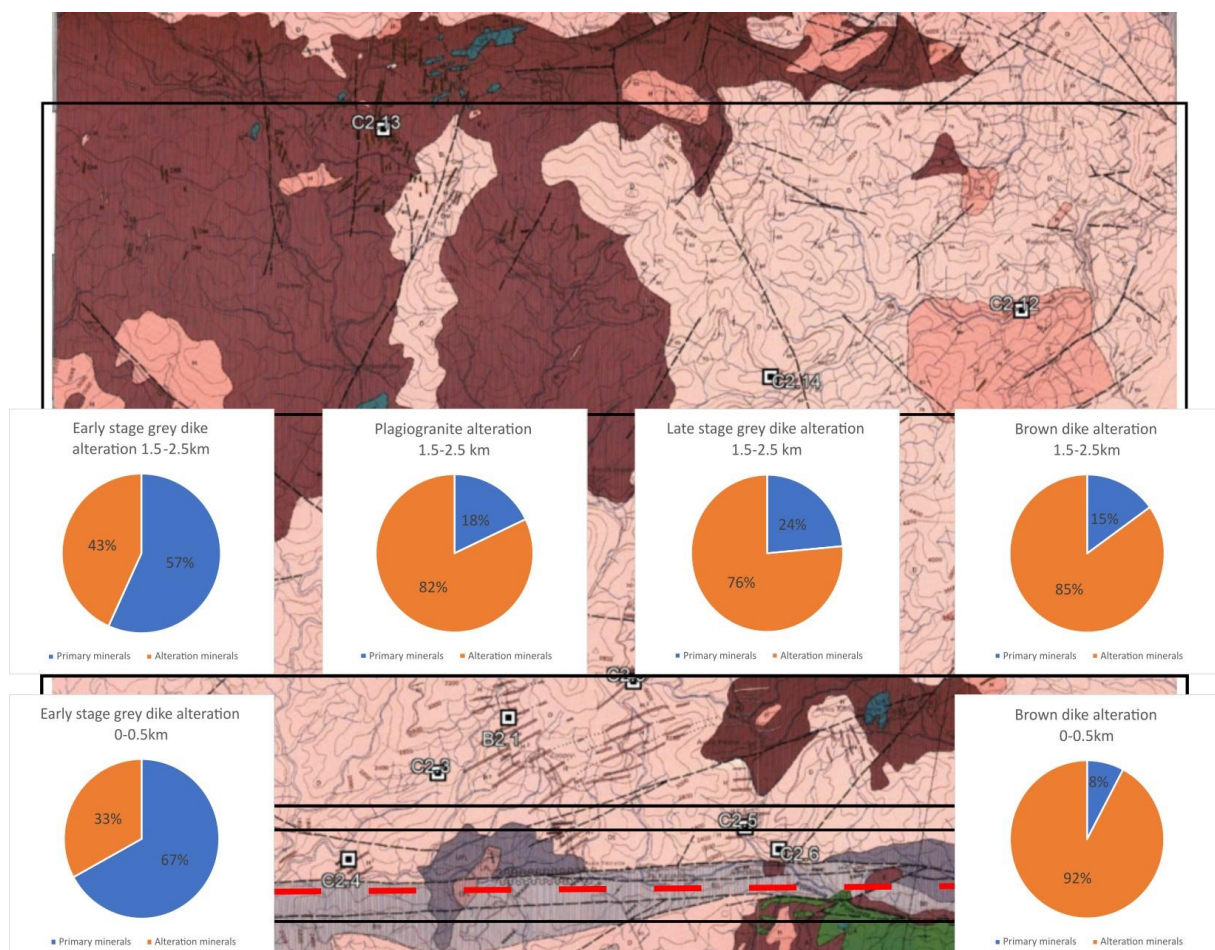
Figure 30 | Map view of pie charts based on average data per dike type per distance to fault. Figure shows the average amount of alteration per dike type relative to the distance to the fault. No data was available for the plagiogranite and late-stage grey dike alterations at 0-0.5 km from the fault (modified after Bear & Morel, 1960).

4.3.2 Alteration diversity between dike types

Next, all data per dike type is combined without regard to the distance from the Arakapas Fault. If alteration happened after formation of the complete intrusive sequence, the most obvious result would be an equal amount of alteration regionally in all dike types. If the alteration process happened continuously during formation, the oldest dikes would be more altered than the youngest dikes, as they had more time in the altering environment. However, in these data a remarkable trend is observed, as can be seen in Figure 31. Younger dikes and intrusions have a progressively higher degree of alteration compared to older dike sets, with the exception of plagiogranite.

Note that for the graphs in Figure 31 it is assumed that the most Ca-rich plagioclase that is present is the primary plagioclase phase. In this case, this means that it is assumed that the plagiogranite and brown dikes have crystallized from a more Na-rich magma (with intermediate plagioclase as primary plagioclase phase) than the early and late-stage grey dikes (with Ca-rich plagioclase as primary plagioclase phase). The plagioclase has a different, felsic source than the other, mafic rocks. It is consistent with this finding that the source magma contains more sodium. For the brown dikes this is possible if the magma matures and becomes more Na-rich over time, causing the primary plagioclase to become the intermediate variety instead of the Ca-rich variety.
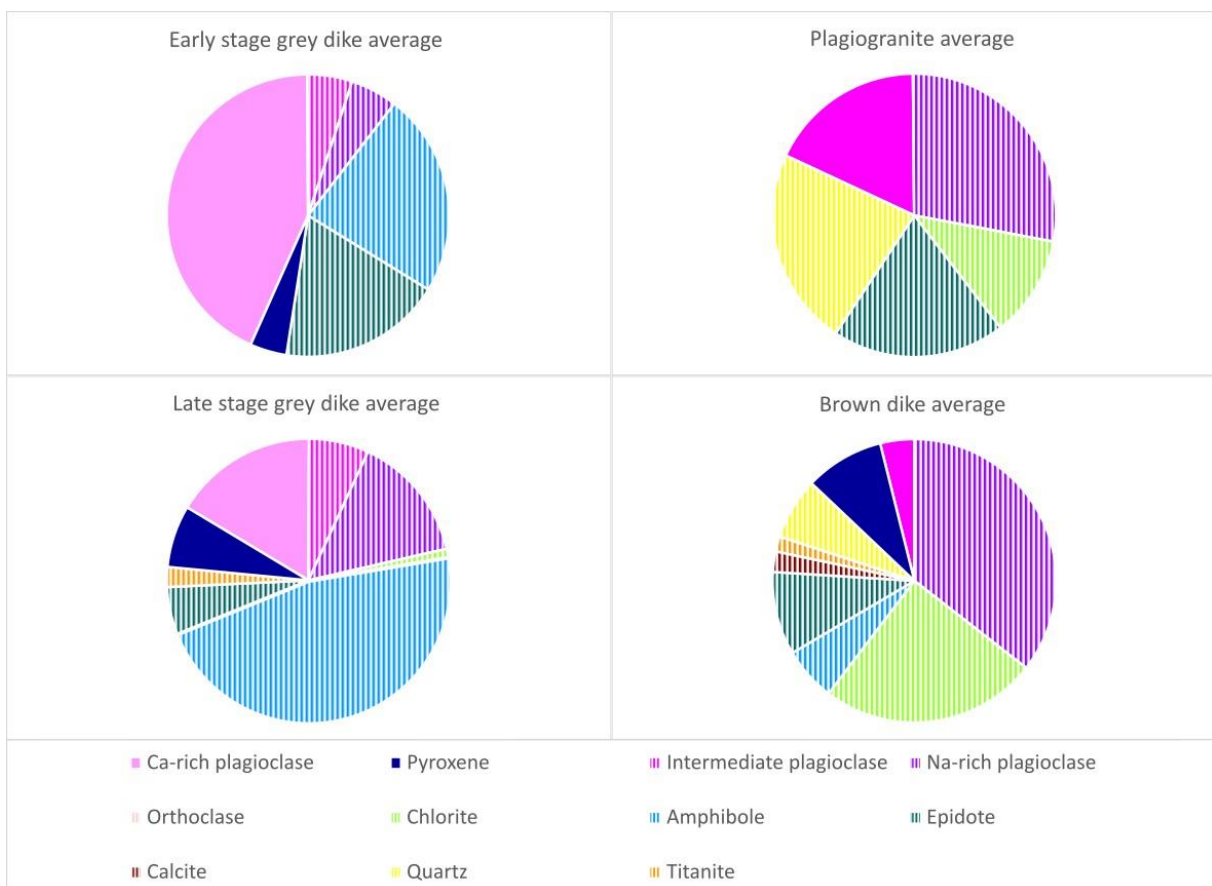
Figure 31 | Average compositions of the dike types with opaque colors indicating primary minerals and striped colors indicating secondary (alteration) minerals.

However, another possibility could be that alteration happened in multiple phases. This would mean that in the cases of plagiogranite and brown dikes the intermediate plagioclase is already a secondary (alteration) mineral. In this case, the primary, Ca-rich plagioclase that crystallized directly from the magma is fully altered into the intermediate plagioclase; no trace of it is left. This would change the pie charts in Figure 32: plagiogranite then fully consists of secondary minerals and the brown dike type has only a small primary fraction of pyroxene left. In this case, the overall trend would not change drastically; it would only be amplified. As the overall trend does not change and thin section and SEM data do not indicate multiple phase alteration, the assumption of one alteration event (as described above) is made.

The difference in composition of these dikes could be a possible explanation for the variety in degree of alteration. The examples above would be most logical for dike sets with similar compositions and structures, but that is not the case in this intrusive set. The composition of plagiogranite is very distinctly different from the greenschist mineral assemblage dike types, as noted above. The brown dikes also somewhat differ in composition from the early and late-stage grey dikes (Figure 31), and besides this, field observations are relevant here: the rocks were so fragile in outcrops that it was often hardly possible to take coherent samples. This may indicate a higher porosity and permeability in brown dikes. These differences open up possible explanations for the differences in degree of alteration: a higher permeability may give way to more fluids, enabling alteration to increase; another option is that the primary minerals in brown dikes and plagiogranites are more susceptible to alteration than the ones in the early and late-stage grey dikes.

4.3.3 Black smoker hydrothermal systems

A potential mechanism for increased permeability in dikes can be found in the activity of black smoker hydrothermal systems (Cann et al., 2012). These are heat-driven systems in which fluids derived from magma and seawater circulate. The rocks in which the circulation takes place can react with the fluids, causing an exchange in components between the two. The fluids finally create massive sulfide deposits (Colín-García, 2016).

Cann et al. (2012) argue that black smoker activity has greatly increased porosity and permeability in some Troodos dikes. The black smoker fluid caused primary dike minerals to dissolute, creating free pore space. The progression of this process led to increased permeability throughout dikes. The created porosity was later filled with the precipitation of new, secondary minerals. It is noted that this did not happen equally throughout all rocks, but instead within one dike at a time. The process created 'stripes' of epidosite, a rock type consisting of primarily epidote and quartz, with less altered rocks in between these stripes (Cann et al., 2012). Epidosites are often found near the boundary between dikes and gabbro and less often in typical, stratigraphically higher diabase dike regions (Jowitt et al., 2012). This implies that black smoker activity also primarily occurred in that region, and not throughout all dikes. Additionally, the mineral assemblage found in the samples of this study mostly corresponds well with the greenschist facies mineral assemblage, and not with the epidosite mineral assemblage.

However, this does not indicate that this mechanism is fully inadequate here. Not all encountered alteration can be explained by greenschist grade metamorphism. For instance, the potassium depletion is counter-indicative for greenschist facies, as it generally contains platy minerals such as micas, which contain K (Bucher & Grapes, 2011b). This suggests that some black smoker influence is likely: both K and Ca depletion in the dikes is balanced out by their enrichment in the massive sulfide deposits on Cyprus, indicating fluid transport of these elements through black smoker activity (Herzig, 1988). Moreover, even on small (cm) scale the degree of alteration to epidosite is very variable (Cann

et al., 2012). In outcrops, green veins were present and in some areas alteration to green minerals throughout the rock was evident. This is likely to be epidotization. As for this study the objective was to collect samples with as little alteration as possible, it is plausible that there was a sample bias to exclude epidosites, which explains why they are not represented in this study. To verify that these green veins and alteration is indeed epidosite and establish the influence of black smokers on rocks throughout the ophiolite, more research on these green-colored minerals is necessary.

The timing of this black smoker activity is uncertain. The alteration of the lastly intruded dike phase, the brown dikes, demonstrates that hydrothermal activity happened either after complete formation of the dike sequence, or both during and after the formation. As black smoker hydrothermal systems rely on magmatic activity for heat and fluids, it is unlikely that alteration happened long after formation of the intrusions. This constrains the time period of hydrothermal activity.

4.4 Evolutionary overview of the Troodos intrusives

To give a clear overview of the intrusive history of the Troodos ophiolite mid-crustal sequence as found in this study, five steps are required (Figure 32). The geological setting during formation of the intrusives of the Troodos ophiolite is as follows: extensional forces caused by subduction rollback create tension in the overriding plate of a subduction zone, while dehydration of the downgoing plate causes melting of the mantle, which generates SSZ magma.

Firstly, extension in the upper plate creates a spreading ridge where early-stage grey dikes rise. They are fed by the mafic magma source underneath, which currently appear as gabbro bodies. Secondly, fractional crystallization of the mafic magma body produces felsic bodies and dikes: the plagiogranites. The dikes cut through the early-stage grey dikes and are never cut by them, implicating that the plagiogranite dikes formed after all early-stage grey dike activity. However, the mixing pattern of plagiogranite and early-stage grey dike (Figure 8) suggests that both were liquid simultaneously; this leads to the conclusion that the activity of the plagiogranite must have immediately followed the early-stage grey dike formation and overlapped in some cases. Thirdly, the late-stage grey dikes intrude. They cut through early-stage grey dikes and both plagiogranite bodies and dikes. They are also observed to cut through gabbro, indicating that their magma source is deeper than the early-stage grey dike source. After this, post-dating all other intrusions, the brown dikes appeared. They cut through all other body and dike types while often going in a different direction than most sheeted dikes. This makes it seem like they follow pre-existing fractures, as their shapes are generally very angular and the direction diverges from usual. The final step is alteration through hydrothermal activity, although the timing is unsure: overlap with one or more previous steps is possible.
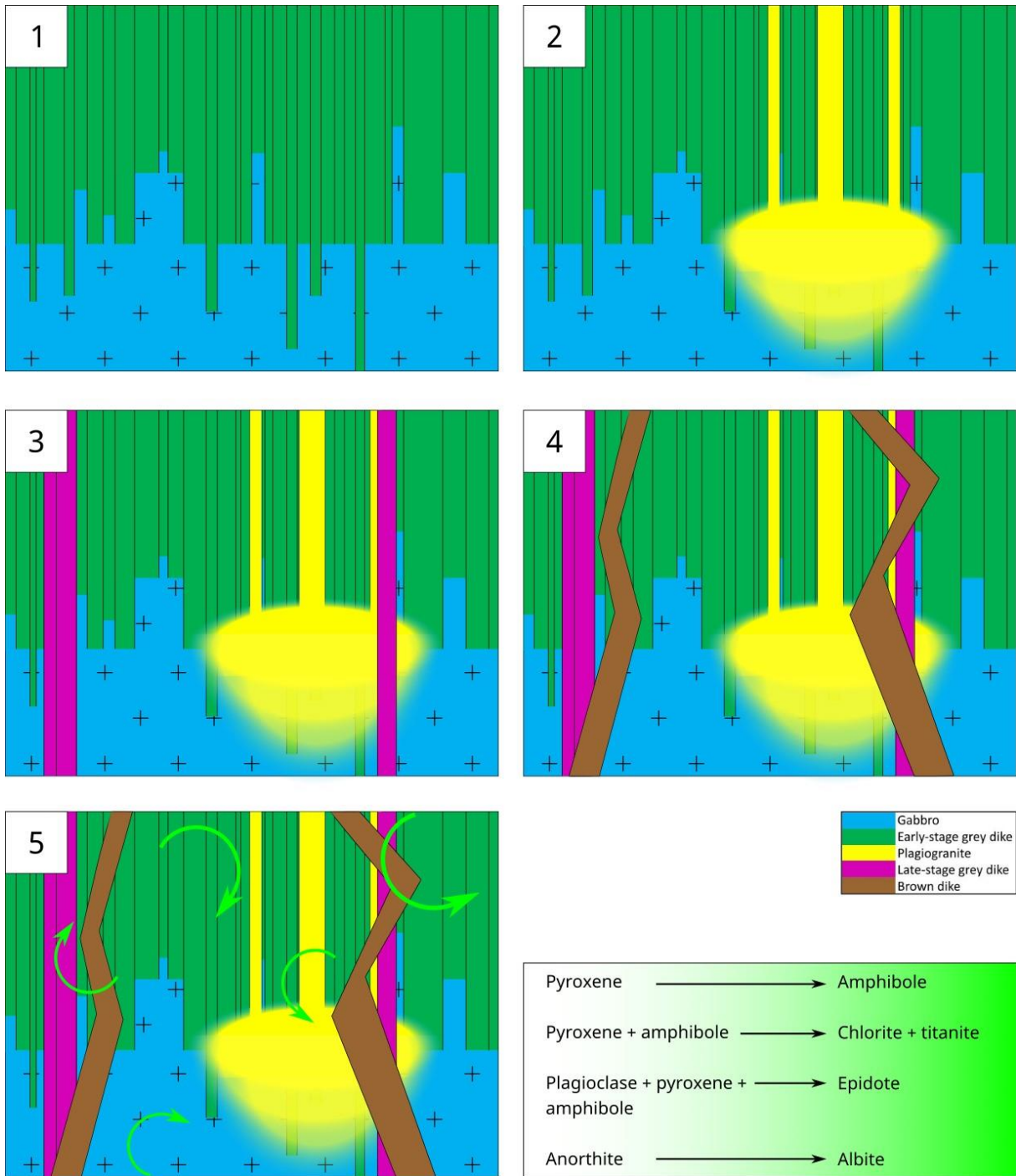
Figure 32 | Evolutionary overview of the intrusion complex of the Troodos ophiolite.

5. Conclusions

1. The Troodos ophiolite dikes can be subdivided into four distinct groups. The early and late-stage grey dike and brown dike types present a (near) greenschist facies mineral assemblage. The fourth group belongs to the plagiogranite classification.

2. Investigation into the minerals of the dikes showed two clear alteration trends in the geochemistry with time:

   i. A decrease in calcium, substituted by an increase in sodium. This presents as alteration from pyroxene to amphibole and from Ca-rich plagioclase to Na-rich plagioclase;

   ii. An increase in SiO_2-content.

3. Additionally, alteration was studied on a larger scale. The relationship between degree of alteration per dike type and distance from the Arakapas Transform Fault was presented. No correlation was found.

4. The degree of alteration between dike types was variable. This may be caused by compositional differences between the groups leading to variation in permeability or primary mineral susceptibility to alteration. The degree of alteration showed an apparent increase with time, which is interpreted to be coincidental. Future research could focus on identifying the cause of variable alteration.

5. Black smoker hydrothermal systems are a potential mechanism to induce an increase in permeability and explain depletion of certain elements in the Troodos ophiolite. Previous work indicates that not the entire dike complex is affected by these hydrothermal systems, potentially excluding (part of) the dikes in this study. Previous work also states that greenschists are altered to epidosites in affected areas, while true epidosites are not found in this study. However, sampling bias towards fresh rocks presumably excluded epidosites from this study. Moreover, the studied samples show indications of hydrothermal activity, such as a depletion in potassium and calcium. More research on veins and alteration in our outcrops is necessary to verify the influence of hydrothermal systems on the selected dikes.

6. Finally, the evolutionary overview shows the Troodos intrusive history in five steps.

   i. In a supra-subduction zone setting, early-stage grey dikes rise in a spreading ridge on the overriding plate from a mafic source.

   ii. Fractional crystallization of the mafic source produces plagiogranitic bodies and dikes, partly temporally overlapping with the gabbro and early-stage grey dike activity.

   iii. Late-stage grey dikes intrude.

   iv. Brown dikes intrude often at a different angle than most sheeted dikes, postdating all other dike types.

   v. Hydrothermal alteration changes the composition of the dikes. Black smoker activity is linked to magmatic activity, indicating that the timing of alteration likely (partly) overlaps with the formation of the ophiolite dikes.

References

Anastasakis, G., & Kelling, G. (1991). Tectonic connection of the Hellenic and Cyprus arcs and related geotectonic elements. *Marine Geology*, *97*(3), 261–277. https://doi.org/10.1016/0025-3227(91)90120-S

Bear, L. M., & Morel, S. W. (1960). *Geological map of the Agros-Apsiou area* (p. 1 map : color; 56 x 46 cm.) [Map]. Geological Survey Department Cyprus.

Bucher, K., & Grapes, R. (2011a). Metamorphic Grade. In K. Bucher & R. Grapes (Eds.), *Petrogenesis of Metamorphic Rocks* (pp. 119–187). Springer. https://doi.org/10.1007/978-3-540-74169-5_4

Bucher, K., & Grapes, R. (2011b). Metamorphism of Mafic Rocks. In K. Bucher & R. Grapes (Eds.), *Petrogenesis of Metamorphic Rocks* (pp. 339–393). Springer. https://doi.org/10.1007/978-3-540-74169-5_9

Burkhard, M. (1993). Calcite twins, their geometry, appearance and significance as stress-strain markers and indicators of tectonic regime: A review. *Journal of Structural Geology*, *15*(3), 351–368. https://doi.org/10.1016/0191-8141(93)90132-T

Cann, J. R., Mccaig, A. M., & Yardley, B. W. D. (2012). Rapid generation of reaction permeability in the roots of black smoker systems, Troodos ophiolite, Cyprus. In *Crustal Permeability* (pp. 193–205). John Wiley & Sons, Ltd. https://doi.org/10.1002/9781119166573.ch17

Colín-García, M. (2016). Hydrothermal vents and prebiotic chemistry: A review. *Boletín de La Sociedad Geológica Mexicana*, *68*(3), 599–620. https://doi.org/10.18268/BSGM2016v68n3a13

Cooke, A. J., Masson, L. P., & Robertson, A. H. F. (2014). Construction of a sheeted dyke complex: Evidence from the northern margin of the Troodos ophiolite and its southern margin adjacent to the Arakapas fault zone. *Ofioliti*, *39*(1), Article 1. https://doi.org/10.4454/ofioliti.v39i1.426

Dilek, Y. (2003). Ophiolite concept and its evolution. In Y. Dilek & S. Newcomb, *Ophiolite concept and the evolution of geological thought* (pp. 1–16). Geological Society of America Special Paper 373. https://doi.org/10.1130/0-8137-2373-6.1

Evans, A. D., Teagle, D. A. H., Craw, D., Henstock, T. J., & Falcon-Suarez, I. H. (2021). Uplift and Exposure of Serpentinized Massifs: Modeling Differential Serpentinite Diapirism and Exhumation of the Troodos Mantle Sequence, Cyprus. *Journal of Geophysical Research: Solid Earth*, *126*(6), e2020JB021079. https://doi.org/10.1029/2020JB021079

Freund, S., Haase, K. M., Keith, M., Beier, C., & Garbe-Schönberg, D. (2014). Constraints on the formation of geochemically variable plagiogranite intrusions in the Troodos Ophiolite, Cyprus. *Contributions to Mineralogy and Petrology*, *167*(2), 978. https://doi.org/10.1007/s00410-014-0978-6

Gass, I. G. (1968). Is the Troodos Massif of Cyprus a Fragment of Mesozoic Ocean Floor? *Nature*, *220*(5162), Article 5162. https://doi.org/10.1038/220039a0

Goldstein, J. I., Newbury, D. E., Michael, J. R., Ritchie, N. W. M., Scott, J. H. J., & Joy, D. C. (2018). *Scanning Electron Microscopy and X-Ray Microanalysis*. Springer. https://doi.org/10.1007/978-1-4939-6676-9

Herrington, R. J., & Brown, D. (2011). The Generation and Preservation of Mineral Deposits in Arc–Continent Collision Environments. In D. Brown & P. D. Ryan (Eds.), *Arc-Continent Collision* (pp. 145–159). Springer. https://doi.org/10.1007/978-3-540-88558-0_6

Herzig, P. M. (1988). A Mineralogical, Geochemical and Thermal Profile Through the Agrokipia "B" Hydrothermal Sulfide Deposit, Troodos Ophiolite Complex, Cyprus. In G. H. Friedrich & P. M. Herzig (Eds.), *Base Metal Sulfide Deposits in Sedimentary and Volcanic Environments* (pp. 182–215). Springer Berlin Heidelberg. https://doi.org/10.1007/978-3-662-02538-3_12

Hynes, A. (1975). Comment on "the troodos ophiolitic complex was probably formed in an island arc", by A. Miyashiro. *Earth and Planetary Science Letters*, *25*(2), 213–216. https://doi.org/10.1016/0012-821X(75)90198-3

Jowitt, S. M., Jenkin, G. R. T., Coogan, L. A., & Naden, J. (2012). Quantifying the release of base metals from source rocks for volcanogenic massive sulfide deposits: Effects of protolith composition and alteration mineralogy. *Journal of Geochemical Exploration*, *118*, 47–59. https://doi.org/10.1016/j.gexplo.2012.04.005

Klein, C., & Dutrow, B. (2007). *Manual of Mineral Science*. John Wiley & Sons.

Malpas, J., Xenophontos, C., & Williams, D. (1992). The Ayia Varvara Formation of SW Cyprus: A product of complex collisional tectonics. *Tectonophysics*, *212*(3–4), 193–211. https://doi.org/10.1016/0040-1951(92)90291-D

Marien, C. S., Hoffmann, J. E., Garbe-Schönberg, C.-D., & Münker, C. (2019). Petrogenesis of plagiogranites from the Troodos Ophiolite Complex, Cyprus. *Contributions to Mineralogy and Petrology*, *174*(4), 35. https://doi.org/10.1007/s00410-019-1569-3

McClain, J. S. (2003). Ophiolites and the interpretation of marine geophysical data: How well does the ophiolite model work for the Pacific Ocean crust? In Y. Dilek & S. Newcomb, *Ophiolite concept and the evolution of geological thought* (pp. 173–185). Geological Society of America Special Paper 373.

McPhee, P. J., & van Hinsbergen, D. J. J. (2019). Tectonic reconstruction of Cyprus reveals Late Miocene continental collision of Africa and Anatolia. *Gondwana Research*, *68*, 158–173. https://doi.org/10.1016/j.gr.2018.10.015

Miyashiro, A. (1973). The Troodos ophiolitic complex was probably formed in an island arc. *Earth and Planetary Science Letters*, *19*(2), 218–224. https://doi.org/10.1016/0012-821X(73)90118-0

Miyashiro, A. (1975). Origin of the troodos and other ophiolites: A reply to hynes. *Earth and Planetary Science Letters*, *25*(2), 217–222. https://doi.org/10.1016/0012-821X(75)90199-5

Moores, E. M. (1982). Origin and Emplacement of Ophiolites. *Reviews of Geophysics*, *20*(4), 735–760. https://doi.org/10.1029/RG020i004p00735

Moores, E. M., Robinson, P. T., Malpas, J., & Xenophontos, C. (1984). Model for the origin of the Troodos massif, Cyprus, and other mideast ophiolites. *Geology*, *12*(8), 500–503. https://doi.org/10.1130/0091-7613(1984)12<500:MFTOOT>2.0.CO;2

Moores, E. M., & Vine, F. J. (1971). The Troodos Massif, Cyprus and other Ophiolites as Oceanic Crust: Evaluation and Implications. *Philosophical Transactions of the Royal Society of London. Series A, Mathematical and Physical Sciences*, *268*(1192), 443–467.

Morag, N., Haviv, I., & Katzir, Y. (2016). From ocean depths to mountain tops: Uplift of the Troodos ophiolite (Cyprus) constrained by low-temperature thermochronology and geomorphic analysis. *Tectonics*, *35*(3), 622–637. https://doi.org/10.1002/2015TC004069

Morimoto, N. (1988). Nomenclature of Pyroxenes. *Mineralogy and Petrology*, *39*(1), 55–76. https://doi.org/10.1007/BF01226262

Morris, A., Creer, K. M., & Robertson, A. H. F. (1990). Palaeomagnetic evidence for clockwise rotations related to dextral shear along the Southern Troodos Transform Fault, Cyprus. *Earth and Planetary Science Letters*, *99*(3), 250–262. https://doi.org/10.1016/0012-821X(90)90114-D

Morris, A., & Maffione, M. (2016). Is the Troodos ophiolite (Cyprus) a complete, transform fault–bounded Neotethyan ridge segment? *Geology*, *44*(3), 199–202. https://doi.org/10.1130/G37529.1

Mukasa, S., & Ludden, J. (1987). Uranium-lead isotopic ages of plagiogranites from the Troodos ophiolite, Cyprus, and their tectonic significance. *Geology*, *15*. https://doi.org/10.1130/0091-7613(1987)15<825:UIAOPF>2.0.CO;2

Niu, Y., & Batiza, R. (1993). Chemical variation trends at fast and slow spreading mid-ocean ridges. *Journal of Geophysical Research: Solid Earth*, *98*(B5), 7887–7902. https://doi.org/10.1029/93JB00149

Osozawa, S., Shinjo, R., Lo, C.-H., Jahn, B., Hoang, N., Sasaki, M., Ishikawa, K., Kano, H., Hoshi, H., Xenophontos, C., & Wakabayashi, J. (2012). Geochemistry and geochronology of the Troodos ophiolite: An SSZ ophiolite generated by subduction initiation and an extended episode of ridge subduction? *Lithosphere*, *4*(6), 497–510. https://doi.org/10.1130/L205.1

Pearce, J. A., Lippard, S. J., & Roberts, S. (1984). Characteristics and tectonic significance of supra-subduction zone ophiolites. *Geological Society, London, Special Publications*, *16*(1), 77–94. https://doi.org/10.1144/GSL.SP.1984.016.01.06

Purdy, G. M., Kong, L. S. L., Christeson, G. L., & Solomon, S. C. (1992). Relationship between spreading rate and the seismic structure of mid-ocean ridges. *Nature*, *355*(6363), Article 6363. https://doi.org/10.1038/355815a0

Ring, U., & Pantazides, H. (2019). The Uplift of the Troodos Massif, Cyprus. *Tectonics*, *38*(8), 3124–3139. https://doi.org/10.1029/2019TC005514

Robertson, A. H. F., & Woodcock, N. H. (1986). The role of the Kyrenia Range Lineament, Cyprus, in the geological evolution of the eastern Mediterranean area. *Philosophical Transactions of the Royal Society of London. Series A, Mathematical and Physical Sciences*, *317*(1539), 141–177. https://doi.org/10.1098/rsta.1986.0030

Robinson, P. T., Malpas, J., Dilek, Y., & Zhou, M. (2008). The significance of sheeted dike complexes in ophiolites. *GSA Today*, *18*(11), 4. https://doi.org/10.1130/GSATG22A.1

Searle, M., & Cox, J. (1999). Tectonic setting, origin, and obduction of the Oman ophiolite. *GSA Bulletin*, *111*(1), 104–122. https://doi.org/10.1130/0016-7606(1999)111<0104:TSOAOO>2.3.CO;2

Small, C. (1994). A global analysis of mid-ocean ridge axial topography. *Geophysical Journal International*, *116*(1), 64–84. https://doi.org/10.1111/j.1365-246X.1994.tb02128.x

Varga, R. J. (2003). The sheeted dike complex of the Troodos ophiolite and its role in understanding mid-ocean ridge processes. In Y. Dilek & S. Newcomb, *Ophiolite concept and the evolution of geological thought* (pp. 323–336). Geological Society of America Special Paper 373.

Varga, R. J., & Moores, E. M. (1985). Spreading structure of the Troodos ophiolite, Cyprus. *Geology*, *13*(12), 846–850. https://doi.org/10.1130/0091-7613(1985)13<846:SSOTTO>2.0.CO;2

Veit, K. M. (1996). Petrological investigation of the sheeted dike zone of the Troodos Ophiolite, Cyprus. *Keck Research Symposium in Geology*, *9*, 249–252.

Appendix

A2.3 map 1
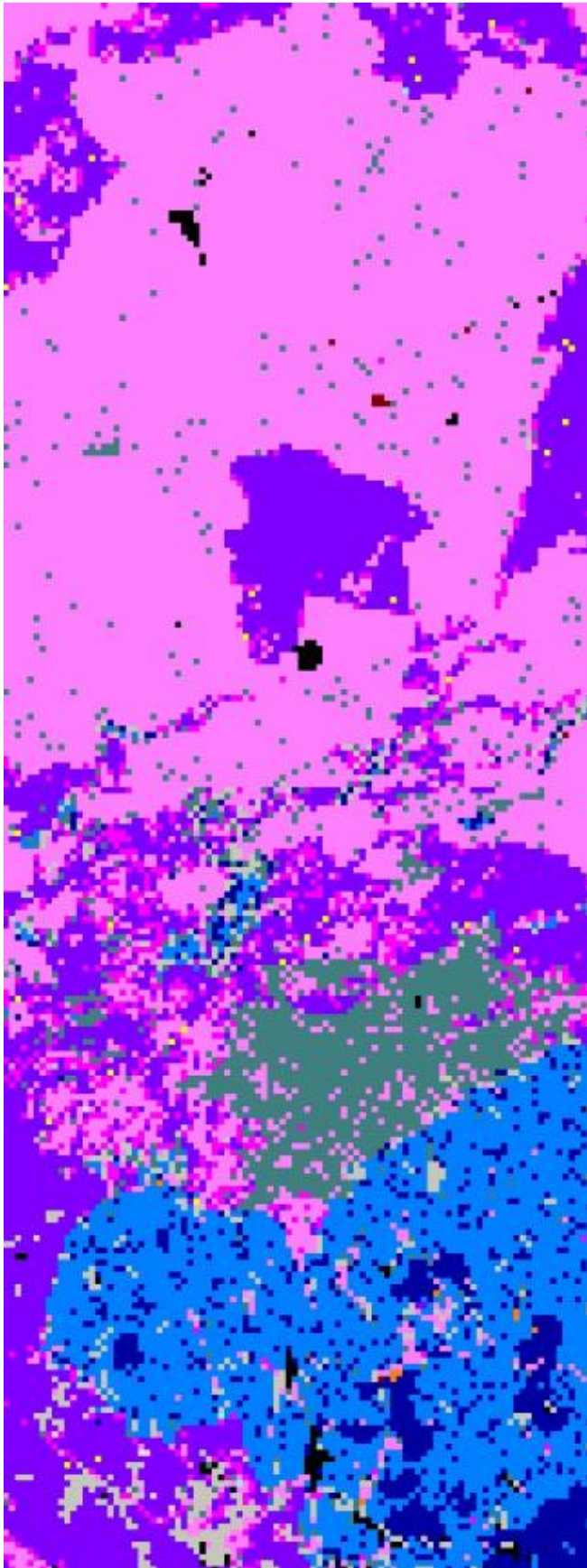
A2.3 map 1
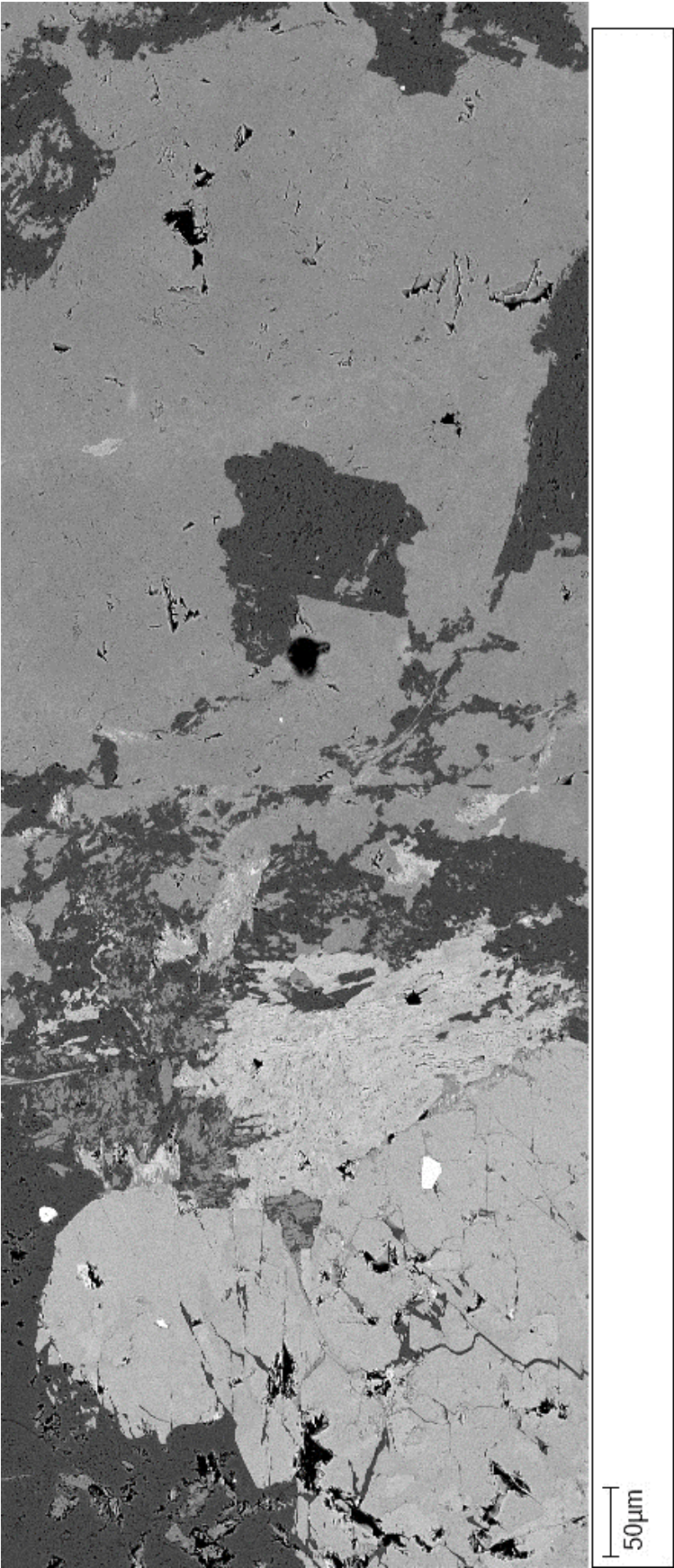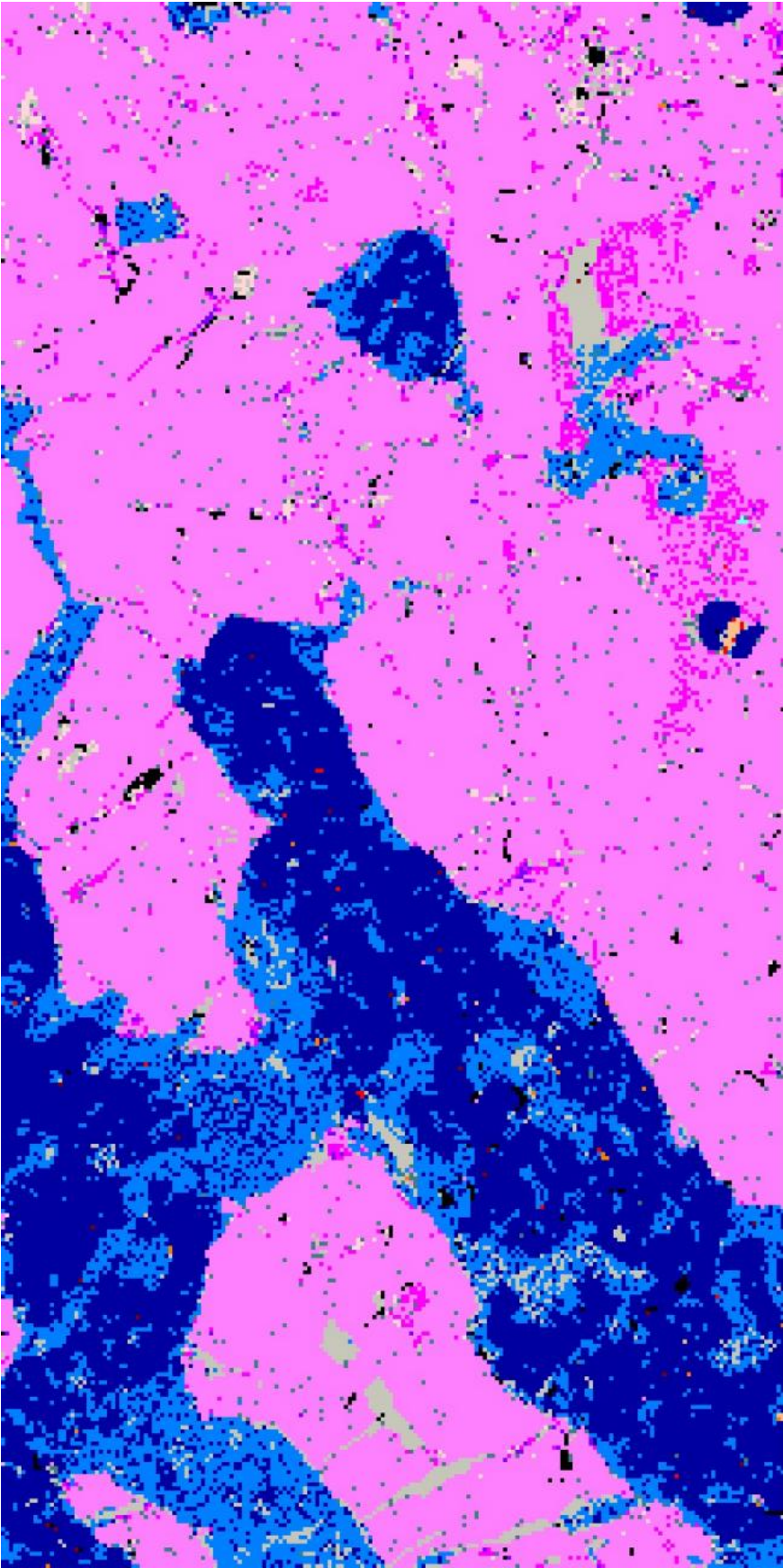
50µm

A2.3 map 2

A2.3 map 1
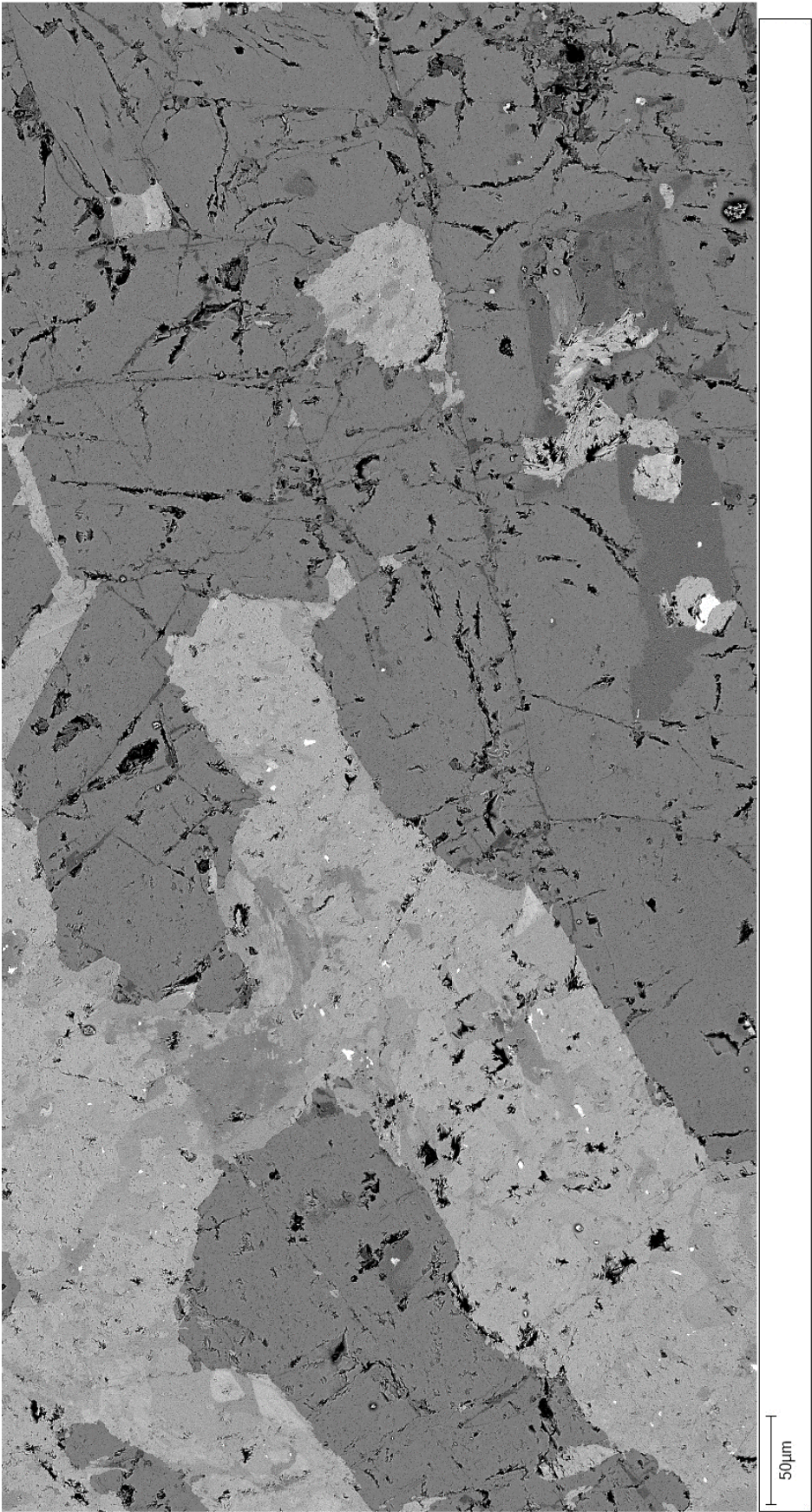
B2.1c
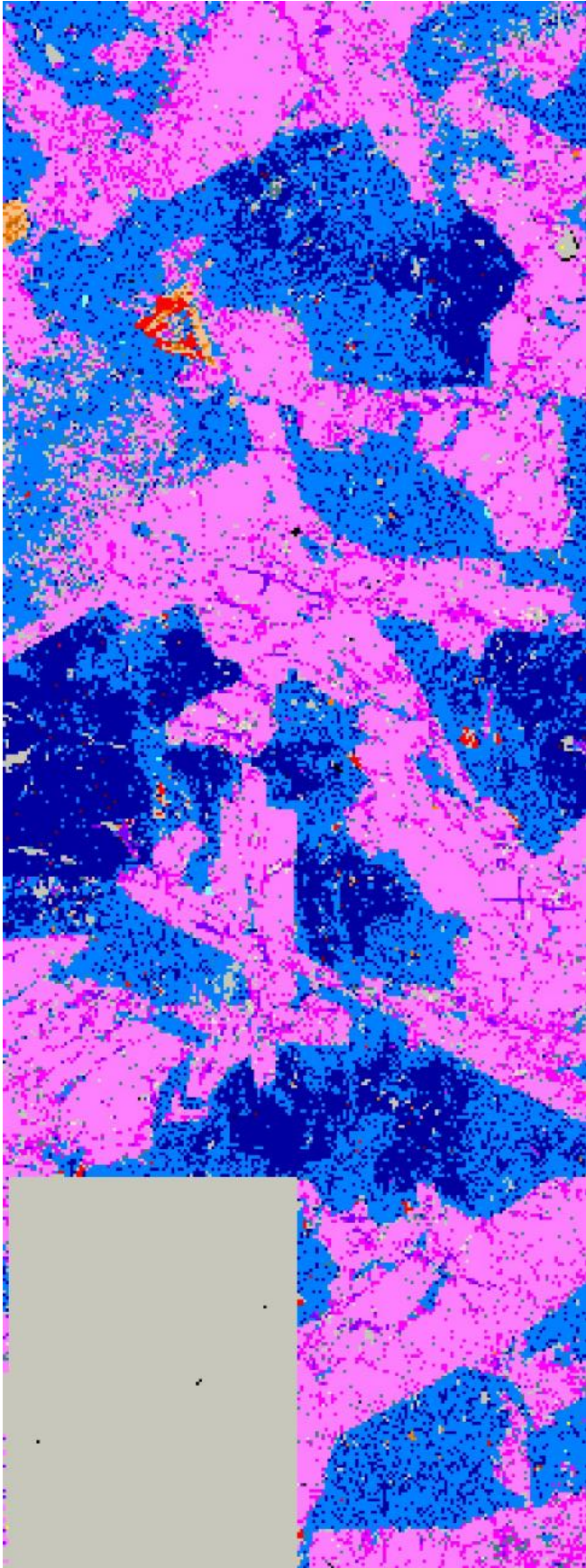
B2.1c
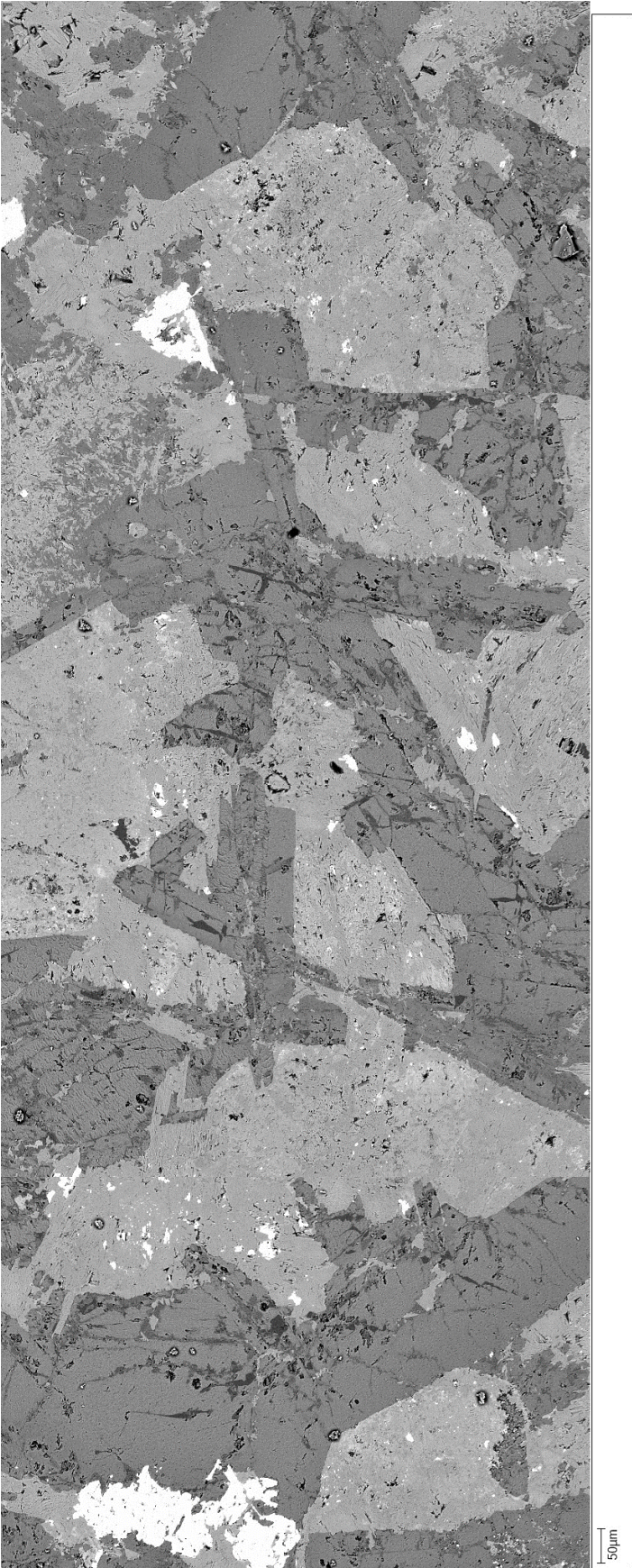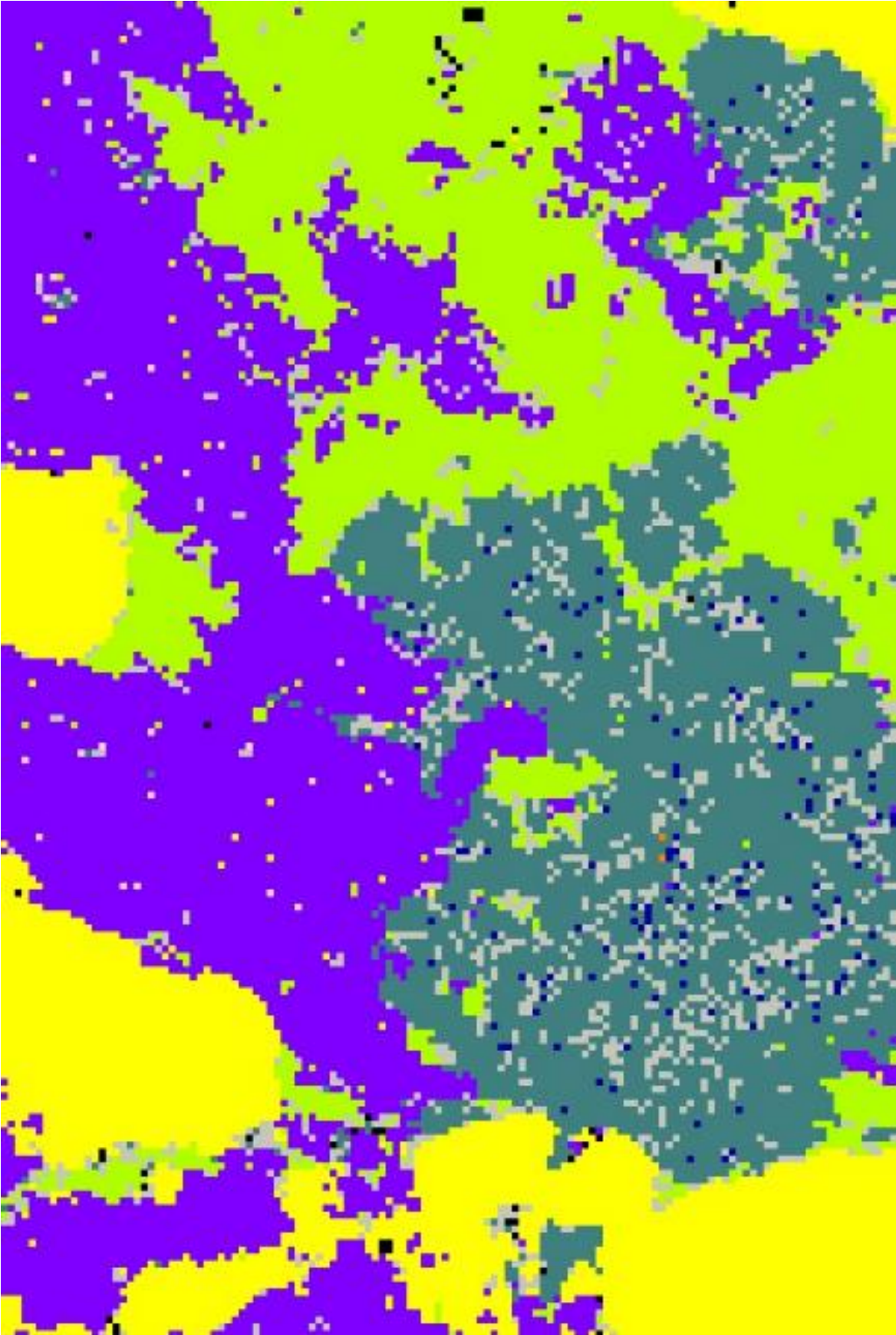
50μm

B2.1ai

B2.1ai
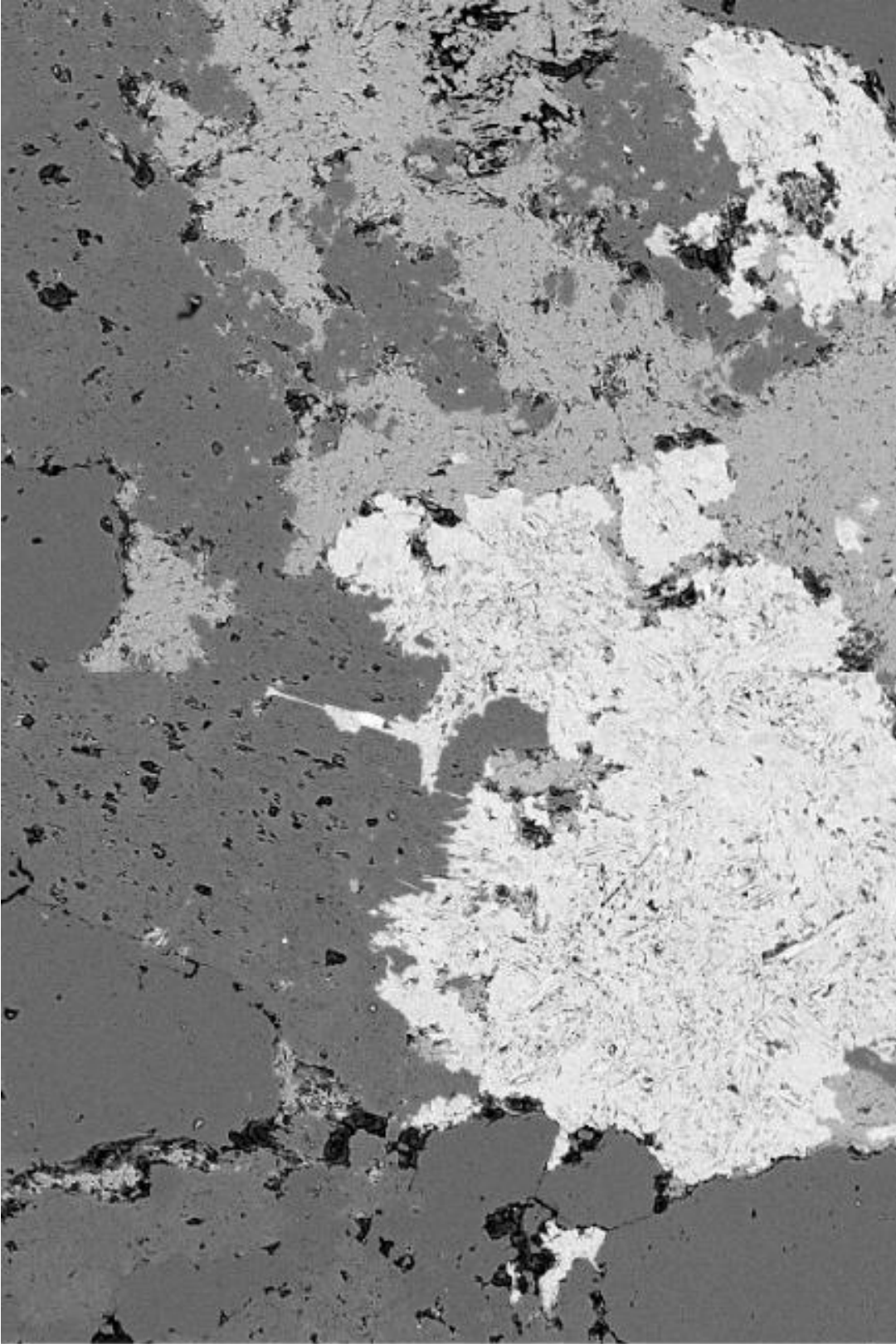
50μm

C2.3c
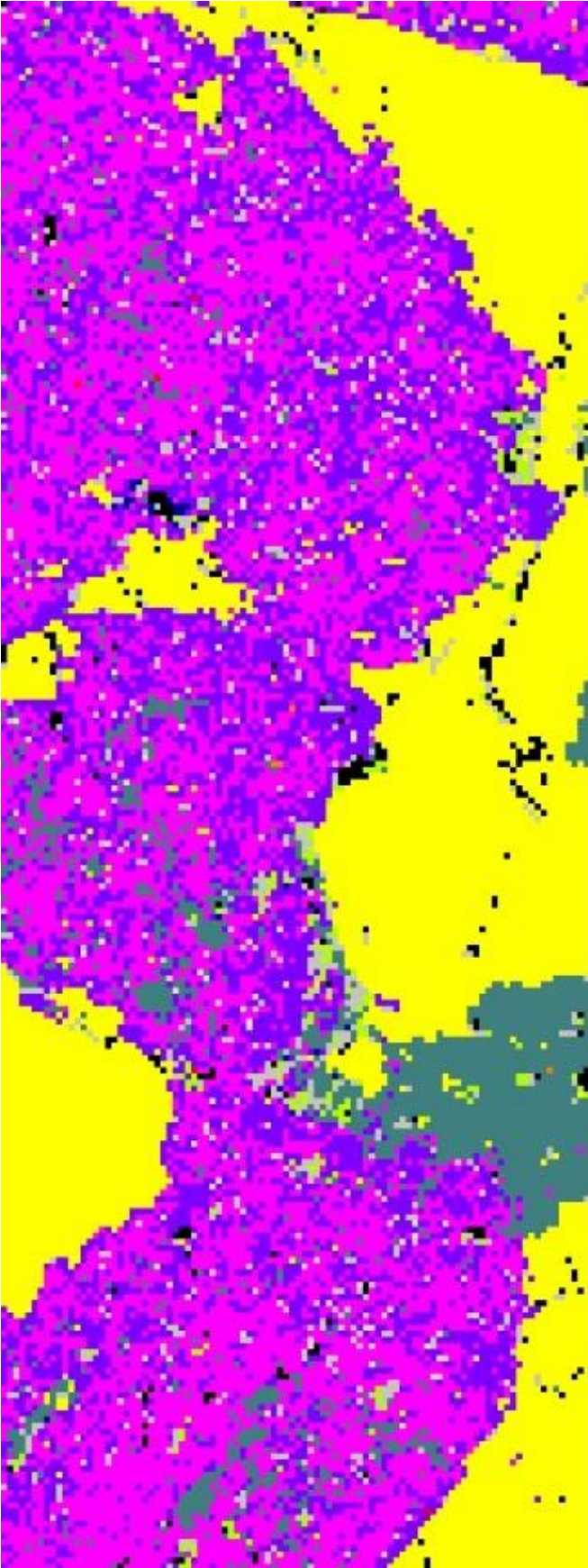
C2.3c
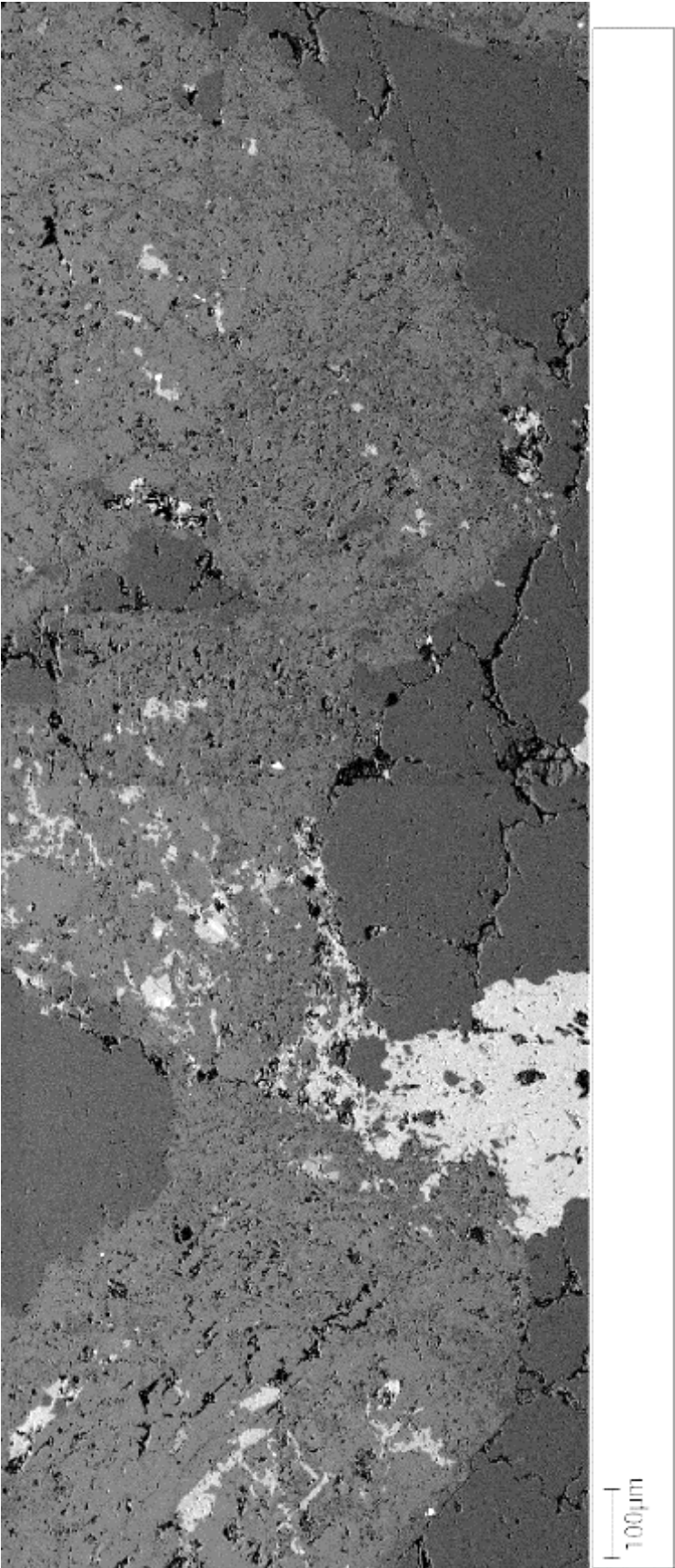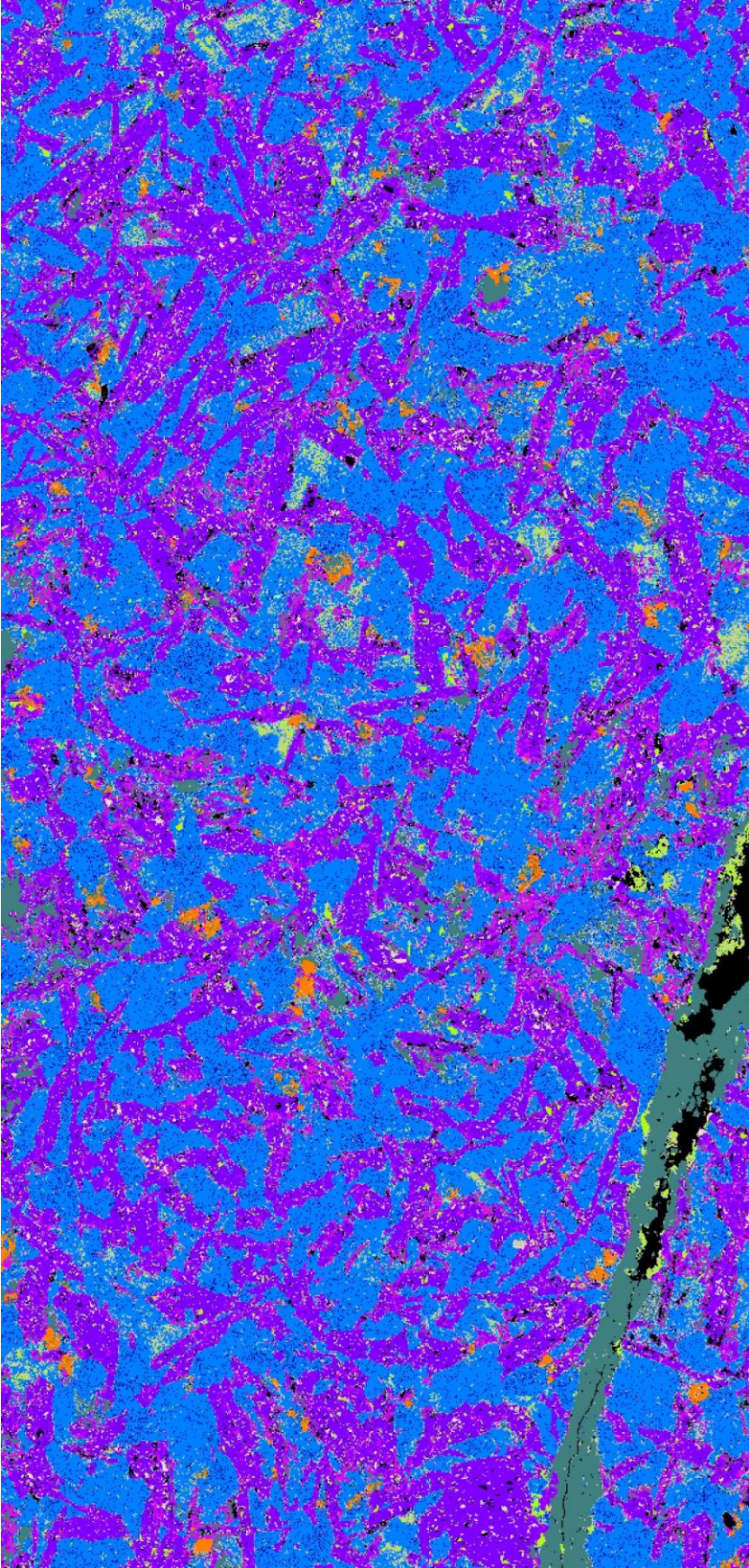
100μm

B2.1b map 1

B2.1b map 1
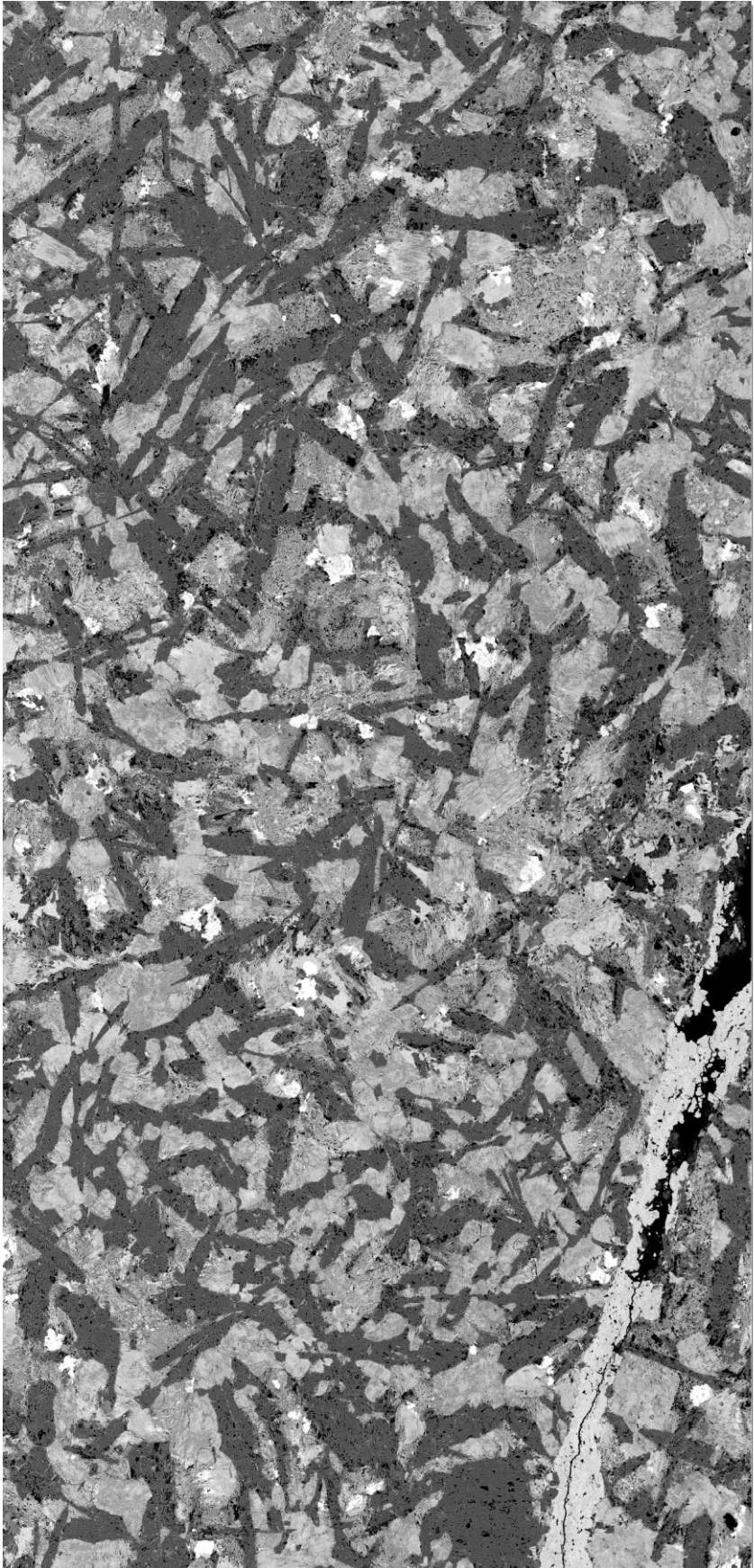
B2.1b map 2
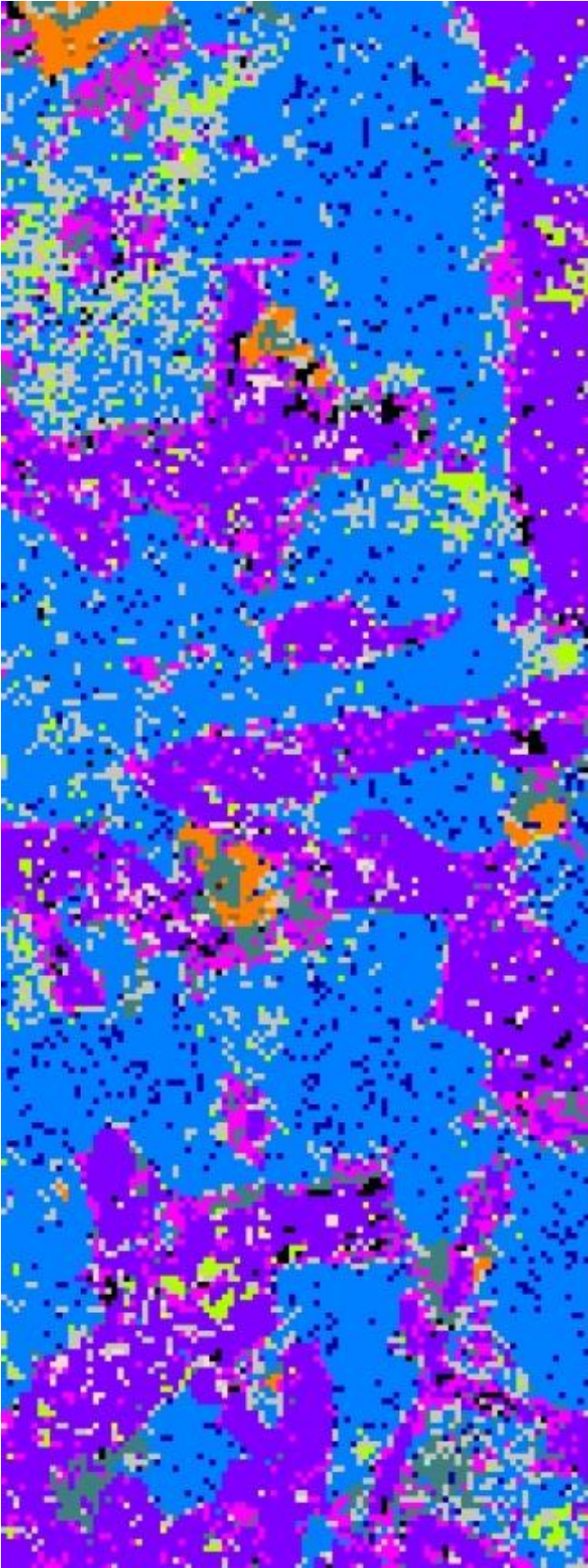
B2.1b map 2
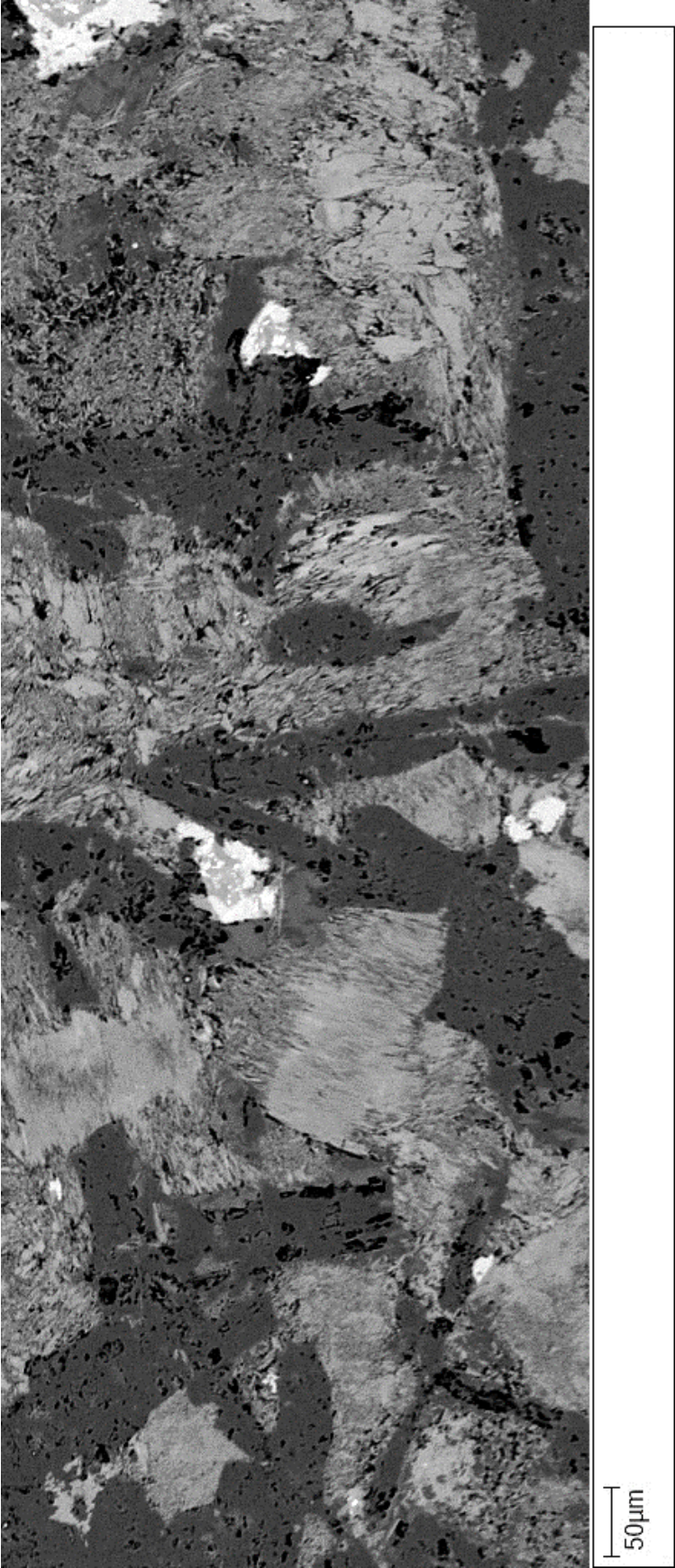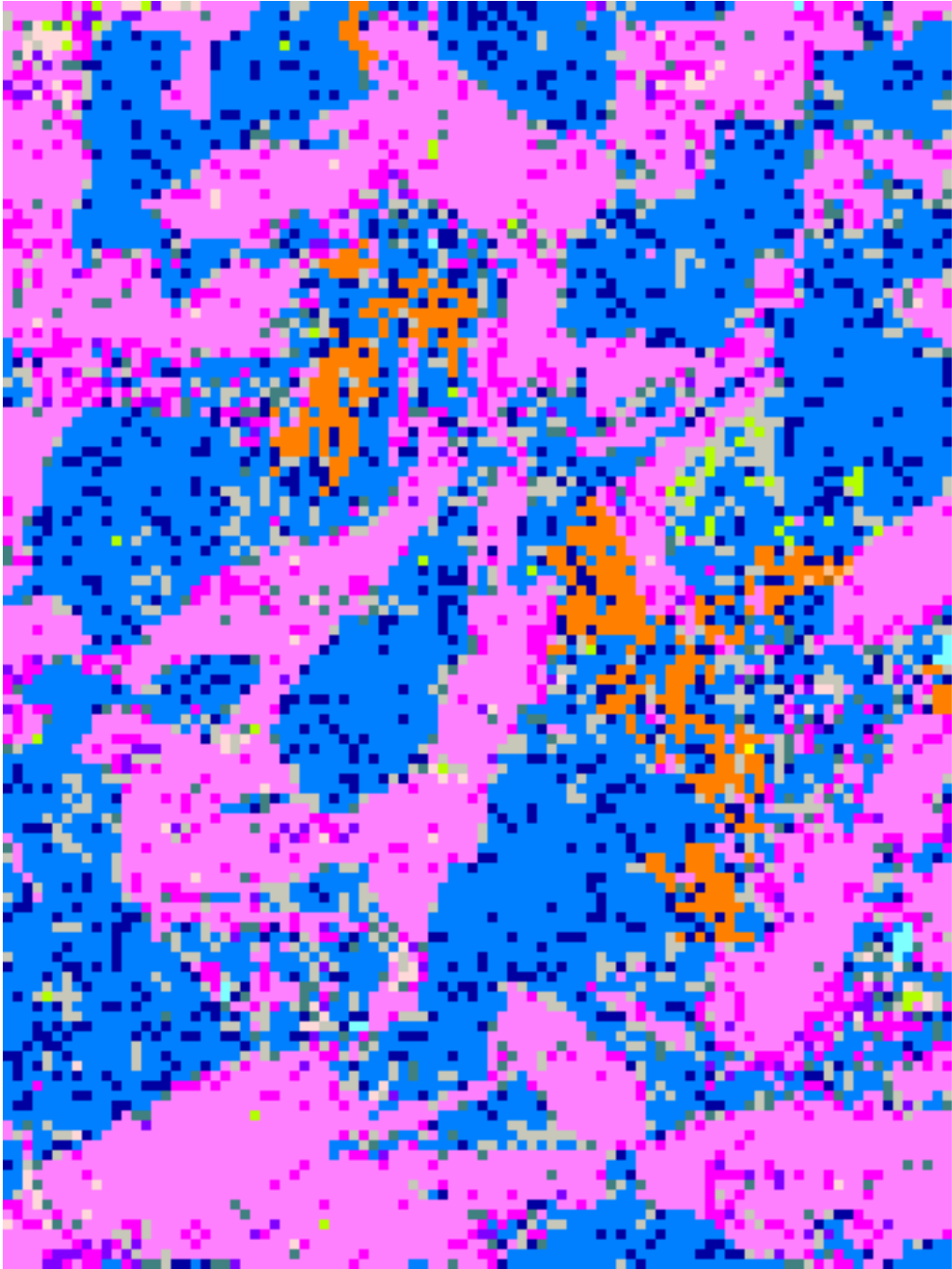
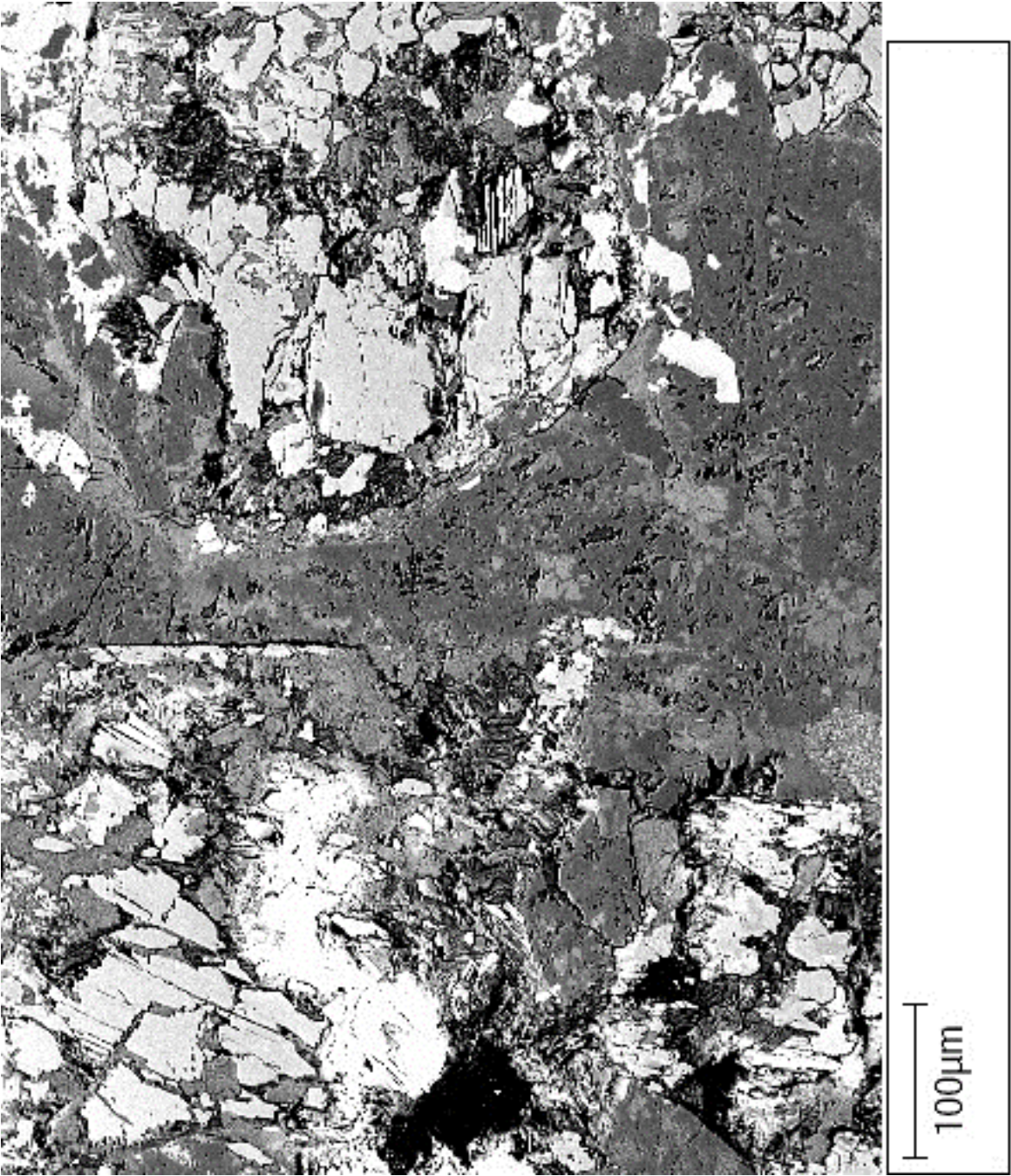50μm

C2.3b map 1

C2.3b map 1
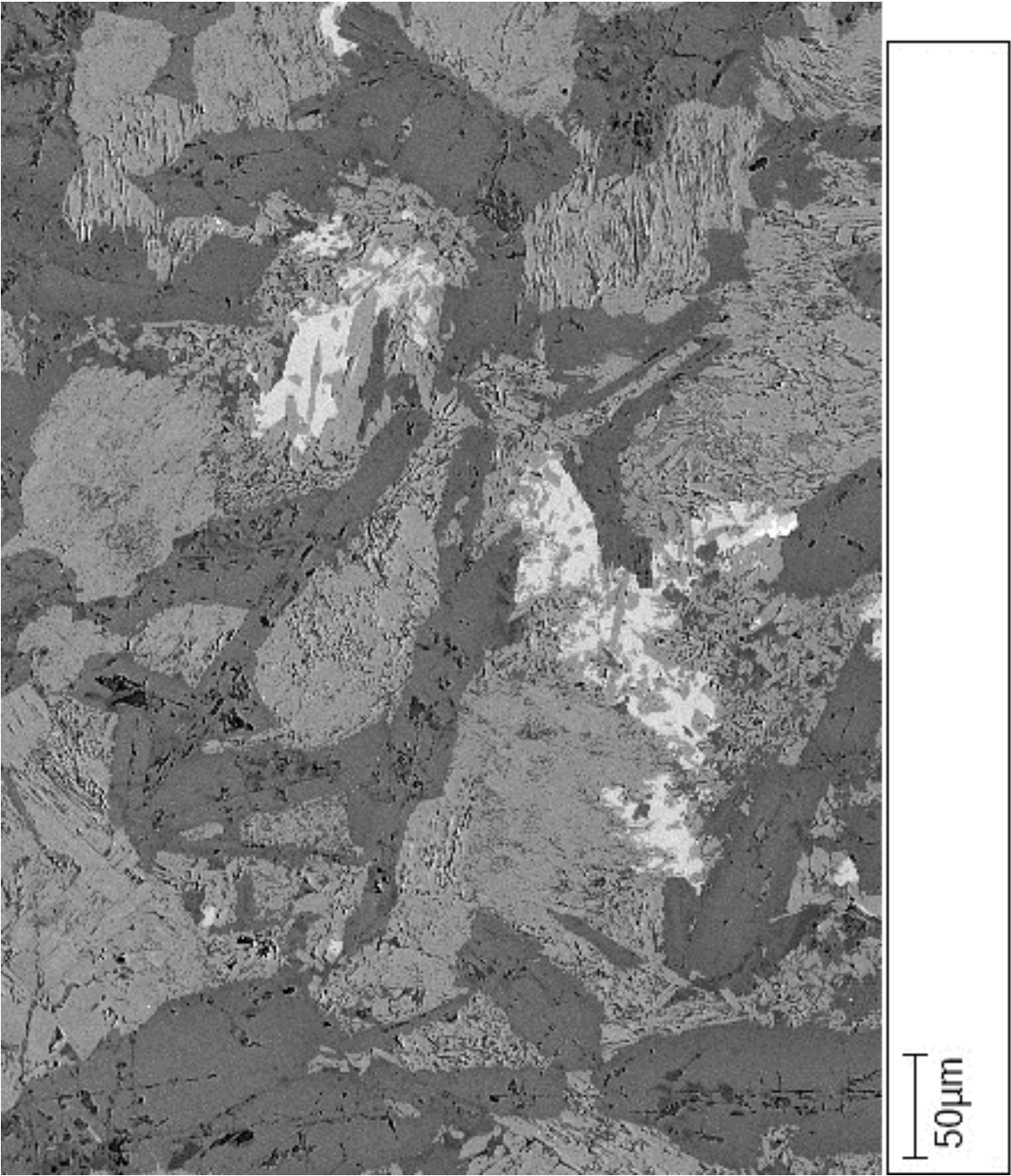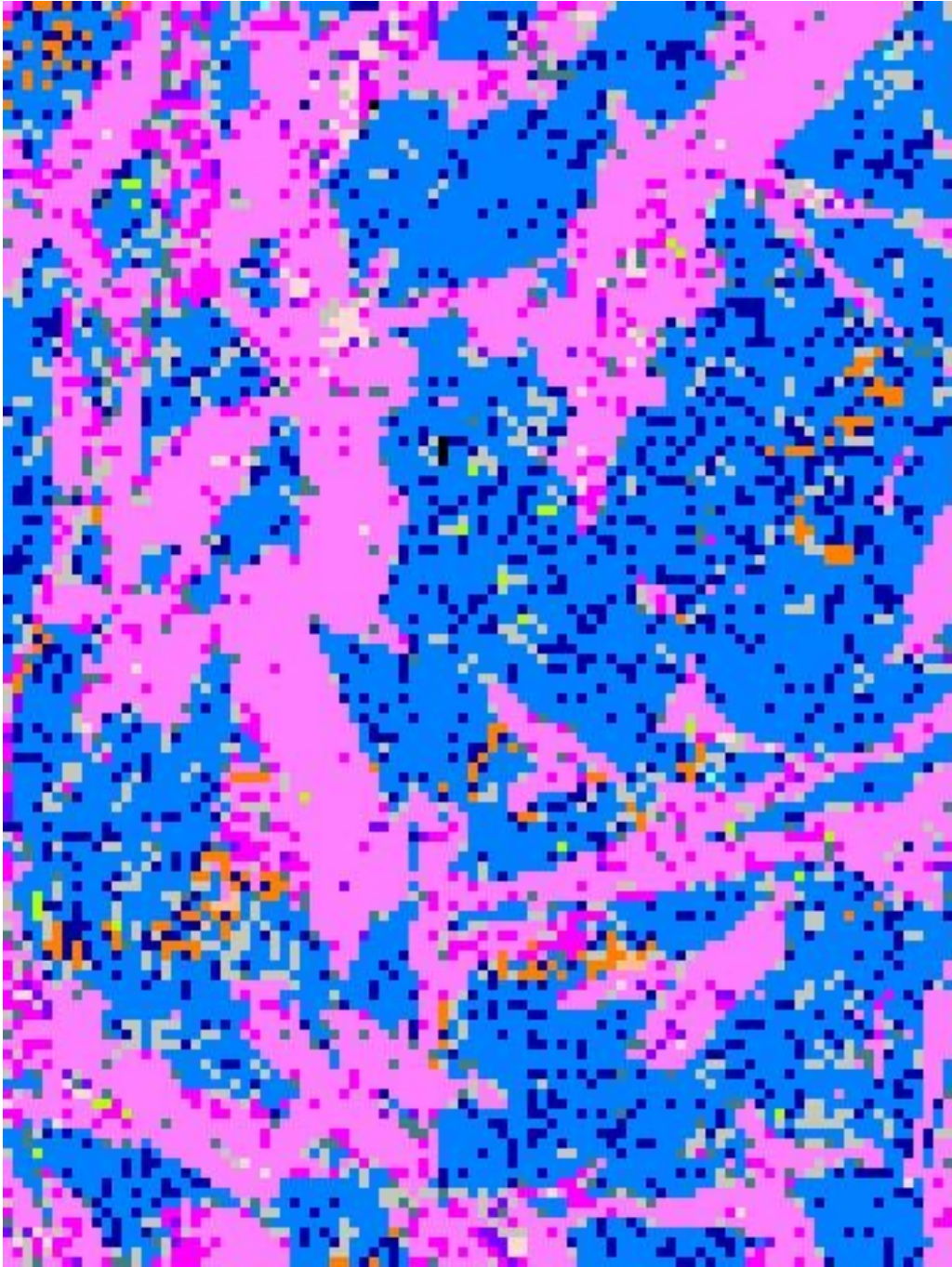
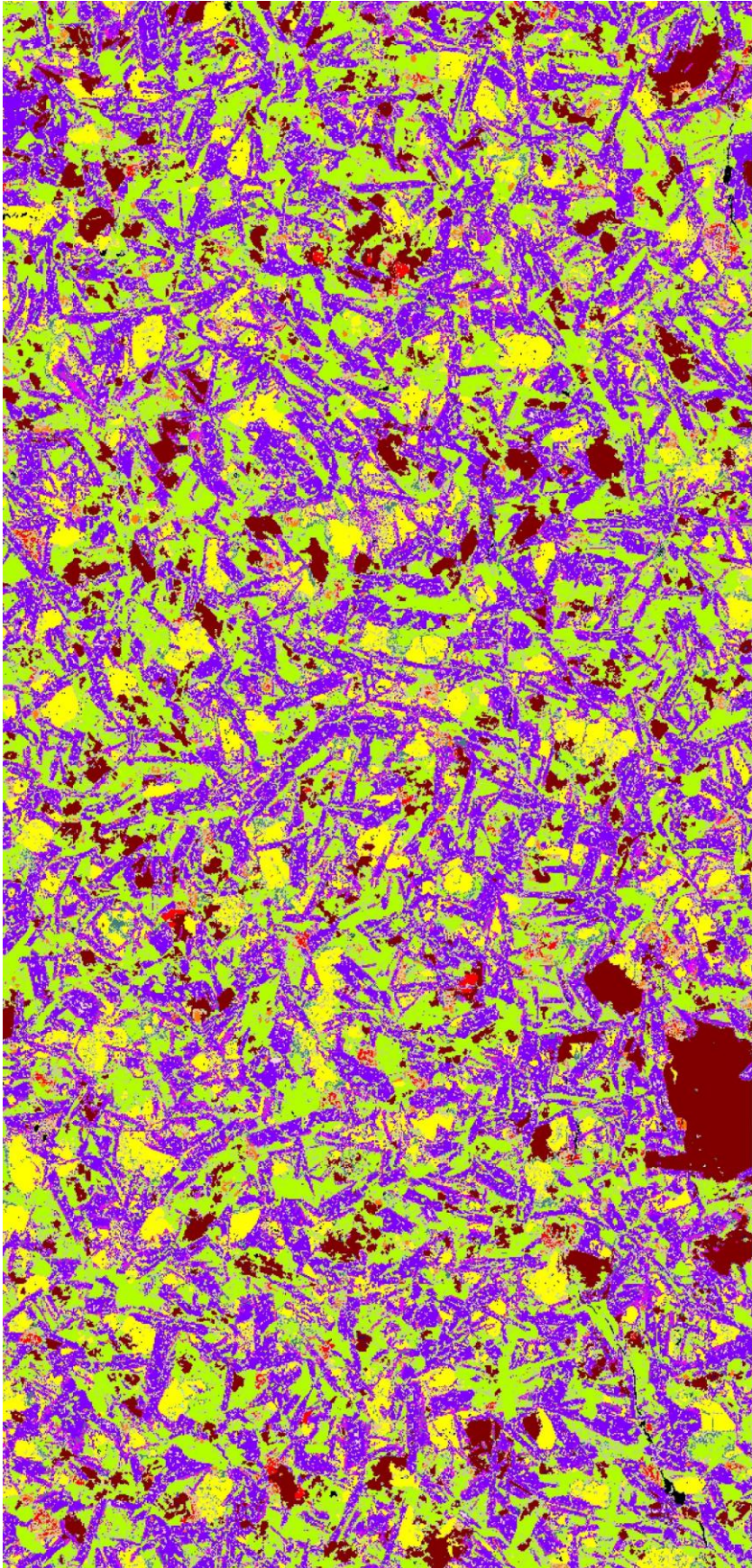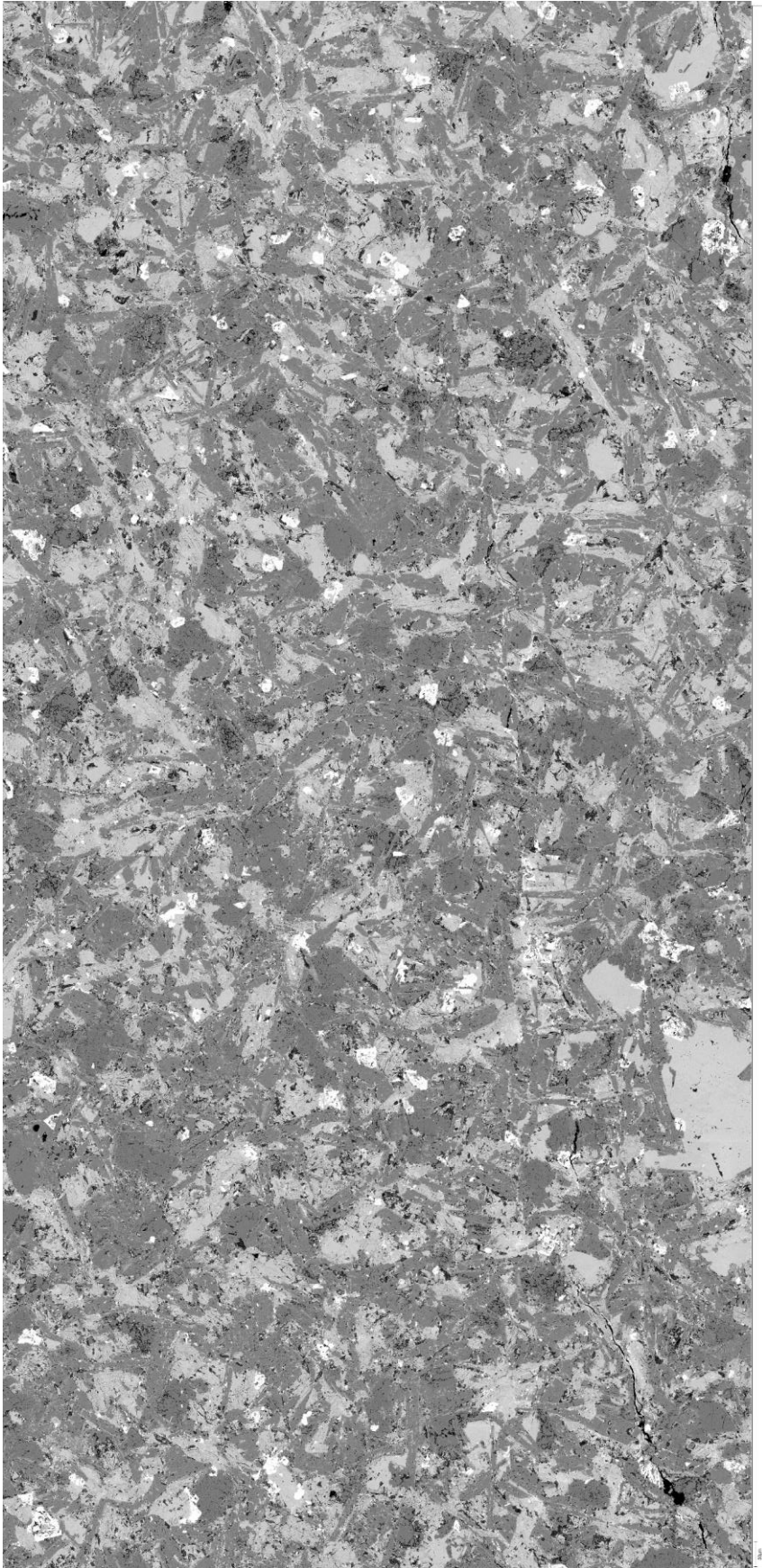50μm

C2.3b map 2

C2.3b map 2
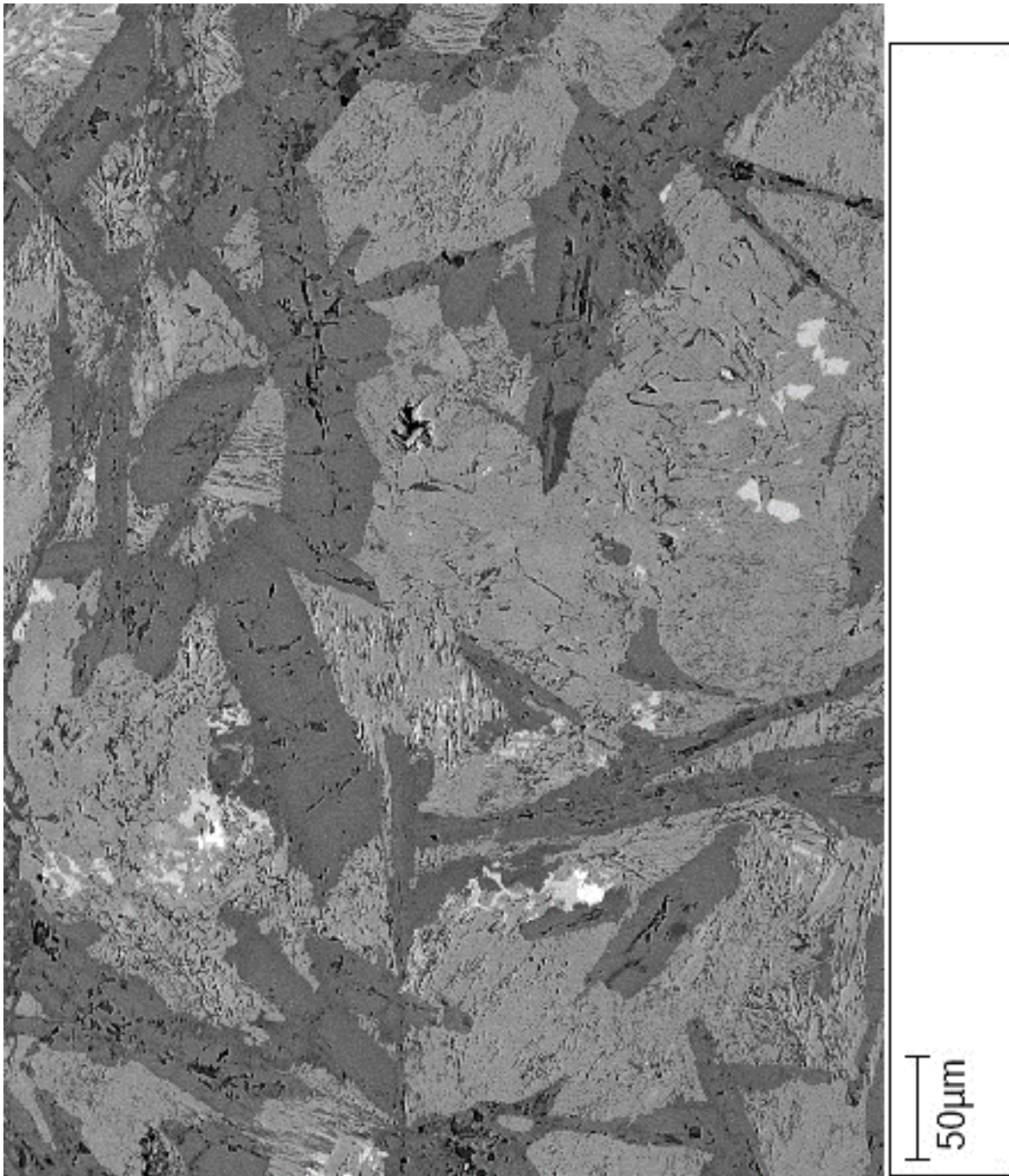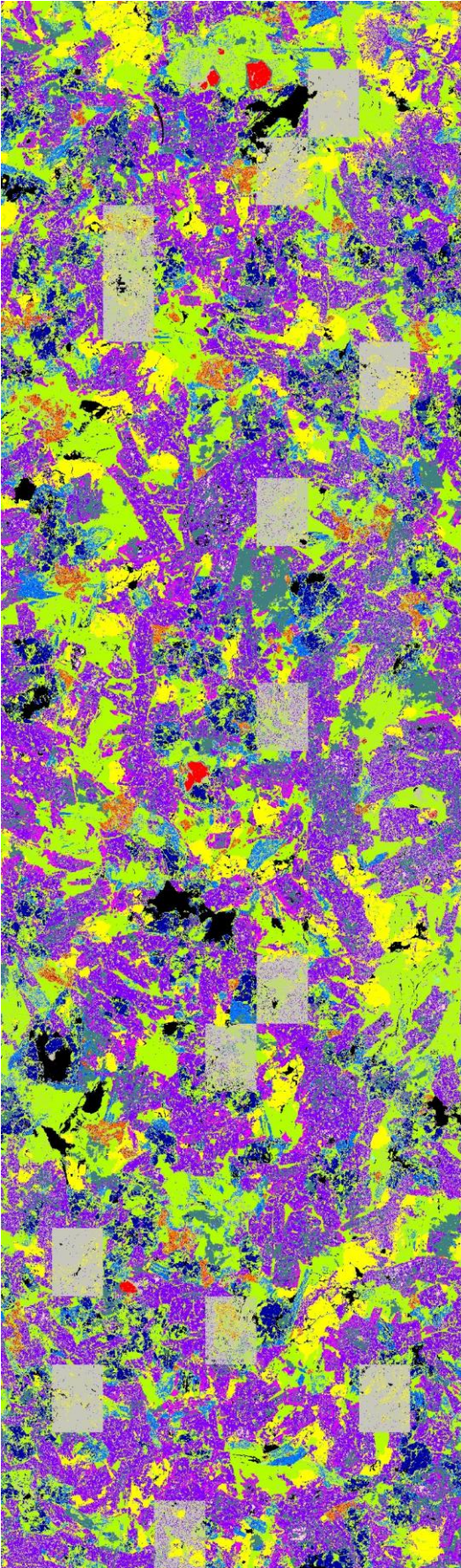
50μm

B2.1h map 1

B2.1h map 1
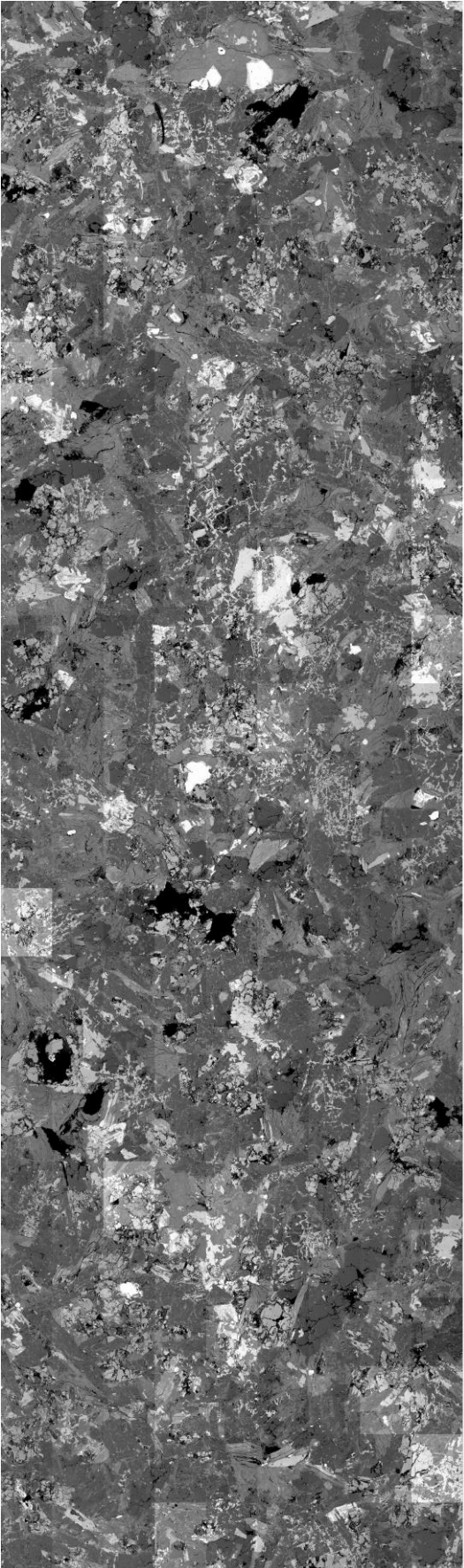
B2.1h map 2
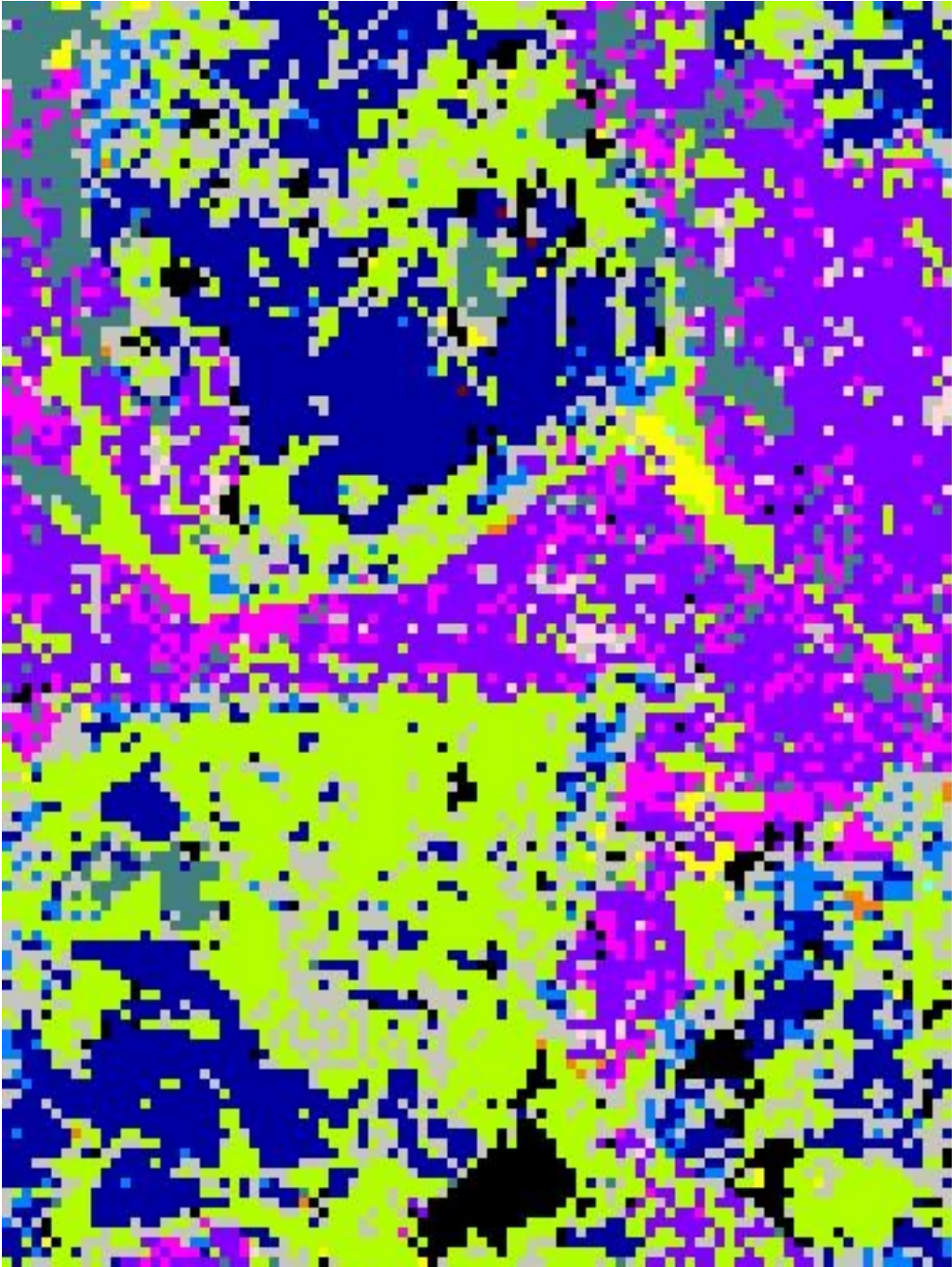
B2.1h map 2

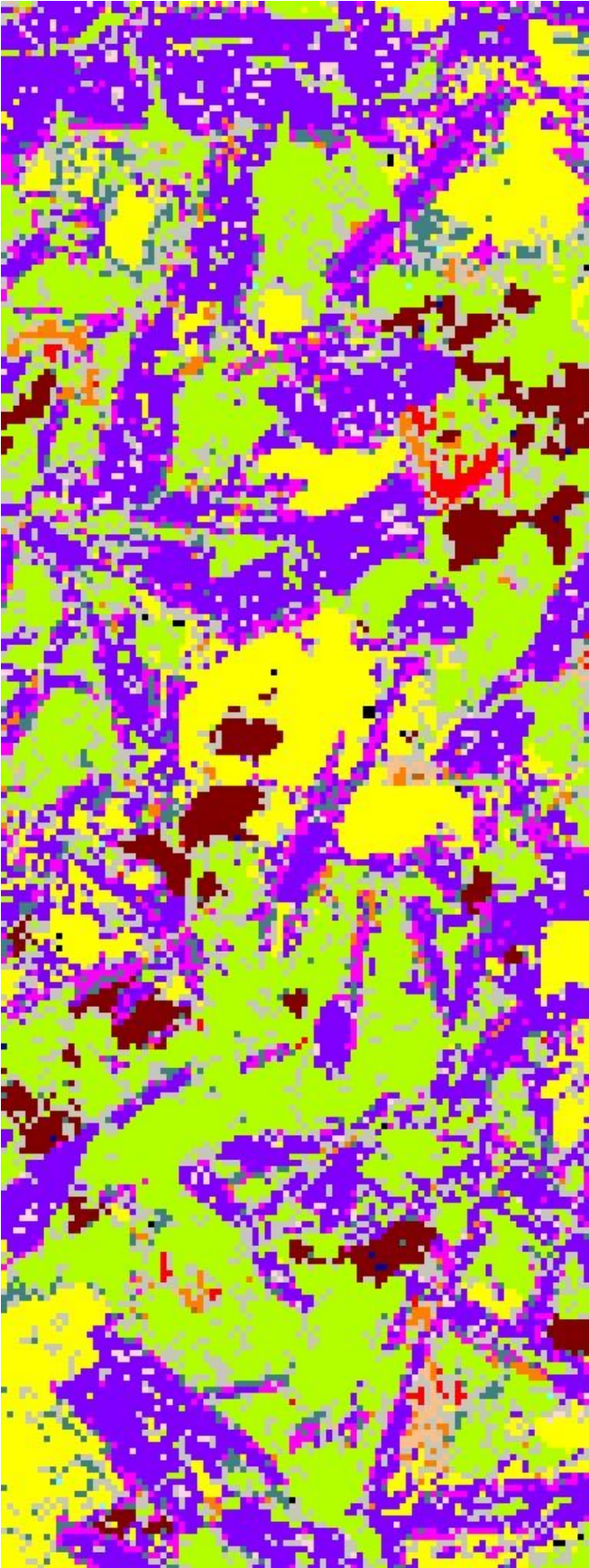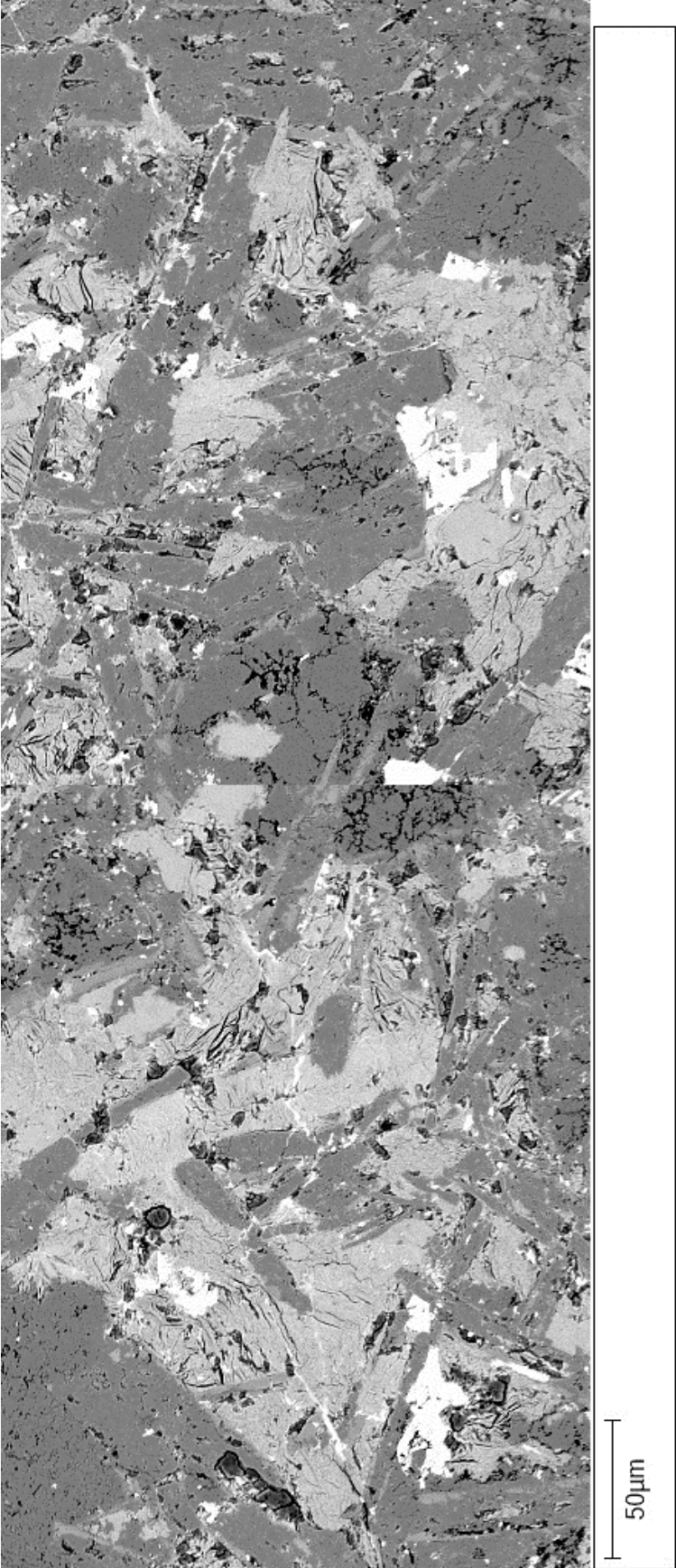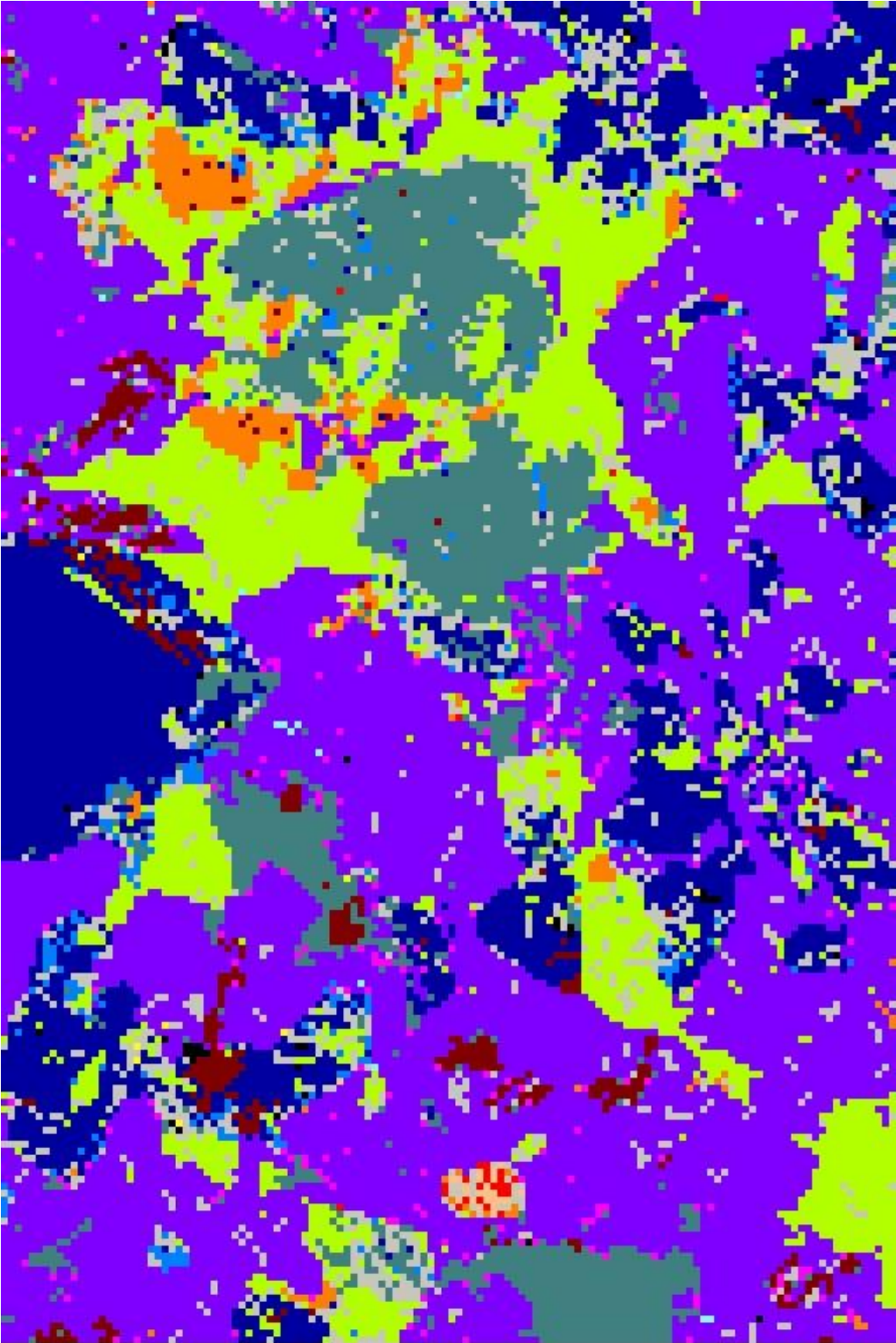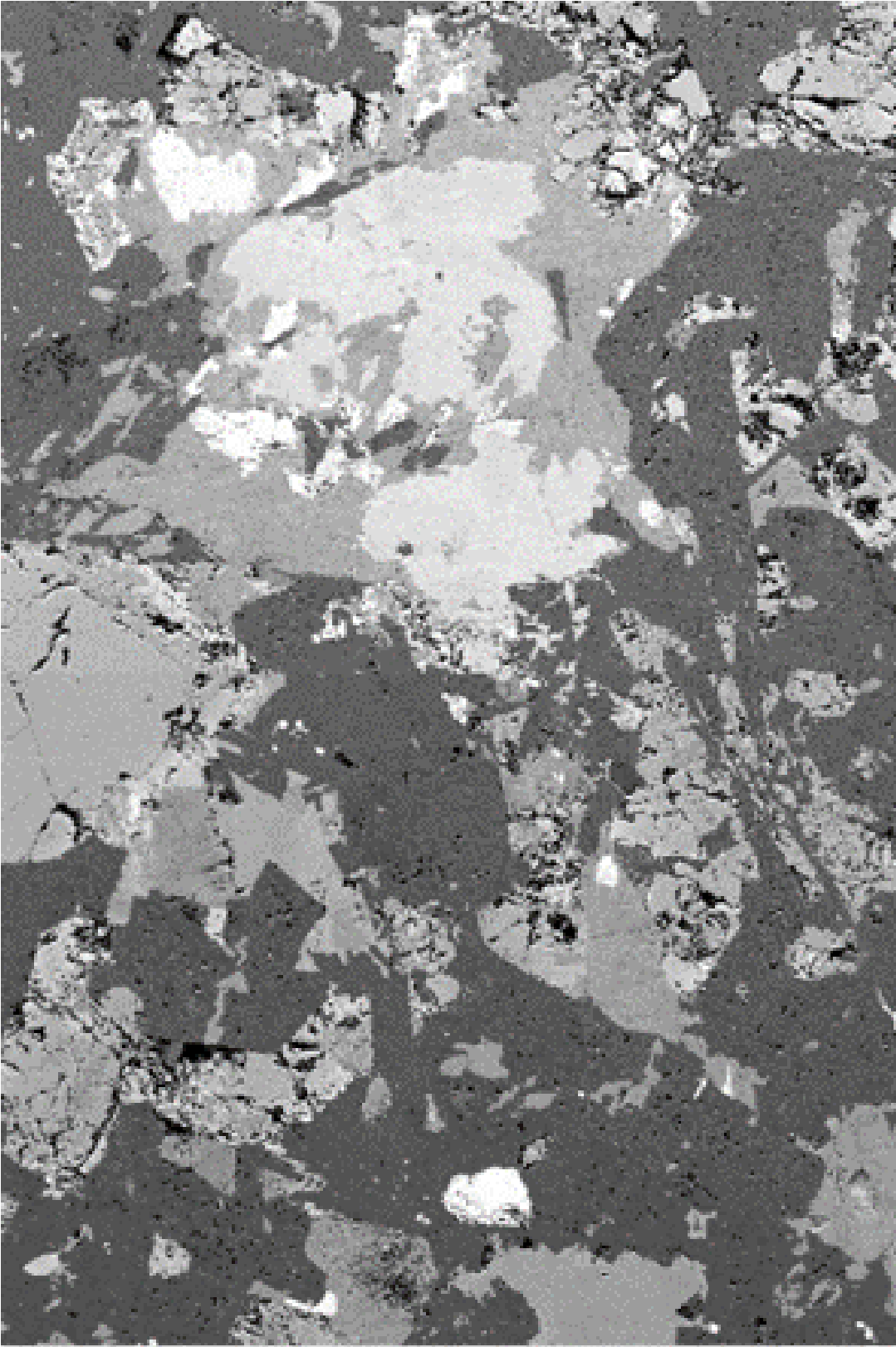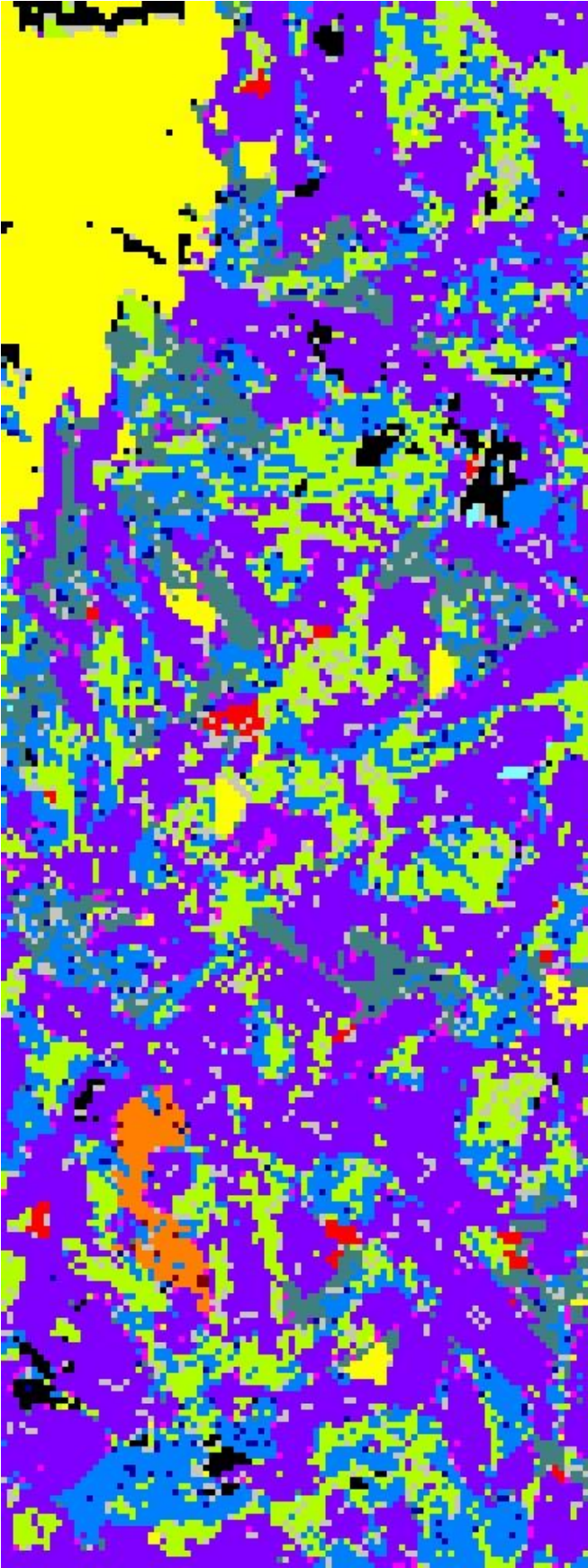B2.2 map 1

B2.2 map 1

B2.2 map 2

B2.2 map 2

50μm

C2.3f

C2.3f

100μm

C2.3g

C2.3g

50μm